JOURNAL OF APPLIED PHYSICS

JOURNAL OF APPLIED PHYSICS

Vol. 18, No. 3 MARCH, 1947

In This Issue

Page

Ordnance Research Laboratory ERIC A. WALKER 263

Contributed Original Research

Theory of Radar Reflection from Wires or Thin Metallic Strips J. H. VAN VLECK, F. BLOCH, AND M. HAMERMESH 274

X-Ray Scattering at Small Angles by Finely-Divided Solids. I. General Approximate Theory and Applications C. G. SHULL AND L. C. ROESS 295

X-Ray Scattering at Small Angles by Finely-Divided Solids. II. Exact Theory for Random Distributions of Spheroidal Particles L. C. ROESS AND C. G. SHULL 308

Excess Noise in Cavity Magnetrons ROBERT L. SPROULL 314

Semi-Polar Form of Fourier Series and Its Use in Crystal Structure Analysis JOSEPH S. LUKESH 321

Insulation of High Voltages in Vacuum JOHN G. TRUMP AND R. J. VAN DE GRAAFF 327

Proceedings of the Electron Microscope Society of America 269

In Every Issue

Here and There 267

Back Number Prices 307

Calendar of Meetings 332

Index to Advertisers xxvi

BOARD OF EDITORS

ELMER HUTCHISSON, *Editor*

Associate Editors

R. BOWLING BARNES
OTTO BEECK
W. F. BUSSE
SELIG HECHT
W. JAMES LYONS
PHILIP MORRISON
PAUL E. SABINE
FREDERICK SEITZ
J. R. TOWNSEND
JOHN VON NEUMANN

Publication of the American Institute of Physics

ADMINISTRATIVE STAFF

HENRY A. BARTON, *Director*
MARGARET S. GRIFFIN, *Publications Manager*
THEODORE VORBURGER, *Business Manager*
JOHN T. TATE, *Adviser on Publications*

GOVERNING BOARD

PAUL E. KLOPSTEG, *Chairman*
WALLACE WATERFALL, *Secretary*
GEORGE B. PEGRAM, *Treasurer*
R. B. DOW
L. A. DUBRIDGE
W. F. FAIR, JR.
FLOYD A. FIRESTONE
HARVEY FLETCHER
R. C. GIBBS
K. S. GIBSON
W. H. MARKWOOD, JR.
A. H. PFUND
JOHN T. TATE
L. W. TAYLOR
A. G. WORTHING

The JOURNAL OF APPLIED PHYSICS, published monthly at Prince and Lemon Sts., Lancaster, Pa., is devoted to physics in its role as the science basic to other natural sciences and to the arts and industries. Previous to 1937 this publication was known as PHYSICS. The JOURNAL OF APPLIED PHYSICS publishes editorials, news of physicists, and reviews, as well as technical papers of applied physics.

Manuscripts should be submitted to Elmer Hutchisson, Editor, Case School of Applied Science, Cleveland 6, Ohio.

Subscriptions and orders for back numbers should be addressed to Prince and Lemon Streets, Lancaster, Pa. or to the American Institute of Physics, 57 East 55 Street, New York 22, N. Y.

Subscription Price

	U.S. AND CANADA	ELSEWHERE
To members and associate members of the American Institute of Physics	$5.00	$5.70
To all others	7.00	7.70

Back Number Prices

Complete set: Vol. 1, July, 1931–Vol. 17, 1946—$124.00
Yearly back number rate: $10.00
Single copies: $1.00 each.

Changes of address and proofs should be addressed to the Publications Manager.

Advertising rates supplied on request. Orders, advertising copy, and cuts should be sent to the American Institute of Physics.

Entered as second class matter January 22, 1937, at the Post Office at Lancaster, Pennsylvania, under the Act of March 3, 1879.
Accepted for mailing at the special rate of postage provided for in the Act of February 28, 1925, authorized May 2, 1932.

Copyright 1947, by the American Institute of Physics.

Journal
of
Applied Physics

Volume 18, Number 3 March, 1947

Ordnance Research Laboratory

BY ERIC A. WALKER*
THE PENNSYLVANIA STATE COLLEGE, STATE COLLEGE, PENNSYLVANIA

THE purpose of the Ordnance Research Laboratory at The Pennsylvania State College is to provide the Navy with an organization which can do research and development in an academic atmosphere. It differs from the Naval Ordnance Laboratory at White Oak, Maryland, and the Naval Research Laboratory in one important respect, namely, that this organization is completely under civilian control and has no Naval officers on its scientific or administrative staff. The organization of such laboratories as the Naval Ordnance Laboratory is too well known to demand further discussion at this time. It is recognized that such an organization cannot be perfect in all respects, and this new Laboratory represents an attempt to meet the problem of providing research for the Navy in a slightly different way.

Although the Laboratory was officially founded on January 1, 1945, it did not start work in its new building until October 1, 1945. However, the organization is much older than this. Many of the members of the staff were recruited from the Harvard Underwater Sound Laboratory, which itself was founded in 1941 and devoted most of its energies to submarine detection problems. Because of the caliber of some of the scientists, the Harvard Underwater Sound Laboratory was asked to undertake an ordnance problem which eventually grew into many and much larger problems, so that by 1943 the Ordnance Division of HUSL was firmly established. The major portion of this group was moved to the Ordnance Research Laboratory during the summer of 1945.

The Laboratory itself is housed in a two-story brick structure built especially for this purpose during the summer of 1945. This building affords approximately 30,000 square feet of space laid out in offices, laboratories, and shops in accordance with the needs. The Laboratory also operates two field groups, one at Newport, Rhode Island, and another at Fort Lauderdale, Florida.

FIG. 1. Exterior of Ordnance Research Laboratory. This Laboratory was designed by Paul Philippe Cret, well-known architect. It is laid out to be both functional and architecturally attractive.

* Director, Ordnance Research Laboratory.

FIG. 2. A view of the Black Moshannon Calibration Station for underwater sound devices. This calibration station is set on piles over a lake in a state forest. The general appearance is that of a Swiss chalet, and it was designed specifically to harmonize with its rural surroundings.

The one at Fort Lauderdale, Florida, will shortly be moved to a new laboratory structure at Key West. Both of these laboratories are modern buildings with office space, laboratory, and shops, but their work primarily is that of field testing the finished product or of obtaining fundamental determinations on which working designs can be based. At each of the field stations there exists a small core of four or five men who are on a permanent basis. The remainder of the staff is composed of scientists who are sent to the field stations for periods of from a few days to several months in order to test their designs.

The relationship between the Laboratory and the College is relatively simple. The Laboratory is established as a department of the School of Engineering in exactly the same way as any other department, such as Aeronautical, Civil, Electrical Engineering, etc. All members of the Laboratory staff are regular employees of the College. The scientists are given the academic titles of Professor, including the usual Associate and Assistant Professorships, or of Research Assistant, which in the usual academic scale corresponds to Instructor. Technicians hired as specialists in a particular field are usually classed as Assistants. The remainder of the staff, including machinists, clerks, and secretaries, carries appropriate designation. The direct line of responsibility between the Laboratory and the remainder of the College is through the Director and the Dean of the School of Engineering.

The relationship with the Navy is a much more tenuous one than that existing with the College, since there is only one Naval officer attached to the Laboratory. In fact, the Navy, by a contract between the College and the Bureau of Ordnance, sets aside a certain fund for the Laboratory to use in doing research and development on underwater ordnance. The Naval Ordnance Officer is expected to be cognizant of all the activities of the Laboratory and must approve certain business transactions which, because of their financial magnitude, seem to require prior Navy approval. The scientific tie between the Laboratory and the Navy is almost placed on a personal basis. The Navy does not write a directive on which the Laboratory must act, but most research programs undertaken by the Laboratory originate with the scientific staff of the Laboratory and are then submitted to the appropriate Naval officers for their approval. Because liaison between Naval officers and the scientific staff is a rather close and cordial one, usually there are a number of discussions preceding any formal proposal, and to date things are so well prepared that no proposal has been made which has not been accepted. This method of problem approval is a valuable one from the Laboratory's viewpoint because it serves as an automatic check on the work of the Laboratory and insures against scientists going off on unprecedented problems, while allowing the staff to judge the worth of the investigation and, to a great extent, to follow their own interests.

The internal organization of the Laboratory is not particularly novel, but it must stress certain factors which have to do with the product of the Laboratory, namely, scientific research. The Laboratory is headed by a Director and several Assistant Directors, but the weekly review of the working operations comes under the cognizance of a Council. This Council consists of the Directors of the Laboratory, including the Business Manager and Personnel Director, the leaders of all the sections, and the project engineers in charge of the major projects of the Laboratory. The scientific staff is organized both horizontally and vertically. There are five major scientific sections: Acoustics, Electronics, Applied Mechanics, Hydro- and Aerodynamics, and Mathematics. These may be further subdivided.

For instance, the Electronics Section is divided into a research division, a development division, and a production division, which undertake the particular functions indicated.

The Applied Mechanics Section is divided in a different manner, since it must fill a service function for the remainder of the Laboratory. It includes a design division which is expected to carry on all mechanical design through the blueprint stage, and the shops, which are expected to produce the mechanisms. This section also employs a number of mechanical designers or engineers who are expected to carry on any research projects which fall into this classification and to serve as representatives of this section in a manner which will be outlined later.

The Acoustics Section has research, development, and construction functions, and also test responsibilities which include the test of any acoustical device which is produced in this Laboratory or a device on which tests may be requested by other organizations.

The Hydro- and Aerodynamics Section is currently being organized. It will consist of two major divisions, the first concerned with the mathematical aspects of aero- and hydrodynamics with special emphasis on body shapes, propellers, and cavitation. The other division will be concerned with operations for the test of these devices either at sea or in the water tunnel.

The Mathematics Section, because of the peculiar nature of its work, has little or no formal organization.

The work of the Laboratory is usually concentrated in a small number of major projects. These projects are almost entirely development work, and therefore they come under the cognizance of a project engineer. In assembling a staff for any particular project, the project engineer may feel that he needs the services of engineers or scientists skilled in particular scientific fields, so he may request the proper section leader to assign to him a scientist who is familiar with the type of problem which he expects to meet. Conversely, the section leader, knowing a project is to be undertaken, may decide that this particular project has a number of features in which his group will be interested. He may then request representation and assign to the group a scientist who will pass on all of the designs which come in his field and who will keep the section leader informed of the progress of the work.

The work in a project usually divides itself into a construction phase which is undertaken at the main laboratory and a test phase which is undertaken at one of the field stations. One of the inviolable principles of operation is that the group which tests a device must be the same group which designed and supervised its assembly at the home laboratory. This serves to preserve continuity of knowledge which exists in unwritten form and which may be of considerable importance in the design and final operation of the device. Some difficulties arise from time to time when an engineer is asked to serve both the project engineer and the section leader. This matter is usually resolved by a ruling that in the field the project engineer is in complete charge, while in the laboratory he must confer with the section leaders.

Every attempt is made to insure complete dissemination of all information about all projects. This is possible because they cover a narrow range of scientific activity. First, a weekly organization report is issued. The material is collected as painlessly as possible by the group secretaries, who visit the various individuals at their work places and ask for their weekly reports. In it each scientific worker in the Laboratory may have his say. Frankness is encouraged, and because the organization report

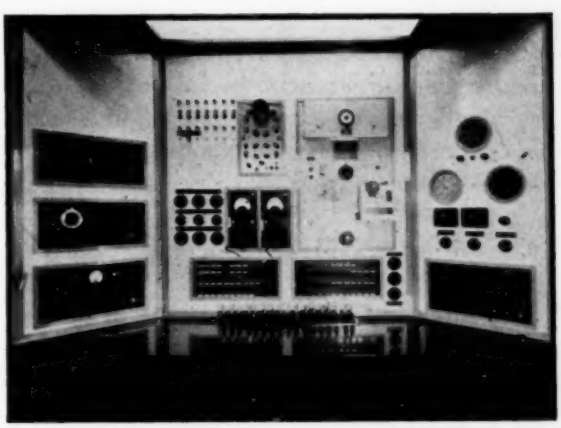

FIG. 3. Front view, Black Moshannon console. A close-up view of the console from which all of the underwater acoustic measurements are made. This panel is so laid out that all measurements can be made from this point and recorded automatically without the operator's leaving the control position.

FIG. 4. This is a view of one of the general shops. This particular shop is devoted to light machine work for the construction of models and test equipment.

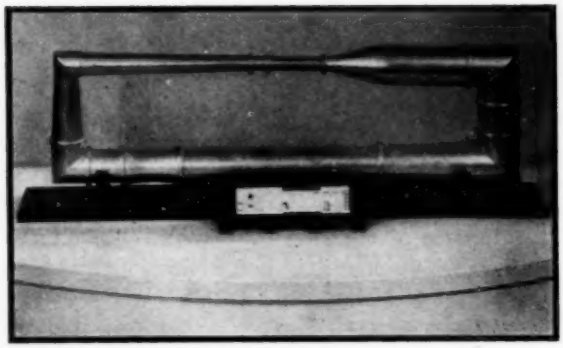

FIG. 5. Scale model of the 48-inch water tunnel which will be built at Penn State in the near future. The large section of the tunnel has a diameter of 12 feet and it is over 100 feet long. The picture shows a full-size railway box car to the same scale.

never leaves the confines of the Laboratory, no editing is encouraged or attempted. The notes published in this organization report may be lengthy or brief, depending on the scientist's mood and on the amount of work he has done during the past week. At times these reports may be deadly reading, but they give every member of the Laboratory a chance to be heard on any subject, scientific, administrative, or otherwise.

The second method is to encourage the frequent writing of internal memoranda. Each member of the staff is told that when he reaches a suitable stopping point in his work, he should write a memorandum addressed to his immediate superior and sent to anyone else in the Laboratory who he feels might be interested in his work. As is expected, these memoranda provoke considerable comment and much constructive criticism.

The third method is by conferences. These are almost never scheduled on a calendar basis but are assembled on short notice by the project engineers when they feel that some clarification is needed.

The reports of the Laboratory take two forms: a monthly report which tells of the progress of all research programs, and reports on a single program which are issued when a suitable tying-off point is reached. Ultimately, the product of the Laboratory will be gadgets or weapons, together with complete sets of prints by which they may be constructed, and the maintenance and instruction manuals which are necessary for their use. Completion reports will include an evaluation of the device which sums up the matter by either saying that the gadget is no good and should be forgotten, or that it is useful and should go to the Fleet for training purposes.

An attempt is made to provide every useful mechanical aid for the scientists, since they, at the present time, are by far the scarcest commodity. Computers are provided to make routine calculations and to plot curves. Draftsmen are provided to put sketches into publishable form, and a library and staff keep the master files and all available useful information. Because these files become quite voluminous it has been found desirable to keep a microfilm file of all documents which are six months old or older. Most of these documents are on the general theme of underwater ordnance and include reports of this and other laboratories, as well as technical accounts of the ordnance used by foreign governments.

In the administration of any such organization, certain aids and methods of operation appear which are peculiar to the personnel employed and which may work in a laboratory of one size and nature and not in another. Experience at ORL has shown that it is desirable to provide almost complete segregation between the business and the scientific functions of the Laboratory. No scientist should be asked or even allowed to waste his time on matters which

belong in a purchasing office. He should not be allowed to hire personnel because he may make commitments which cannot be honored. He should not be asked to waste his time securing tickets or hotel reservations if it can better be done by someone attached to the Business Office. One other peculiarity arises from the fact that in a research organization very often only one item of a kind is made. Many scientists feel that such an item can best be designed "on the lathe." It is quite obvious that no machine shop of any size can be run in this manner, so at ORL the stipulation is made that all machine shop work is done either to blueprint or to approved sketches. This still leaves the possibility that in some cases the scientist's contention may be correct, and it is not worth the time to make detailed drawings or elaborate sketches before construction is started. For this reason, a small and well-equipped machine shop is provided in which any scientist can do his own work. For the safety of both the scientist and the machines, an expert machinist is always in attendance who may actually do the job or, if necessary, guide the scientist while the job is being done. Such an arrangement, although a rather elaborate one, seems to remove many causes of irritation and friction.

Every attempt is made to get publications into the scientific press, and for this purpose an Editorial Office exists and may be called upon to give assistance if the author wishes or requires it.

Here and There

New Appointments

G. Howard Carragan has been appointed head of the Department of Physics at Rensselaer Polytechnic Institute. He succeeds Robert A. Patterson, who recently left to serve as an assistant director of Brookhaven National Laboratory, atomic research center at Camp Upton, Long Island.

Walter Evans Receives Army Award

The War Department has announced the award of the Army Certificate of Appreciation to Walter Evans, vice president in charge of all radio activities for the Westinghouse Electric Corporation, for "his contribution to the Signal Corps in connection with the development and production of radio and radar equipment during World War II."

Duane Roller Receives Oersted Medal

The American Association of Physics Teachers has awarded the Oersted Medal to Duane Roller, professor and head of the Department of Physics of Wabash College, Crawfordsville, Indiana. The award is made annually "for notable contributions to the teaching of physics."

Through the *American Journal of Physics*, which he has edited since it was founded in 1933, Dr. Roller had made probably the most notable contribution to the teaching of physics at the college and university levels since the subject was introduced into our educational system. If the *Journal* were his sole contribution (which it is not), Dr. Roller would richly deserve this signal honor.

He attended Culver Military Academy and did his undergraduate work at the University of Oklahoma. He also received the Master's degree at Oklahoma and taught there for thirteen years partly before and partly after his work for the Doctorate at California Institute of Technology, which he received in 1929. Subsequently he was a research associate at Columbia and an associate professor at Hunter College. During the first world war he was a pilot and during the recent war he was Chief Technical Aide of the National Defense Research Committee.

Former recipients of the Oersted Medal, which has been awarded every year since 1936, include W. S. Franklin of Lehigh, M.I.T., and Rollings; R. A. Millikan of Columbia, Chicago and Caltech; Henry Crew of Northwestern, and G. W. Stewart of Iowa. Last year's award was to R. L. Edwards of Miami University.

The formal award was made at the January 31 session of the annual meeting of the American Association of Physics Teachers, which occurred at Columbia University. In his address of acceptance Dr. Roller discussed one of his chief professional interests, physical terminology, another field in which he has made notable contributions, both to the teaching of physics and to the science itself.

Chicago I.R.E. Conference

The second Chicago Conference of the Institute of Radio Engineers will be held on Saturday, April 19, at Northwestern Technological Institute. It will feature an all-day series of technical sessions and discussions on the practical side of electronic engineering, with emphasis on applied electronics.

The Bulletin of Mathematical Biophysics

Following is the table of contents of the March 1947 issue of *The Bulletin of Mathematical Biophysics:*

Suggestions for a Mathematical Biophysics of Some Psychoses— N. RASHEVSKY
A Problem in Mathematical Biophysics of Interaction of Two or More Individuals Which May Be of Interest in Mathematical Sociology— N. RASHEVSKY

Mathematic Theory of Motivation Interactions of Two Individuals: I.—ANATOL RAPOPORT
The Mechanism of the Middle Ear: I. The Two Piston Problem—MARTINUS H. M. ESSER

The University of Chicago Press, Chicago, Illinois, Volume 9, Number 1.

New Physics Laboratory at Carnegie Tech

The Buhl Foundation of Pittsburgh has made a grant of $300,000 to Carnegie Institute of Technology for the partial support of a plan to build a 200-million-volt synchrocyclotron and nuclear physics laboratory. A condition of the grant provides that at least $250,000 shall be subscribed by others for the same purpose. Dr. Charles F. Lewis, Director of The Buhl Foundation, said of the grant, "It is confidently expected that this program will notably strengthen Pittsburgh's position as one of the nation's outstanding centers in scientific research."

Institute of Navigation

The Institute of Navigation held its eastern regional meeting on February 13 and 14 in New York City. The Institute was founded during the war by members of the Armed Services and by civilians as a non-profit scientific and technical society devoted to the modern science of navigation in the air and on the sea. The membership is composed chiefly of astronomers, mathematicians, navigators, aviators, physicists, and engineers. The president of the Institute is Commander Gordon A. Atwater, Director of the Hayden Planetarium, New York City.

Frontiers in Chemistry Lectures

The sixth annual series of Frontiers in Chemistry lectures at Western Reserve University, Cleveland, Ohio, will occur in February, March, and April. Among the twelve scientists to appear in the series are Dr. Glenn T. Seaborg, Dr. Harold C. Urey, and Dr. K. C. D. Hickman. The lectures will be divided into two sections. The first will deal with recent advances in physical and inorganic chemistry, and the second with modern theories of organic chemistry. The course is designed chiefly for graduate chemists and physicists.

Physics Research at Northwestern

In January it was announced that Northwestern University would begin immediately a $500,000 three-year program of fundamental research in physics that is expected to lead to new and improved communication devices. Financed by the Navy, the program will be directed by Professors Walter S. Huxford and Robert J. Cashman of the Department of Physics. It is an extension of wartime research in which they developed a new invisible-ray telephone and many new types of photoelectric cells used in the phone and in various Army and Navy secret weapons.

Hugh L. Dryden Elected to International Committee

Hugh L. Dryden, associate director of the National Bureau of Standards, was elected a U. S. representative to the International Committee at the Sixth International Congress for Applied Mechanics held at the Sorbonne, Paris, September 1946. The Congress brought together for the first time since the war those scientists from each major country interested in theoretical and experimental work on the elastic and plastic properties of materials and structures, fluid mechanics, vibration, sound, friction and lubrication, thermodynamics, combustion, and heat transfer. The International Committee, consisting of outstanding scientists from member nations in the field of applied mechanics, is the managing body of the Congress, which is concerned with the international cooperation, advancement and standardization of the sciences of applied mechanics.

General Electric Fellowships at Case School

Case School of Applied Science will offer fifty fellowships to high school teachers of physics for a six-weeks program of study during the summer of 1947. Recognizing the fact that industrial research and progress stem largely from a knowledge of physics, The General Electric Company has provided these fellowships for high school and preparatory school teachers of physics. The program is designed to acquaint teachers with recent scientific developments. The fellowships include all tuition fees, room and board, and travel expenses. High school and preparatory school teachers of physics from the following states are eligible to apply: Ohio, Michigan, Western Pennsylvania, West Virginia, Kentucky, Indiana, Illinois, Wisconsin, and Maryland.

Research in Mineral Flotation at MIT

Armour and Company has established a fund of $12,000 for a graduate research program in the fundamentals of mineral flotation at the Massachusetts Institute of Technology. This program, which provides for grants-in-aid for several assistantships and fellowships, will concentrate on the operation of cationic collectors, particularly the organic compounds known as amines and amine salts.

Harvey L. Curtis Retires from Bureau of Standards

Dr. Harvey L. Curtis, physicist at the National Bureau of Standards since 1907, has retired. His major scientific achievement has been in the field of absolute electrical measurements. He has written the standard textbook on the subject, and his conclusions will form the basis for United States proposals in establishing a fixed relationship between the absolute and international electrical measurement units at the next International Electrical Congress. During World War II he assumed responsibility for interior ballistics research at the Bureau.

Journal of Mathematics and Physics

The Journal of Mathematics and Physics is published by the Massachusetts Institute of Technology in annual volumes of four numbers. Papers which appear in this journal deal with mathematical problems from the fields of engineering and applied physics and with mathematical methods of interest for the applications.

Individual members of the American Institute of Physics may subscribe to the Journal at the special rate of $3 per year. The regular subscription price is $4 per year. Subscription orders and other correspondence may be sent to the Journal of Mathematics and Physics, Massachusetts Institute of Technology, Boston 39, Massachusetts.

Reinforced Concrete Research at Bureau of Standards

The American Iron and Steel Institute is supporting a research program on reinforced concrete now under way at the National Bureau of Standards. The prime objectives are improved design of concrete reinforcing bars and engineering data that will enable engineers and builders to make more effective use of reinforced concrete.

Awards

Two members of the staff of the Naval Research Laboratory recently received the Distinguished Civilian Service Award from the Secretary of the Navy for their contributions to the war effort: George R. Irwin, director of the ballistics section, and Wayne C. Hall, head of the electrical division.

The War Department has awarded the Bronze Star Medal to Harold O. Wyckoff, associate physicist in the X-Ray Section, National Bureau of Standards. Dr. Wyckoff served in the European Theater as assistant chief of the Operational Research Section of the Ninth Air Force.

Radio Engineering Meeting

On May 3 in Cambridge, Massachusetts, there will be an all-day New England Radio Engineering Meeting under the sponsorship of the North Atlantic Region of the Institute of Radio Engineers. All persons interested in radio and electronic engineering are cordially invited to attend. There will be six technical sessions, none held concurrently, exhibits by the leading manufacturers in New England, a luncheon and a banquet. The entire program will be held at the Continental Hotel in Cambridge. A complete program announcement will be made later.

German Physical Society

A conference of German physicists was held October 4–6, 1946, at Göttingen, Germany, in the British Zone of Occupation. About three hundred physicists were present. A German Physical Society was organized for the British Zone. Following are the titles of papers presented: "Theory of the diffraction of electro-magnetic waves on a circular disk," "Measurements on the slowing-down of neutrons," "On neutron processes in beryllium, aluminum and lithium," "Experiments on photographing by means of neutrons," "Changes of sensitivity on light counter tubes," "On a method for the determination of energy and energy distribution of ionizing particles," "On the age of the world," "On the isotope displacement effect in the *E I*-Spectrum," "Experimental detection of the von Schmidt headwave in optics," "Collision discharge in highest pressure mercury lamps," "The accommodation time of the electron temperature in a stationary electric discharge," "Determination of the altitude of the sodium layer shining in the night sky," "Oxide layers on metals," "The optical and electrical qualities of synthetic Greenockite," "Density of sublimed salt layers," "Thermal dissociation in the radiation black body cavity," "Deformation of electron clouds by the collision of gas molecules," "Intuitive models for the theory of super-conductivity," "Superconductivity and the periodic system of elements," "Electron theory of superconductivity," "Sublimation, condensation, saturation pressure and critical point in a model experiment," "Does the lattice constant change for very small particles?" "Optical analyses on electrolytic solutions. Measurements on absorption coefficients," "Thermal effects of gliding friction," "Equation of state of water at high densities," "Exact viscosity measurements up to 2000 atm." "Hydrogen bonding, resonance and the formation of molecular chains," "Remarks on the statistical theory of turbulence.".

Dr. Max von Laue was elected Chairman of the Society. The question of journals was discussed but no action was taken.

The following note at the end of the program is significant. "This program may at the same time be regarded as a ticket. . . . Ration cards, including those for potatoes, are necessary."

Necrology

George A. Scott, assistant professor of physics at the University of Pittsburgh, passed away suddenly following a heart attack in January.

PROCEEDINGS OF THE ELECTRON MICROSCOPE SOCIETY OF AMERICA

THE annual meeting of the Electron Microscope Society of America was held at the Mellon Institute in Pittsburgh, Pennsylvania, December 5–7.

Titles and abstracts of the papers presented are given below:

1. Trends in X-Ray Diffraction Work. DAVID HARKER, *General Electric Company, Schenectady, New York.*

2. Trends in the Use of the Electron Microscope in the Study of Fine Structure. JAMES HILLIER, *Radio Corporation of America, Princeton, New Jersey.*

3. The Application of Electron Diffraction Methods in the Study of Fine Structure. ROBERT HEIDENREICH, *Bell Telephone Laboratories, Murray Hill, New Jersey.*

4. First-Order Theory of the Three-Electrode Electron Gun with Plane Electrodes. S. G. ELLIS, *University of Toronto, Canada.*—On the simplifying assumption of linear

potential variations within the electron gun it is possible to deduce the position of the image of the cathode, the magnification and the angular aperture of the beam external to the gun. The results are compared with those of Johannson. The area of the specimen illuminated in the electron microscope is discussed. It is shown that in general an electron gun can be operated either with or without the production of a cross-over.

5. Some Observations on the Shadow Cast Formvar Replica Technique. BEATRICE M. DEACON, S. G. ELLIS, AND W. G. CROSS, *University of Toronto, Canada.*—Formvar replicas of polished glass surfaces containing sleeks were examined in the electron microscope both with and without shadow casting. In another experiment several replicas from the same region of a glass surface were examined. The nature of the replicas and the limitations of the method are discussed.

6. Electron Microscopy of Colloid Systems. JOHN TURKEVICH, *Princeton University* AND JAMES HILLIER, *Radio Corporation of America, Princeton, New Jersey.*—Typical colloidal systems such as gold, silver, platinum, alumina, ferric oxide, tungsten oxide, vanadium pentoxide, cadmium sulfide, arsenic sulfide, etc., were examined under high resolution with the electron microscope. The form of the colloidal particle and its size were determined as a function of the variables used in the preparation. A method will be described for obtaining gold particles of very uniform size and suitable for calibration standards. The behavior of particles of alumina on steam treatment will be illustrated with electron microphotographs.

7. Electron Microscope Examination of the Microphysical Properties of the Polymer Cuprene. JOHN H. L. WATSON, *Shawinigan Chemicals Limited, Shawinigan Falls, Quebec.*—The microphysical structure of cuprene is described from electron micrographs and suggestions are made from them concerning the mechanism of the formation and catalysis of this material. Copper is detected in the electron diffraction pattern. Cuprene samples prepared by polymerization of acetylene in the presence of finely divided cuprous oxide are shown as hollow fibers characterized by both longitudinal and transverse structure and a very thin skin. The striking appearance of this type of cuprene serves to identify it in clogging deposits taken from acetylene lines. This is illustrated by a deposit taken from a reactor used in the process of hydrogenation of acetylene to ethylene. "Cuprene" specimens formed by alpha-ray bombardment of acetylene gas are shown as round particles joined by short necks about 500 to 1000A in length. An oxidized sample has round particles of mean diameter 4900A and unoxidized sample of mean diameter 3800A. The alpha-ray cuprene is quite unlike the catalyzed solid material in appearance and in addition possesses characteristics of a very viscous liquid in the electron micrographs.

8. An Effect of Electron Bombardment upon Carbon Black. JOHN H. L. WATSON, *Shawinigan Chemicals Limited, Shawinigan Falls, Quebec.*—A significant change is reported in mean particle size and shape characteristics of carbon black due to specimen contamination while under examination in electron microscopes. The effect is described for a number of well-known commercial blacks and examples are given in micrograph, graphical and tabular form to illustrate expected variations in mean particle size with continued bombardment. At normal focusing intensities, the particle size usually will have changed more than 5 percent in 30, or sometimes in as little as 15 seconds. The change is detected with other materials but is more pronounced with carbon black. Chromium shadow cast specimens seem to change to a less degree than uncoated samples. The contamination is explained as arising from the well-known polymerization and condensation processes which occur when organic vapors and gases are bombarded by charged particles. Suggestions are made for minimizing the effect.

9. The Electron Microscope Examination of Greases. S. G. ELLIS, *University of Toronto, Canada.*—A method is described for examining the soap component of lubricating greases with the electron microscope. The soap component is mounted on Formvar films from a dispersion in ether. The specimen is shadow cast by the method of Williams and Wyckoff. The deduction of the shape of the soap particles is discussed.

10. Artifacts Produced by Poor Resolution. L. H. WILLISFORD, *Goodyear Tire and Rubber Company, Akron, Ohio.*—A micrograph of round objects may show the following two opposite conditions: (1) the individual objects of a group will have a tie or rod connection with each adjacent individual of that group and (2) isolated individual objects will have smooth profiles with no evidence of any portion of a tie or rod. This condition of rod connection is caused by imperfect resolution. A simple set-up has been devised for casting shadows which simulate continuous changes from good to poor resolution. When two disks under conditions of poor resolution approach each other, the space between them remains clear until the distance is just less than the limit of resolution, at which distance a misty connection appears. With closer and closer approach, the connection darkens; and before the disks are in contact the connection has the appearance of reality. When slightly overlapped, the disks have a pronounced dumbbell effect. This artifact rod has been confirmed by destroying the resolution of a standard micro-tessar lens; in fact, the "rod" effect is quite universal, and an audience participation demonstration will be given which will duplicate the clues of poor resolution to be looked for in regular and stereo micrographs of round objects.

Some structural patterns in biological systems. FRANCIS O. SCHMITT, *Massachusetts Institute of Technology, Cambridge, Massachusetts.*

11. Remarks on the Borderline of Physics, Chemistry, and Biology. L. MARTON.—A dual conception of life phenomena is proposed in a manner somewhat similar to the

dual conception of wave mechanics. The probability of "creation of order from order" depends on the size of the elementary unit of a chemical compound and on the *non-periodic* complexity of its components. "Life" is therefore not restricted to the group of so called "living organisms," the probability function has a finite value for the simplest chemical compounds, although its value may be immeasurably small. For large chemical compounds, which are considered often on the border line between chemistry and biology, it depends on the experiment whether the "chemical" or the "life" character will be predominant. These considerations necessitate also a critical survey of the molecular concept. A more statistical definition of the molecule is attempted and experiments are proposed to prove the conclusions of the paper.

12. Applications of the Phase Microscope in Electron Microscopy. OSCAR W. RICHARDS, *American Optical Company, Buffalo, New York.*—The Spencer Phase Microscope controls light passing through it so that invisible phase differences arising from optical path differences in the specimen are converted into visible amplitude or intensity differences. In phase microscopy the contrast in the image may be increased, decreased or reversed, and either increased or decreased. The instrument and its use will be described. The Phase Microscope, within its limits of resolution, is useful for the examination of transparent specimens (e.g., replicas). The relation of phase and electron microscopy will be discussed.

13. Preparation of Tissue for High Speed Sectioning. MARY C. SCHUSTER AND CLIFFERD E. GRAY, *Interchemical Corporation, New York, New York.*—The standard techniques of tissue preparation for light microscopy produce distortions that become apparent with the increased resolution of the electron microscope. An adaptation of standard technique is made in the following manner: the tissue is washed free of soluble proteins using isotonic saline solution; fixation is started at very great dilution, and the concentration of fixative is increased slowly to the desired level; when fixation is complete, dehydration and embedding are performed with similar care. Preparation of various tissues with various reagents is discussed and illustrated. It is believed that the procedures described will add to the effectiveness of the joint techniques of high speed sectioning and electron microscopy.

14. Electron Microscope Studies on the Structure of Chlorophyll "Crystals," "Crystalline Alpha Carotene," "Crystalline Beta Carotene" and "Crystalline Vitamin A." EDITH A. ROBERTS, *Vassar College, Poughkeepsie, New York.*—Electron microscope studies of the above show that they are composed of structural units less than 100 ängströms, some of units close to 10 ängströms. These units appear to be protoplasmic entities comparable to those present in plastids rather than "crystals."

15. Further Electron Microscope Studies of the Structure of the Starch Grain. MILDRED D. SOUTHWICK, *Vassar College, Poughkeepsie, New York.*—Electron microscope studies of the structural organization of starch grains, either fresh or commercially prepared from the seeds, roots, stems, or leaves from different genera of plants belonging to the *Bryophyta*, *Pteridophyta*, and *Spermatophyta* indicate the same essential morphology of all starch grains. All show the presence of structural units, comparable to those in the chloroplast—the larger units, plastidules, and the smaller units, plastid granules, as well as the units of a still smaller size which would approach the smallest functional protoplasmic units known.

16. The Mounting of Bacteria for Electron Microscope Examination. JAMES HILLIER AND R. F. BAKER, *Radio Corporation of America, Princeton, New Jersey.*—In the case of some bacteria grown on solid media it is possible to remove a young culture from the medium intact. In other cases a modification of the light microscopists impression technique is found to be very satisfactory.

17. A Study, with the High Voltage Electron Microscope, of the Endospore and the Life Cycle of Bacillus Mycoides. GEORGE KNAYSI, *Cornell University, Ithaca, New York* AND R. F. BAKER AND JAMES HILLIER, *Radio Corporation of America, Princeton, New Jersey.*—A study of strain C_2 of *bacillus mycoides* at 150 kv shows that the endospores obtained from old agar-slant cultures present considerable differences in appearance. Most common are those which are uniformly opaque, those which show a black outline and a shrunken content, and those with transparent lateral areas and thick folds. The exine is thick and surrounded by a thin, elastic pellicle. The intine can sometimes be seen. Germination is initiated by an increased transparency to the electrons and by lateral bulging. This is followed by cracking of the exine, the two halves of which usually remain attached but occasionally are totally severed. In ordinary media, the germ cell and subsequent generations are semi-transparent but show no differentiation in their protoplasm until the fatty inclusions which usually appear before sporulation are formed. We were unable to observe these granules at 50 kv. The forespore appears homogeneous. The mature spore often shows a dark outline and a slightly shrunken protoplasm within the mother cell. High voltage is of distinct advantage in the study of this problem.

18. Demonstration, with the Electron Microscope, of Nucleus-like Bodies in Cells of *Bacillus Mycoides* Grown in Nitrogen-Free Media. GEORGE KNAYSI, *Cornell University, Ithaca, New York* AND R. F. BAKER, *Radio Corporation of America, Princeton, New Jersey.*—The endospore of *bacillus mycoides* contains a relatively considerable quantity of ribonucleic acid which is an excellent source of nitrogen but a very poor source of energy. In ordinary nutrient media, this material is also readily formed by the vegetative cell and is diffuse throughout the protoplasm in an apparently combined form. It is the reason why such cells stain homogeneously and are opaque to electrons. When the endospore germinates in a medium without a nitrogen source, the ribonucleic acid is used up and the subsequent generations of vegetative cells become poorly

stainable and transparent to electrons even at 30 kv. In such cells one observes one to several opaque bodies which appear to divide and which are finally enclosed in the forespore; this behavior indicates their nuclear nature. There is also a variable number of smaller bodies of unknown significance. The best results were obtained with a medium consisting of 0.2 g of glucose+0.2 g of Na acetate+100 ml of distilled water.

19. Observation on Actin and Myosin Extracted from Muscle. M. A. JAKUS AND C. E. HALL, *Massachusetts Institute of Technology Cambridge, Massachusetts.*—Actin has been extracted from striated muscle according to the method of Straub. The addition of neutral salts or hydrogen ions to an aqueous solution of actin brings about a reversible transformation of the globular protein into a fibrous form. Electron micrographs of actin at different stages of linear aggregation will be shown. A water-soluble muscle component designated as "myosin" by Szent-Györgyi has also been prepared and examined. Micrographs of this protein will be presented and compared with those of myosin extracted in alkaline salt solution after the method of Greenstein and Edsall.

20. Size Distribution of Tobacco Mosaic in the Early Stages of Infection. GERALD OSTER, *The Rockefeller Institute for Medical Research, Princeton, New Jersey.*—A method is described whereby the contents of the hair cells from leaves of Turkish tobacco plants diseased with tobacco mosaic virus may be examined by means of the electron microscope. It was found that 68 percent of the rod-like particles present in the hair cells of plants infected for 25 days are about 280 mu in length. The contents of hair cells infected with the virus were also examined less than one day after innoculation, and particles less than 280 mu in length were found to be present. The size distribution of virus preparations subjected to sonic treatment was determined. The virus activity of the sample is proportional to the number of particles 280 mu in length that are present.

21. Studies on the Newcastle Disease Virus (California Strain). A. R. TAYLOR, *Duke University School of Medicine, Durham, North Carolina.*—The infectious agent responsible for Newcastle disease of fowls has been concentrated and purified by ultracentrifugation. Studies of the concentrates have been made by means of electron micrography, analytical ultracentrifugation, and chemical analysis. The virus is a sperm-shaped particle with a head of about 70-mu width and 180-mu length and a thin tail of about 500-mu length. Well-defined internal structure was observed in the head-piece. The virus consists of protein and lipid in association with a small amount of mucleic acid. The results of elementary and component analyses will be given in detail.

22. An Electron Microscope Study of the Structures of Some Virus Protein Crystals. R. W. G. WYCKOFF, *National Insitute of Health, Bethesda, Maryland.*—This is a discussion, illustrated with electron micrographs, of the kinds of regularity of particle arrangement obtained when suspensions of several crystallizable macro molecules are desiccated in the presence and in the absence of salts. These kinds of order are compared with that observed by electron microscopy in preformed crystals of these substances.

23. Immunochemical Aspects of Sonic Treated Tobacco Mosaic Virus. SAUL MALKIEL, *The Rockefeller Institute for Medical Research, Princeton, New Jersey.*—In preparing tobacco mosaic virus from the juice of infected plants, Sigurgeirsson and Stanley found small non-infectious particles about $\frac{1}{3}$ of the usual length of the tobacco mosaic virus particles in the supernatant liquids after centrifugation of the normal virus particles. Preparations of this small particle were compared quantitatively with the 280×15-mu sized rod by means of the precipitin reaction. More antibody was precipitated by the rod of normal size. A solution of freshly prepared tobacco mosaic virus was subjected to sonic vibrations in order to yield small particles. By fractional centrifugation, the normal sized tobacco mosaic virus particles were removed, leaving a supernatant liquid containing a preponderance of smaller particles as checked by distribution measurements of electron micrographs. In order to investigate and compare more fully the immunochemical behavior of these particles with normal tobacco mosaic virus, the stoichiometric relationship of antigen to antibody in specific precipitates was determined by means of the quantitative precipitin reaction. Both heterlogous and homologous antisera were used for this investigation. These findings and the possible theoretical considerations are presented.

24. Specimen Preparation for Electron Micrographs and Diffraction Patterns. LELAND L. ANTES, *University of Texas, Austin, Texas.*—Several simple and effective methods of dispersing fine powders which have a tendency to agglomerate when in suspension are outlined. As applied to such materials as carbon black, metallic oxide pigments and catalysts, these methods may be roughly classified into dry smear and surface film techniques. The results of these methods are compared with others which are generally used. Methods of preparing water-soluble salts for diffraction patterns are discussed, and the advantages of electron diffraction methods in determining crystal structure are pointed out. A means of directly comparing the intensities of diffraction pattern spots or rings is suggested.

25. Alterations and Additional Equipment for an R.C.A. Console Electron Microscope. HENRY C. FROULA, *Armour Research Foundation, Chicago, Illinois.*—Alterations and additional equipment were made for an R.C.A. console electron microscope to simplify maintenance and operation and to improve performance. The items involved include: (1) controls for more positive gun-alignment, (2) equipment for testing the vacuum system for leaks, (3) panel control of illumination, (4) calibration of intensity and focus controls, (5) functionally improved control dials, (6) cassette markings for more certain identification of exposures, and (7) simple holder for storage of specimens. The usefulness of these items will be discussed.

26. Spherical Aberration of Compound Magnetic Lenses. L. MARTON AND K. BOL, *Stanford University, Palo Alto, California.*

27. Further Studies on the Magnetic Electron Microscope Objective. J. HILLIER AND E. G. RAMBERG, *Radio Corporation of America, Princeton, New Jersey.*—Fresnel diffraction fringes observed in through-focus series are shown to be a sensitive criterion for the existence of asymmetries in the electron microscope objective. It is shown that sufficiently accurate symmetry in the objective field can be attained by empirical compensation. The method of compensating the objective is described in detail and some of the results in which resolving powers of 10A were obtained are shown. Further experiments with a new high contrast objective are described.

28. Bias Focused Electron Gun. JOHN H. REISNER, *Radio Corporation of America, Camden, New Jersey.*—History of the gun—A qualitative description of the action of the gun; field plots to be given; effect of circuits on the operation; physical parameters affecting spot sizes and intensities; desirable uses of the gun; effect on alignment; effect of vacuum; filament shapes; constructional materials.

29. Photographic Plates for Use in Electron Microscopy and Electron Diffraction. ROBERT G. PICARD AND W. F SWANN, *Radio Corporation of America, Camden, New Jersey.*—A summary of work carried out jointly by Eastman Kodak and R.C.A., to provide a plate especially suited to the requirements of electron microscopy. After many attempts, an emulsion having long scale, medium contrast, fine grain and adequate speed has been developed. Special, practically grainless plates admirably suited for electron diffraction and subsequent microphotometry have also been tested and will be described.

30. Calculated Magnitude of Fresnel Diffraction in Shadow Casting. C. E. HALL, *Massachusetts Institute of Technology, Cambridge, Massachusetts.*—The intensity curve of the diffraction pattern near the edge of a shadow cast by an evaporated beam is calculated for a Maxwellian distribution of velocities in the beam. Effects other than diffraction which may contribute to unsharpness of the edge are neglected. The results indicate that when heights of the order of 100A are to be measured accurately by the shadow-casting technique, the width of the shadow edge may be appreciable in comparison to the total length of the shadow.

31. Electron Microscope Goniometry. A. F. KIRKPATRICK, EVELYN GAGNON, AND T. G. RECHOW, *Stamford Research Laboratories, American Cyanamid Company, Stamford, Connecticut.*—The frequent occurrence of crystals in electron micrographs presents the problem of their identification. The silhouette angles observed on the photographic plate are functions of the true interfacial angles of these crystals. The interfacial angles of a suspected compound, available in the literature, can be used to calculate the angles that would be formed by the orthographic projection of the crystal edges upon the plane of the photographic plate. A comparison of the calculated angles with those measured on the electron micrograph serves to identify the crystals. Thus a measurement of a physical constant can be made with the electron microscope. The calculations can be made by geometrical construction with the use of stereographic projections. Examples of the use of electron microscope crystallography in the identification of crystals will be presented.

32. Preparation and Uses of Silica Replicas in Electron Microscopy. C. H. GEROULD, *The Dow Chemical Company, Midland, Michigan.*—A detailed description of the preparation of silica replicas and substrates and their many and varied uses is presented with photographs and electron micrographs. The question of "up and down" in stereo pictures of silica replicas is definitely settled by adding a metal oxide smoke (MgO) to the polystyrene replica before the silica evaporation. A successful powder dispersing technique consists of dispersing the powder in an ethyl cellulose lacquer and depositing upon a silica substrate. A method of preparing silica replicas of specimens which cannot be subjected to the temperatures and pressures of the ordinary technique is described. It consists of applying a polystyrene lacquer to the specimen surface in place of the conventional molding. Several other techniques are also included.

33. Procedure for Preparing Latex Samples for Electron Micrographs. WALTER E. BROWN, *The B. F. Goodrich Company.*—It is difficult to obtain good electron micrographs of latices consisting of soft particles such as natural and synthetic rubbers because the particles tend to flatten and merge. These particles can be hardened by bromination to give good micrographs. For GR-S and Hycar OR 15 this treatment results in a swelling of about 9 percent of the diameter. There is no other apparent change that might cause difficulty in interpreting the results. The reliability of the method is shown by: (1) comparison with a vulcanized GR-S latex; (2) by combining two latices of different particle sizes and obtaining the size distribution for the mixture; and (3) observing a particle in random orientation. The complete technique for making such samples is discussed. It is especially important that all of the materials used be very clean and this involves the use of freshly distilled water and solvents. Generally, it is necessary to wash the sample after drying.

34. A Review of Some Recent Advances in Electron Microscopy Microtomy. E. FULLAM, *General Electric Research Laboratories, Schenectady, New York.*

35. Round Table Discussion of Cross Sectioning for the Electron Microscope—Invited Speakers and Discussion from the Floor.

36. Round Table Discussion on Particle Size Problems in Electron Microscopy—Invited Speakers and Discussion from the Floor. MARY C. SCHUSTER, *Interchemical Cooperation, New York, New York,* Moderator.

Contributed Original Research

Theory of Radar Reflection from Wires or Thin Metallic Strips*

J. H. VAN VLECK,** F. BLOCH,† AND M. HAMERMESH††
Radio Research Laboratory, Harvard University, Cambridge, Massachusetts
(Received September 3, 1946)

Knowledge of the radar response of wires or thin metallic strips, as a function of their length and thickness, and of the radar frequency is important in the design of reflectors for radar. In view of the difficulty of this theoretical problem and the necessity of making approximations, as well as the dearth of adequate experimental data, two independent procedures for solution are presented. Detailed quantitative results are obtained for the angular dependence of the cross section, and also for the mean cross section, of randomly-oriented wires or, more generally, of metallic strips, which behave electromagnetically like cylindrical wires of a certain "equivalent radius." When expressed in terms of a unit of area equal to the square of the wave-length, these cross sections depend on the dimensions of the wire only through the two ratios

$$\frac{2l}{a}=\frac{\text{length of wire}}{\text{equivalent radius of wire}},\qquad \frac{2l}{\lambda}=\frac{\text{length of wire}}{\text{wave-length}}.$$

The mean cross section is shown to take on maximum values when $4l/\lambda$ is slightly less than an integer ($n=1$, 2, etc.). The shift of these "resonances" from integral values depends on the ratio $2l/a$, becoming greater as $2l/a$ decreases. The value of $\bar{\sigma}/\lambda^2$ at resonance increases slowly with the order n of the resonance; it depends only very slightly on the ratio $2l/a$, increasing as $2l/a$ decreases. For values of $4l/\lambda$ away from resonance, $\bar{\sigma}/\lambda^2$ decreases rapidly, reaching minimum values near $4l/\lambda=3/2$, $5/2$, etc. The value of $\bar{\sigma}/\lambda^2$ at these minima is strongly dependent on $2l/a$, increasing as $2l/a$ decreases. Also as $4l/\lambda$ increases, the heights of the minima increase and approach the height of the resonance peaks. A brief comparison with preliminary experimental results is given.

I. DESCRIPTIVE SURVEY

INTRODUCTION: In the use of radar, an electromagnetic wave is sent out from a transmitter; the wave impinges on a target and some of the energy is scattered back in the direction of the radar. There it is received and presented on a screen. The strength of the return signal (echo) will depend, among other factors, on the scattering properties of the target. These can be described completely, for our purposes, by introducing the concept of "radar cross section" σ defined as 4π times the quotient of power returned per unit solid angle in the direction of the radar to the power density incident upon the target.

The customary targets for radar observation are aircraft, ships, and topographical features. Since these objects have not generally been constructed from the point of view of their use as radar reflectors, one finds that they are rather inefficient in this respect—one can obtain radar responses comparable to those of an aircraft or ship by using properly designed reflectors of much smaller dimensions. These reflectors can perform several functions.

They may be used to present echoes to a radar for purposes of identification of a target, or for marking a geographical location, thus replacing complicated beacons.

For military purposes they can be used to present "false" echoes to a radar operator for purposes of deception or confusion.

Useful types of reflectors for these purposes are flat sheets, spheres, corner reflectors, and metallic wires or strips. Reflectors for use by aircraft require special consideration as regards weight, size, and ease of handling. The most convenient type of reflector in this case is the bundle of strips, known as window, which, when dropped from the aircraft, will produce the required radar signal. Though strips are most convenient for

* The work reported in this paper was done at the Radio Research Laboratory, Harvard University under contract with Division 15 of the National Defense Research Committee.
** Now at Harvard University, Cambridge, Massachusetts.
† Now at Stanford University, Palo Alto, California.
†† Now at New York University, University Heights, New York, New York.

practical use, we shall refer to the reflectors as "wires," and assume that they are circular cylinders. This assumption involves no loss of generality since, as shown in another paper by F. Bloch and M. Hamermesh,[1] a thin antenna of arbitrary cross-sectional shape has the same electrical characteristics as a circular cylinder of the same length and having an equivalent radius a. For a flat strip the equivalent radius is one-fourth the width of the strip.

In designing these reflectors it is of importance to know the radar response of the wire as a function of its length and thickness, and the wave-length used by the radar. There will be an optimum length for producing echoes at a given radar wave-length; the band of wave-lengths to which the wire responds strongly will depend on its thickness. Wires cut for one wave-length may produce undesirable responses at other wave-lengths (effect of "harmonics").

The calculation of the radar response of wires is also of interest from the point of view of general antenna theory. The problem presents most of the pertinent features of the receiving or transmitting antenna; at the same time it does not involve the complication presented by the gap at the center in such instruments. Thus it represents our best opportunity for comparing theoretical predictions with experiment.

The problem of radar reflection from a wire can be formulated as follows: A transmitter emits a linearly polarized wave which impinges upon a wire, the direction of incidence being at an angle θ to the axis of the wire. The wave scattered back along this same direction is picked up by a receiver ordinarily polarized parallel to the transmitter. We wish to calculate the power returned to this receiver as a function of the angle of incidence θ, the direction of polarization, the wave-length, and the length and radius of the wire.

Notation: We shall use the following symbols:

λ = wave-length.

$\beta = 2\pi/\lambda$; $\omega = 2\pi c/\lambda$; c = velocity of light.

$2l$ = length of wire.

a = equivalent radius of wire.

E_0 = amplitude of the electric field of the incident wave.

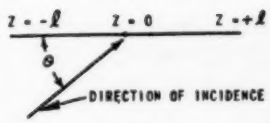

FIG. 1.

φ = angle between the electric field of the incident wave and the plane of Fig. 1.

$q = \beta \cos\theta$.

$I(z)$ = current in the wire at z, the coordinate giving position along the wire (Fig. 1).

log = logarithm to base e.

The cross section σ is defined as:

$$\sigma = 4\pi \frac{\text{Power reflected backwards (per unit solid angle)}}{\text{Power density incident upon the target}}$$

$\bar{\sigma}$ is the "average cross section" which will be observed when the signal is reflected from a bundle of randomly oriented wires. It can be computed from σ by averaging:

$$\bar{\sigma} = (1/4\pi) \int\int \sigma \sin\theta d\theta d\varphi.$$

$\sigma(\theta) = (1/2\pi) \int \sigma d\varphi$ is the average return signal for fixed direction of incidence and random polarization. The average power returned to a rotating dipole antenna from a wire in fixed orientation would be given by $\sigma(\theta)$.

Methods of Solution: The first step in the solution of our problem is to calculate the current induced in the wire. (This is essentially the problem of the receiving antenna.)

A simple method, which has been used in similar problems is that of Siegel and Labus.[2] This method starts from a reasonable assumption concerning the form of the expression for the current, and evaluates the numerical magnitudes in this expression by applying the requirement of conservation of energy (e.m.f. method). Rigoristically speaking, it is not a method for deducing the solution to the antenna problem. A second, more satisfactory procedure, is to try to satisfy the Maxwell equations and to fulfill the boundary conditions at the surface of the wire, using a method of successive approximations. The tangential component of the total electric field must vanish on the surface of the wire (assumed to be a perfect conductor). This

[1] F. Bloch and M. Hamermesh, Report 411–TM125 of the Radio Research Laboratory (NDRC Division 15).

[2] E. Siegel and J. Labus, Hoch: tech. u. Elek: akus. **43**, 166 (1934).

total field consists of the incident field plus the field produced by the induced current in the wire. For sufficiently thin wires the current at the ends may be set equal to zero. The mathematical equivalent of these statements is the integral equation[3]

$$\int_{-l}^{+l} d\xi I(\xi)\frac{e^{-i\beta r}}{r}=\frac{i\omega\cos\varphi E_0 e^{iqz}}{\beta^2\sin\theta}$$

$$+A_1\cos\beta z+A_2\sin\beta z \quad (1)$$

with

$$r=[(z-\xi)^2+a^2]^{\frac{1}{2}}, \quad I(\pm l)=0.$$

These equations assume that the current is located at the center of the wire rather than residing on its surface, but it is well known in antenna theory that the resulting error is not serious (the reason being essentially that any infinitely long cylindrically symmetric charge distribution gives the same exterior potential as though concentrated at the center).

King and Harrison[3] solved the integral Eq. (1) for the receiving antenna by a method of successive approximations due to E. Hallén.[4] In its original form, the Hallén method suffered from the defect that the convergence of the successive approximations becomes poorer as l/λ increases. Even for $l=\lambda$, a reasonably accurate solution would require the use of complicated higher approximations.

This difficulty, however, is avoided by following procedures introduced by Miss Gray,[5] and especially by King and Middleton,[6] who start from the same integral equation but who choose different procedures of successive approximation. The Gray procedure was intended primarily for the transmitting antenna but, as explained more fully in the last part of the appendix, it is more suitable for the receiving antenna. It leads to difficulties when the wire is so very long that it contains a large number of wave-lengths (a case which does not usually arise in practice). The most refined scheme of approximation is that recently published by King and Middleton.

We have obtained solutions of the problem by two methods:

(A) A combination of a judicious guess based on the solution of King and Harrison (with some corrections à la Gray or King and Middleton), and the application of the principle of conservation of energy.

(B) An approximate solution of the integral equation for the receiving antenna. The procedure which we employed is one which we deemed at the time a modification of the Gray method, since it resembled the latter rather more than that of Hallén. After our investigations were completed, however, the paper of King and Middleton was published. It turns out that actually our scheme for approximating the integral equation involves the same kind of attack as that used by King and Middleton in the antenna problem, though the superficial language is rather different. The point is discussed more fully at the end of the appendix. The mathematical details of the approximate solutions by methods (A) and (B) will be described in Sections II and III, respectively.

In both methods (A) and (B) the current along the wire is assumed to be of the form

$$I(z)=C_1\cos qz+C_2\cos\beta z+C_3\sin qz+C_4\sin\beta z, \quad (2)$$

where C_1, C_2, C_3, C_4 are functions of the angles θ, φ and of l, λ, a. We shall refer to the terms in $\sin qz$ and $\sin\beta z$ (or $\cos qz$ and $\cos\beta z$) as the forced and resonant parts, respectively, of the solution, inasmuch as the phase of the impressed field along the wire is qz, and inasmuch as the amplitude C_2 (or C_4) is abnormally large, because of resonance, if $\beta l/\pi$ is a half-integer (or integer). The cosine and sine terms will be characterized as the even and odd members, respectively. In method (A) the values of C_1, C_2, C_3, C_4, are determined by the conservation of energy and a supplemental assumption concerning the form of the solution away from resonance. In (B) one calculates the C_1, C_2, C_3, C_4 in a more dynamical fashion from the integral equation. In (A) it is

[3] R. King and C. Harrison, Proc. I.R.E. **31**, 548 (1943); and **32**, 18 and 35 (1944).
[4] E. Hallén, Nova Acta (Uppsala), Series 4, **11**, 1 (1938).
[5] M. C. Gray, J. App. Phys. **15**, 61 (1944).
[6] R. King and D. Middleton, Quart. App. Math. **3**, 302 (1946). For an interesting critical comparison of the various schemes which have been proposed for approximate solution of the integral equation for the transmitting antenna, see D. Middleton and R. King, J. App. Phys. **17**, 273 (1946). Our approximation is, we believe, comparable with what these authors call "first-order King-Middleton," as we do not essay the refined but rather lengthy calculation of the second order terms included in the articles of Bouwkamp and of King and Middleton.

assumed that

$$\frac{C_1}{C_2}=-\frac{\cos\beta l}{\cos ql};\quad \frac{C_3}{C_4}=-\frac{\sin\beta l}{\sin ql}, \tag{3}$$

so that the boundary conditions $I(\pm l)=0$ are automatically satisfied. In (B) the ratios C_1/C_2, C_3/C_4 have somewhat different values than (3), especially near resonance. At first sight this fact may seem to imply that in (B) the boundary conditions are not satisfied, but this is not really the case, as in satisfying the latter in (B) certain extra terms are included which we have not written down in the expression (2) for $I(z)$. It is consistent to carry these higher order terms only in satisfying the boundary conditions,[7] but not in computing the radiation, since most of the radiation comes from parts of the wire not near the ends, whereas the correction terms are abnormally important at the ends, especially in the interesting resonance region where $\cos\beta l$ or $\sin\beta l$ is nearly zero. In (A) the amplitude of one of the forced terms drops to zero at resonance, since (3) shows that C_1 and C_3 vanish with $\cos\beta l$ and $\sin\beta l$, respectively. Actually, this is not correct, as the forced vibration is unaffected by resonance rather than suppressed by it. In consequence of the fact that (B) uses a more refined current expression than does (A) in satisfying the boundary condition, (B) is able to yield various effects and details which (A) is incapable of describing.

Chu's Theory: A simple and ingeneous, though crude, method for obtaining expressions for the radar response, was used by Chu (unpublished). (We shall not give the details of this method since, as shown in Sec. II, the results can be obtained as a special case of Method A.)

For resonant wires (length a multiple of $\lambda/2$) Chu proceeds as follows: The current is assumed to be a pure sine function vanishing at the ends of the wire. Then the magnitude of the current is determined by applying the law of conservation of energy (as in our method (A), which differs from Chu in the choice of current form). The expression for $\bar{\sigma}$ at resonance is

$$\bar{\sigma}=\frac{3\lambda^2}{16\pi}\frac{4\pi^2 l/\lambda-\frac{3}{2}+3\log(8\pi l\gamma/\lambda)-\log 2}{[\log(8\pi l\gamma/\lambda)]^2}, \tag{4}$$

where γ denotes Euler's constant 1.78. The variation of cross section with angle of incidence, i.e., $\sigma(\theta)$, may be obtained from the diagrams on page 788 of Terman's Handbook. One must, however, take the fourth power of the radial coordinate shown in his plots, as the cross section involves power rather than voltage, and as there is an extra square because on back-scattering the angular factor occurs both in incidence and reflection.

The other case treated by Chu is that of long wires. Here only forced terms are considered (i.e., $C_2=C_4=0$ in Eq. (2)) and he obtains

$$\sigma=\frac{4\pi l^2\sin^2\theta(\sin x/x)^2}{(\pi/2)^2+(\log\{\lambda/\gamma\pi a\sin\theta\})^2}\cos^4\varphi, \tag{5}$$

with the abbreviation $x=(4\pi l/\lambda)\cos\theta$. Averaging over all θ and φ, Chu finds

$$\bar{\sigma}=\tfrac{3}{8}l\lambda\frac{\pi/2-\lambda/8\pi l}{(\pi/2)^2+(\log\{\lambda/\gamma\pi a\})^2}. \tag{5a}$$

Chu's method has the advantage of extreme simplicity, but it suffers from several defects:

(a) It gives no information on the response in the intermediate region between the peaks corresponding to the resonant lengths, and the valleys corresponding more to the case of long wires.

(b) It does not predict any shifts in the resonance maxima from the values $\lambda=4l/m$, where m is an integer. Actually, the experimentally observed maxima are somewhat on the long wave-length side.

(c) At resonance it neglects the effect of the forced oscillation, which is not negligible for broadside response or at the higher maxima (large values of m).

(d) It makes an error in the values of the height of the resonance peaks because the resonance shifts (effect b) alter the damping constant, and hence the amplitude.

(e) The heights of the valleys are furnished by the Chu theory only if one assumes that away

[7] The current can be made to vanish at the end even in the first approximation if one iterates in such a way that at each stage the solution at the end of the wire is subtracted from that at the middle. This is done, for instance, in the papers of Hallén and of King and Middleton. Such a difference in procedure from ours is, however, a rather superficial one. It amounts, so to speak, to merely a different system of book-keeping for the various terms which necessarily appear as the iteration progresses.

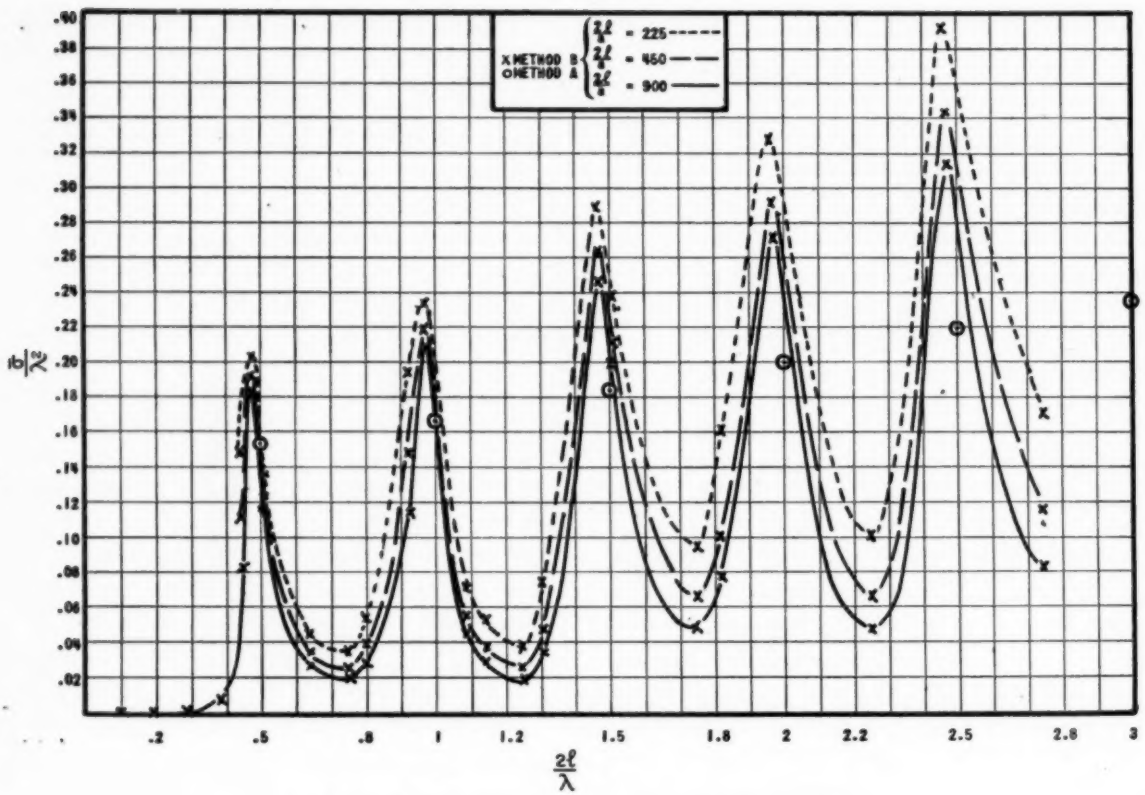

FIG. 2. Radar response of wires: average cross section.

from resonance practically all the response is caused by the forced rather than resonant terms, so that one can use his result (5a) for infinitely long wires. Actually, for wires of practical length the effect of the resonant members cannot be neglected even in the valleys.

Relative Merits of Methods (A) and (B): The results of Chu may be roughly characterized as a zero-order theory, which suffers from the defects mentioned in items (a)–(e) inclusive. Method (A) gives formulas for all wave-lengths, thus removing difficulty (a), but it is open to the objections (b–c–d). It is more than just an interpolation scheme between the various Chu formulas as it does include the effect of the resonant terms away from the maxima, and so is not subject to the drawback (e). Hence (A) usually agrees quite closely with (B) in the valleys, but near the peaks (A) gives results which practically coincide with those given by the Chu resonance formula. Quite irrespective of the additional refinement connected with (b), (c), (d), method (B) has the advantage that it yields formulas that are much more tractable than those supplied by (A), as it gives closed expressions for the cross section averaged over all angles. Hence most of our comparison with experiment will be based on (B) and, because of the labor involved, only a few points will be computed by means of (A).

Results

(1) *Variation of the Averaged Cross Section with Wave-Length:* It is perhaps well first to take a bird's-eye view of the response curves furnished by the theory for the cross section averaged over all angles, i.e., for a random distribution of wires. This is provided by Figs. 2 and 3. The curves are those furnished by method (B). Each curve of Fig. 2 refers to a different value of the ratio $2l/a$ of the wire length to radius. In Fig. 2, the cross section is plotted out to $l/\lambda = 1.25$ (five peaks), while in Fig. 3 the curve is extended to the 20th peak for the special case $2l/a = 900$. The points actually calculated by method (B) are indicated by crosses in Fig. 2, and it is seen that, except for a few selected instances, most of the points

beyond the second or third maximum have been calculated only for the peaks and valleys, i.e., for resonance and antiresonance. No monumental accuracy should be attached to the precise values of the coordinates in the transition region where the curves slope very steeply and cannot be determined precisely without calculating a very large number of points. In the additional region covered by Fig. 3, only the peaks and valleys have been calculated, except that the shape of the curve has been computed in some detail for the 19th peak in order to examine whether there are any important changes in the band width at the higher resonances. It is seen from Fig. 3 that, measured in frequency, the band width increases slowly as one passes to the higher resonances, and is over 3 times as great for the 19th as for the first peak. On the other hand, the percentage change in frequency required to detune from resonance is obviously much smaller at the higher peaks, simply because the frequency is higher. As one would expect, the peaks are sharper, the smaller the radius of the wire in comparison to its length. No attempt has been made to calculate a detailed curve by method (A). Instead, the points calculated with this method are indicated by circles in Figs. 2 and 3. As can be seen from the curves, the two methods agree quite well away from resonance. The circles at $2l/\lambda=\frac{1}{2}$, 1, $1\frac{1}{2}$, $2\cdots$ are the peak maxima for method (A), and have practically the same values as those given by the simple resonance theory of Chu.

It should be noted that the percentage difference between resonance and antiresonance diminishes as the length of the wire, measured in multiples of wave-length, increases. For instance, Fig. 3 shows that the first peak is ten times as high as the first valley, whereas the ninth peak has only three times the height of the ninth valley. For infinitely long wires the difference between the peaks and valleys would disappear entirely.

As we go from one valley to another the height of the valley floor does not increase uniformly, but rather increases in an alternating fashion. The first and second valleys, for instance, are approximately equal in elevation. Similar remarks apply to the third and fourth, which are both considerably higher than the first and second. This result is yielded by both (A) and (B), and is in accord with the experimental data.

(2) *Positions of the Maxima:* Both experimentally and theoretically (method (B)), the resonance maxima come at somewhat longer wave-lengths than in the usual approximate formula $4l/\lambda=m$. The displacements are greater the larger the radius of the wire; for an infinitely thin wire the resonance would be at exactly $4l/\lambda=m$. With finite radii, the expression for the resonance maxima furnished by method (B) is approximately

$$\begin{pmatrix}\cot\beta l\\ -\tan\beta l\end{pmatrix}=\tfrac{1}{4}\pi[2\log(\lambda/\pi a)+\tfrac{1}{2}\log(2\pi l/\lambda)-1.87]^{-1}. \quad (6)$$

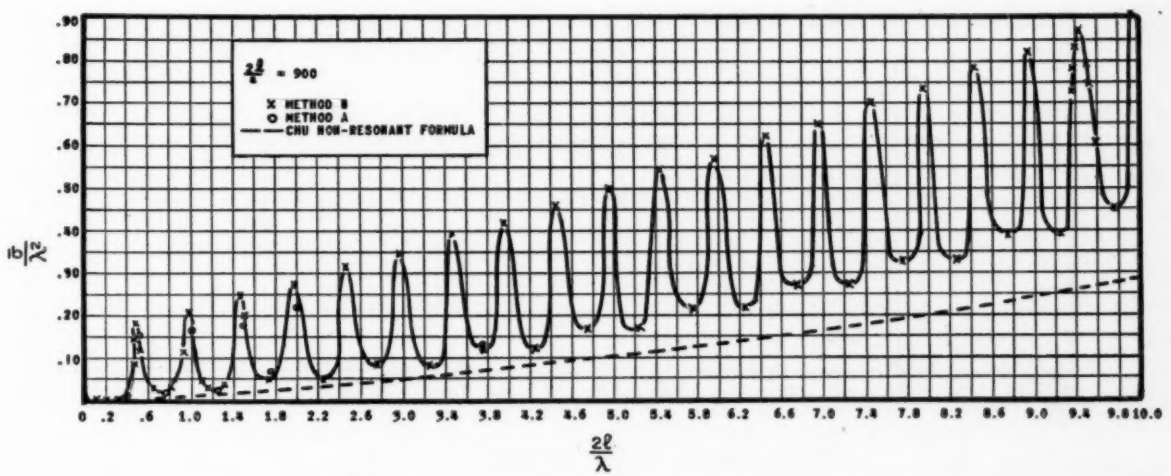

FIG. 3. Response of wires: average cross section.

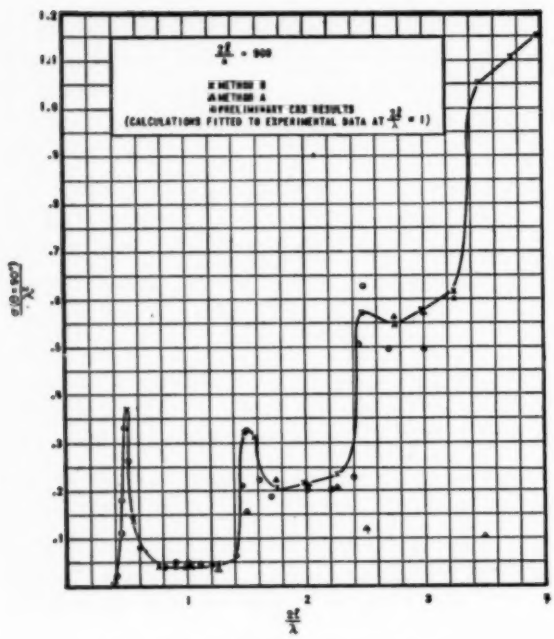

FIG. 4. Broadside response of wires.

(See Eq. (36) of Sec. III, where one will find a more complete discussion of expressions for the resonance maxima, including formulas (36′) and (36″) which are more accurate than (6) under certain conditions.) Here the cotangent applies to the resonances 1, 3, 5, etc., and the tangent to 2, 4, 6···.

The positions of the maxima furnished by method (B) are in quite good accord with experiment. For $2l/a=900$, it predicts that the successive maxima should come at $4l/\lambda=0.95$, 1.94, 2.93$\underline{5}$, 3.93, 4.92$\underline{5}$ whereas the observed values are $4l/\lambda=0.96$, 1.88, 2.94, 3.90, 4.92.

(3) *Influence of Forced Terms at Resonance-Broadside Response:* If we consider only the averaged cross section, the amplitude at resonance is determined almost entirely by the resonant term (C_2 or C_4 in Eq. (2)) and but little harm is done in omitting the "forced" members C_1 and C_3 in calculating the amplitudes of the first few peaks ($m=1, 2, 3$). When however, we do not average over all orientations of the target, but instead consider only the broadside response (at $\theta=90°$), this is no longer true. The theory is particularly simple for the broadside case, as the phase of the incident electric vector is the same for all parts of the wire. The curve furnished by method (B) for the cross section as a function of $2l/\lambda$ for broadside setting of the wire is shown in Fig. 4.[8] It is in quite good agreement with the experimental data indicated by circles. On the other hand, method (A) gives results not in accord with experiment at the odd resonances. (The even resonances have no particularly large broadside scattering.) The reason why the forced vibrations cannot be neglected, as in method (A), for broadside response at resonance, especially at the higher maxima, is the following:

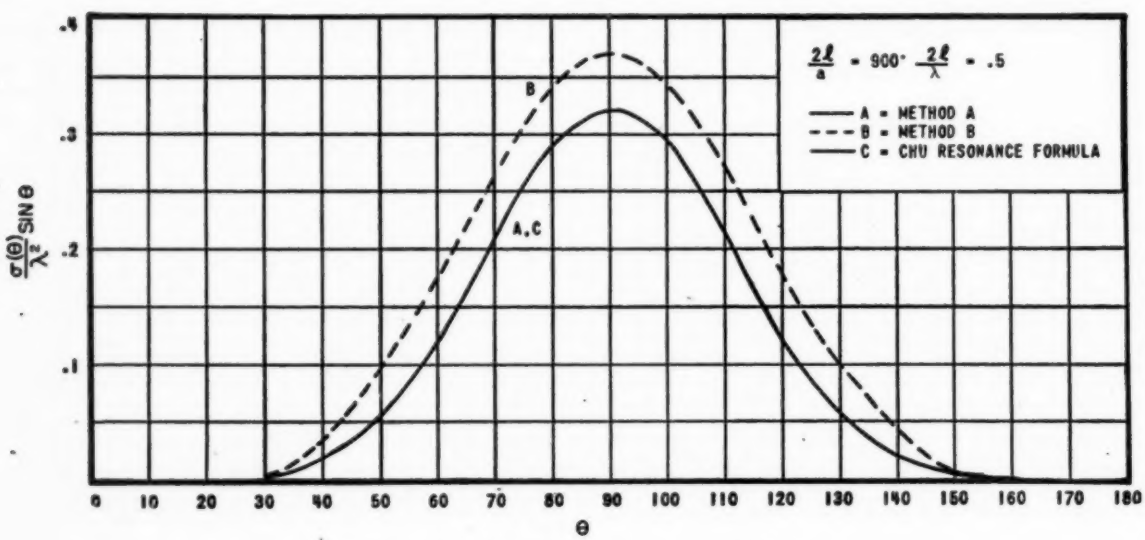

FIG. 5. Angular distribution of response of wire.

[8] The quantity plotted in Figs. 4–8 is $\sigma(\theta)$ which is connected with σ by the relation $\sigma=(8/3)\cos^4\varphi\,\sigma(\theta)$.

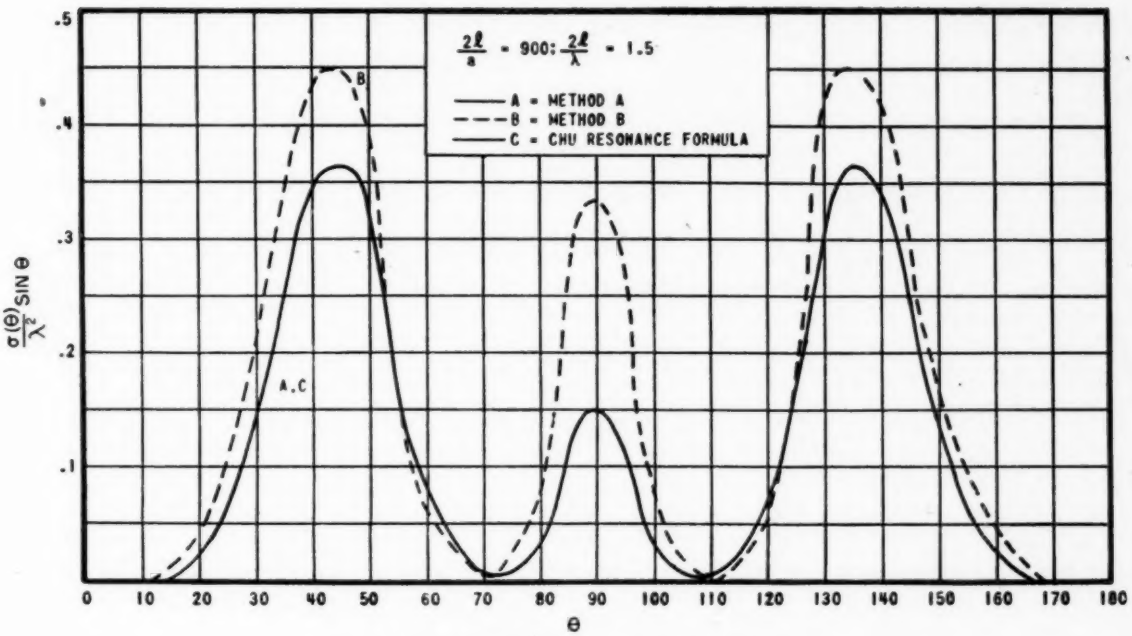

FIG. 6. Angular distribution of response of wire.

When we average over all orientations, the important term at resonance is usually that corresponding to resonant rather than forced oscillation (i.e., of structure $\sin\beta z$ or $\cos\beta z$ rather than $\sin qz$ or $\cos qz$ in Eq. (2)). In the broadside case, however, we are interested in scattering perpendicular to the wire (the equatorial zone). The forced oscillations C_1, C_3 in Eq. (2) give a particularly strong perpendicular scattering, whereas except for the first resonance or two, the major lobes due to the resonant vibrations C_2, C_4 are nearer the poles than the equator. For this reason the forced radiation is abnormally important in the broadside case, and at the higher resonances actually exceeds the resonant, despite the fact that the latter is associated with a far larger current amplitude. As an example we cite some numerical results obtained by method (B) for a wire having $2l/a=900$. Here at the first, third, fifth, seventh resonances, the contribution due to the resonant oscillations represents respectively 95, 54, 24, 11 percent of the total broadside cross section, the remainder being caused by the forced oscillations. It is because method (A) artificially suppresses the forced vibrations at resonance that it actually gives minima rather than maxima in the broadside response curves at resonance.

(4) *Height of the Maxima in the Averaged Cross Section:* The height of the resonance peaks as given by method (B) is higher than that given by method (A) or by the Chu formula. For instance, if $2l/a=900$, the maxima corresponding to $m=1$, 3, 5, 10, 20 are, respectively, 20, 32, 42, 66, 112 percent higher than given by Chu's expression. This difference, which would disappear for infinitely thin wires, is ascribable to two causes. One is the neglect of forced oscillations by (A), or by the Chu expression (our Eq. (4)), at resonance maxima. We have already discussed in paragraph (3) how this affects the results at broadside. For the first two or three maxima, the peaks of the averaged cross section are not affected appreciably by the forced oscillations. However, if, for example, $2l/a=900$, inclusion of the forced oscillations in method (B) makes the first, third, and tenth maxima ($m=1$, 3, 10), respectively, 6, 11, 29 percent greater than if the forced members are neglected (i.e., if C_1 and C_3 are taken equal to zero in Eq. (2)). The other effect which makes the maxima given by (B) higher than those given by (A) or by Chu is the fact that (B) takes into account the displacement of resonance to a slightly longer wave-length than that furnished by the ordinary expression $l/\lambda=m/4$. The theory of Part III shows that the

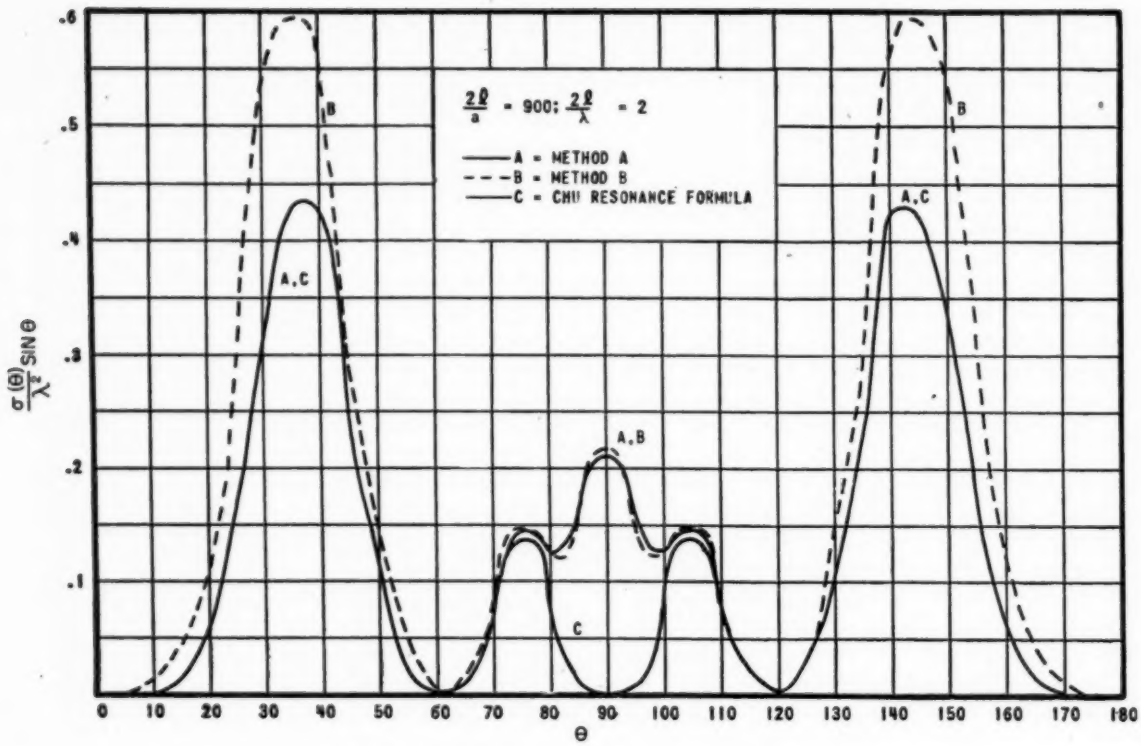
$\frac{2l}{a}$ = 900; $\frac{2l}{\lambda}$ = 2
A = METHOD A
B = METHOD B
C = CHU RESONANCE FORMULA
A,C
B
A,B
C
$\frac{\sigma(\theta)}{\lambda^2}$ SIN θ
θ
0 10 20 30 40 50 60 70 80 90 100 110 120 130 140 150 160 170 180
.1 .2 .3 .4 .5 .6

FIG. 7. Angular distribution of response of wire.

shift in the resonance decreases the damping and so increases the amplitude.[9] It is particularly noteworthy that this displacement effect makes the peak for $m=1$ higher than it would be otherwise, since this particular peak is often used for calibration. (Equation (4) shows that according to Chu the cross section at the first peak is $0.153\lambda^2$, regardless of the value of l/a. With method (B), on the other hand, it depends on the radius of the wire, and has the values of $0.184\lambda^2$, $0.194\lambda^2$, $0.204\lambda^2$ for $2l/a=900$, 450, 225, respectively.)

(5) *Height of the Valleys:* Here methods (A) and (B) agree quite well. The cross section furnished by the Chu non-resonant formula (Eq. (5a)), is indicated by the dotted line in Fig. 3. We see that even the deepest parts of the valleys are considerably higher than the dotted line. This means that even as far removed as possible from resonance, the effects of the resonant terms are not completely negligible. Stated in a different way, a finite wire, even when it is non-resonant, is far from behaving like an infinite wire. It should be noted that the valley floors depend on the radius much more than do the peaks.

(6) *Angular Distribution:* It is interesting to plot $\sigma(\theta)$ for a fixed wave-length. This has been done for the first, third, and fourth resonance maxima in Figs. 5–7. The types of angular variation predicted by methods (A) and (B) are not much different and are in general agreement with experiment. The angular patterns given by method (A) for the first few resonances are almost identical with those obtained by the simple theory of Chu. For higher maxima such as the 2 peak, however, the corrections to the simple theory are important, as shown by Fig. 7, especially at 90°.

As typical of an angular response well removed from resonance, the angular pattern for $2l/\lambda=1.25$ is given in Fig. 8, for which methods (A) and (B) give the same distribution.

(7) *Comparison with Experiment:* Unfortu-

[9] Mathematically, this is expressed in the fact that the "resonance denominators" $\Psi^2+\Xi^2$ appearing in the expressions for G and H in Eq. (35) are smaller in numerical magnitude for $\beta l<(m+\frac{1}{2})\pi$ and $\beta l<m\pi$, respectively, than for $\beta l=(m+\frac{1}{2})\pi$ and $\beta l=m\pi$.

nately, one will not find in the present paper elaborate curves comparing theory with experiment. This is because the existing data are, in our opinion, not yet satisfactory. In the absence of well-established experimental material, obviously more reliance must be placed on theory than would otherwise be the case, and this is one reason why we have developed the theory in detail in the two forms, (A) and (B); it is perhaps reassuring to have two independent theoretical approaches. Two results of the theory, for which significant comparison with experiment can be made at present have already been discussed, *viz.*, (a) shift in the positions of the resonance maxima from the "zero-order" positions $l=\frac{1}{4}m\lambda$; and (b) broadside response. Experiments on either of these features are easier than on the averaged cross section. Obviously (a) does not involve any intensity measurements, while (b) does not involve a variety of angular settings such as are needed in finding the averaged cross section. A more important feature of measurements of the broadside response is that they avoid polarization effects in the suspensions used to support the wires during laboratory measurements. The dielectric properties of the suspension may alter the charge distribution and hence the current in the wire. However, in the broadside case the current is a symmetrical function of the distance from the center of the wire, so that at the center we have $\partial I/\partial z=0$. Furthermore, the equation of continuity gives $\partial I/\partial z=i\omega\rho$, and hence there will be no charge near the center of the wire. Thus the polarization difficulties will not occur if the wire is supported at its center.

Limitations of the Theory: It is essential that the reader should appreciate that the antenna problem is so difficult that even these somewhat involved calculations apply only under the assumption that the wire is long compared to its radius. The calculations involve an expansion in descending powers of $\Omega=2\log(2l/a)$, where l is the half-length of the wire, and a is the radius of the equivalent wire. The fact that the expansion is in terms of reciprocal powers of $\log 2l/a$, rather than of $2l/a$, itself shows that under no conditions can the accuracy be monumental. For values of $2l/a$ of the order 10^3 it is doubtless quite good (say within a few percent) and for $2l/a\sim 100$ it is probably adequate, but for very "fat" wires of the order $2l/a=10$ the calculations can at most be relied on only for orders of magnitude. Even when l/a is very large, the theory may involve considerable percentage of error in its expression for the amplitude of the resonant vibrations, if the wire is so very long as to contain

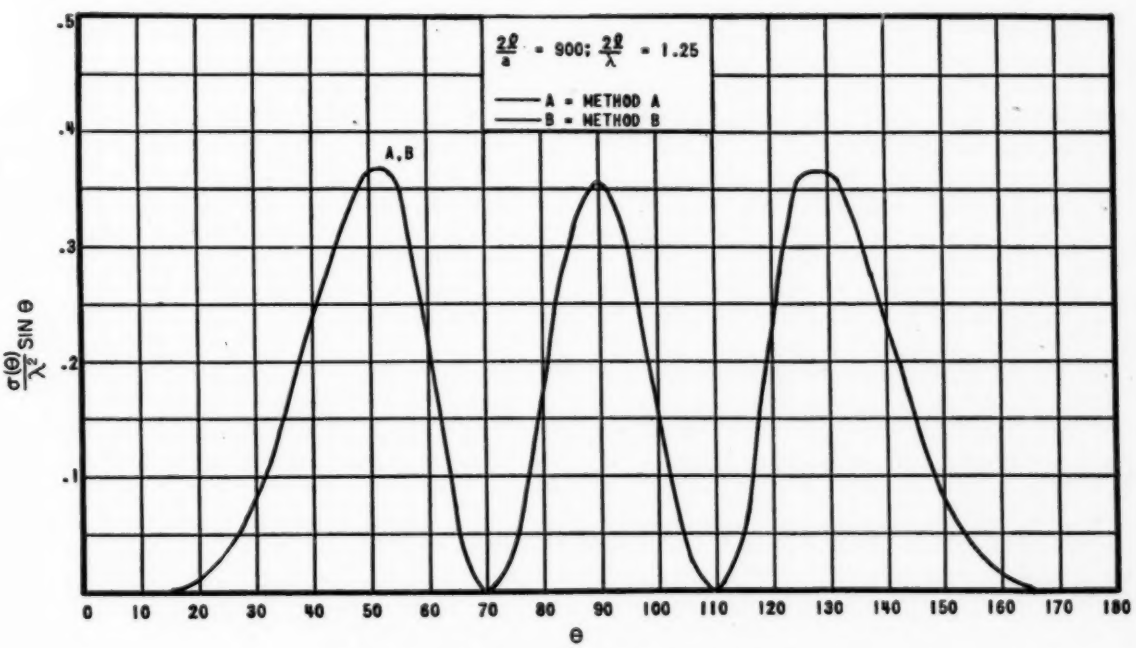

FIG. 8. Angular distribution of response of wire.

a large number of wave-lengths (see discussion in latter part of appendix). However, this difficulty is not serious, because for such exceedingly long wires the resonant vibrations are of minor importance compared to the forced ones.

II. DETAILS OF METHOD A

The projection of the incident field on the antenna is $E_0 \sin\theta \cos\varphi e^{iqz}$. (We omit everywhere the time factor $e^{-i\omega t}$.) We choose our current in a form suggested by the solution of King and Harrison[3]:

$$I(z)=-\frac{i\omega E_0}{\beta^2 \sin\theta}\frac{\cos\varphi}{\Omega}\left[\frac{\cos qz\cos\beta l-\cos\beta z\cos ql}{\cos\beta l+(i/\Omega)f(l,q)}+i\frac{\sin qz\sin\beta l-\sin\beta z\sin ql}{\sin\beta l+(i/\Omega)g(l,q)}\right]; \tag{7}$$

$$\Omega=2[\log(2/\gamma\beta a)+\mathrm{Ci}2\beta l];\quad \gamma=1.78;\quad \mathrm{Cix}=-\int_x^\infty\frac{\cos t}{t}dt. \tag{8}$$

In Eq. (7) we shall refer to the first term in brackets as the even part and to the second as the odd part. To determine the functions f and g we use the procedure of calculating the work done on the antenna, and equate to the total energy flux radiated from the antenna; i.e., we set

$$\mathrm{Re}\int_{-l}^{+l}\mathbf{E}\cdot\mathbf{I}^*dz=\frac{c}{4\pi}\mathrm{Re}\int(\mathbf{E}\times\mathbf{H}^*)R^2d\omega=\frac{c}{4\pi}\int|\mathbf{E}|^2R^2d\omega, \tag{9}$$

where $\mathbf{E}$, $\mathbf{H}$ are the fields produced by the induced currents in the antenna, F^* is the conjugate complex of F, and Re denotes the real part. The first integral is taken over the antenna, while the second is taken over the surface of a large sphere of radius R.

On the antenna we have

$$\int_{-l}^{l}\mathbf{E}\cdot\mathbf{I}^*dz=-\frac{i\omega E_0^2\cos^2\varphi}{\beta^2\Omega}\left[\frac{\cos\beta l\{l+h(2q)\}-\cos ql\{h(q+\beta)+h(q-\beta)\}}{\cos\beta l-(i/\Omega)f(l,q)}\right.$$
$$\left.+\frac{\sin\beta l\{l-h(2q)\}-\sin ql\{h(q-\beta)-h(q+\beta)\}}{\sin\beta l-(i/\Omega)g(l,\beta)}\right] \tag{10}$$

with the abbreviation $h(x)=\sin xl/x$. Again we shall refer to the first term as the even part, and to the second as the odd part.

The field produced by the current I at $\measuredangle\theta'$ and distance R is

$$E=\frac{i\beta}{c}\frac{\sin\theta'}{R}\int_{-l}^{+l}I(z)e^{i\beta z\cos\theta'}dz. \tag{11}$$

The flux density is

$$\frac{c}{4\pi}|E|^2=\frac{c}{4\pi}\frac{\beta^2}{c^2}\frac{\sin^2\theta'}{R^2}\int_{-l}^{+l}\int_{-l}^{+l}I(z)I^*(z')e^{i\beta(z-z')\cos\theta'}dzdz'. \tag{12}$$

The total flux is

$$\frac{c}{4\pi}\int_0^{2\pi}d\varphi'\int_0^{\pi}\sin\theta'd\theta'|\mathbf{E}|^2R^2=\frac{1}{\omega}\left\{\int_{-l}^{+l}\int I^*(z')\frac{\sin\beta(z-z')}{z-z'}\left[\left(\beta^2+\frac{d^2}{dz^2}\right)I(z)\right]dzdz'\right.$$
$$\left.-\int_{-l}^{+l}dz'I^*(z')\left(\frac{dI(z)}{dz}\frac{\sin\beta(z-z')}{z-z'}\Bigg|_{z=-l}^{z=+l}\right)\right\}. \tag{13}$$

We have written the current as the sum of an even and an odd function of z. As can be seen from Eq. (13), integrals involving products of even and odd parts of the current vanish; i.e., the total flux consists of two parts, one in which we choose for $I(z)$ only the even part of the current; the other in which we use only the odd part.

We shall satisfy Eq. (9) (which is actually simply a statement of the law of conservation of energy) separately for the odd and even parts. Using only the even part of $I(z)$ from Eq. (7) in Eq. (13), and performing the integrations, we obtain for this part of the total flux the value

$$\frac{1}{\cos^2\beta l+f^2/\Omega^2}\frac{1}{\omega}\frac{\omega^2E_0^2\cos^2\varphi}{\beta^4\sin^2\theta\Omega^2}[\beta\gamma(\beta)\cos^2ql+K\sigma(q)-L\gamma(q)-M\cos^2\beta l], \tag{14}$$

where

$$K=(\beta^2-q^2)\{l+h(2q)\}\cos^2\beta l+2\cos\beta l\cos ql(q\sin ql\cos\beta l-\beta\cos ql\sin\beta l),$$

$$L=(\beta^2-q^2)\cos^2\beta l(\cos 2ql/2q)+q\cos^2\beta l\cos 2ql+\tfrac{1}{2}\beta\sin 2ql\sin 2\beta l,$$

$$M=(\beta+q)\sin^2(\beta-q)l+(\beta-q)\sin^2(\beta+q)l,\quad \sigma(q)=\mathrm{Si}2(\beta+q)l+\mathrm{Si}2(\beta-q)l,$$

$$\gamma(q)=\mathrm{Cin}2(\beta+q)l-\mathrm{Cin}2(\beta-q)l,\quad \mathrm{Si}x=\int_0^x\frac{\sin t}{t}dt;\quad \mathrm{Cin}x=\int_0^x\frac{1-\cos t}{t}dt=\log x+0.577-\mathrm{Ci}x.$$

Equating (14) to the even part of Eq. (10), and solving for $f(l, q)$, we obtain

$$f=\sigma(y)\cos x+A^{-1}\{\gamma(x)\cos^2xy-\gamma(y)[\tfrac{1}{2}y^{-1}(1+y^2)\cos^2x\cos 2xy+\tfrac{1}{2}\sin 2x\sin 2xy]$$
$$-\cos^2x[(1+y)\sin^2x(1-y)+(1-y)\sin^2x(1+y)]\}, \tag{15}$$

where

$$x=\beta l;\quad y=\cos\theta=q/\beta;\quad \sigma(y)=\mathrm{Si}2x(1+y)+\mathrm{Si}2x(1-y);\quad \gamma(y)=\mathrm{Cin}2x(1+y)-\mathrm{Cin}2x(1-y);$$
$$\gamma(x)=\mathrm{Cin}4x;\quad A=(1-y^2)(x+\tfrac{1}{2}y^{-1}\sin 2xy)\cos x-\cos xy\{(1+y)\sin x(1-y)+(1-y)\sin x(1+y)\}.$$

By a similar procedure, using the odd part of the current, we obtain

$$g=\sigma(y)\sin x+B^{-1}\{\gamma(x)\sin^2xy+\gamma(y)[\tfrac{1}{2}y^{-1}(1+y^2)\sin^2x\cos 2xy-\tfrac{1}{2}\sin 2x\sin 2xy]$$
$$-\sin^2x[(1+y)\sin^2x(1-y)+(1-y)\sin^2x(1+y)]\}, \tag{16}$$

where

$$B=(1-y^2)(x-\tfrac{1}{2}y^{-1}\sin 2xy)\sin x-\sin xy\{(1+y)\sin x(1-y)-(1-y)\sin x(1+y)\}.$$

Having determined the functions f and g, we now calculate the scattering cross section in the backward direction θ. The scattering cross section is defined as $\sigma=4\pi R^2|E|^2/|E_0|^2$ when E is the scattered field in direction θ, as given by Eq. (11). After performing the integration, we can write E in terms of x and y as

$$E=\frac{E_0\cos\varphi}{\beta\Omega(1-y^2)}\left[\frac{A}{\cos x+if/\Omega}-\frac{B}{\sin x+ig/\Omega}\right], \tag{17}$$

$$|E|^2=\frac{E_0^2\cos^2\varphi}{\beta^2\Omega^2(1-y^2)^2}\left[\frac{A^2}{\cos^2x+f^2/\Omega^2}+\frac{B^2}{\sin^2x+g^2/\Omega^2}-\frac{2AB(\sin x\cos x+fg/\Omega^2)}{(\sin x\cos x+fg/\Omega^2)^2+\Omega^{-2}(g\cos x-f\sin x)^2}\right]. \tag{18}$$

We assume that both transmitter and receiver are polarized parallel to each other. This gives an extra factor $\cos^2\varphi$. The average over all polarizations give $\langle\cos^4\varphi\rangle_{Av}=\frac{3}{8}$ (if the polarizations of receiver and transmitter were crossed, we would be concerned with $\langle\sin^2\varphi\cos^2\varphi\rangle_{Av}=\frac{1}{8}$, making the cross section one-third as large). Thus we have

$$\frac{\sigma(\theta)}{\lambda^2}=\frac{3}{8\pi\Omega^2}\frac{1}{(1-y^2)^2}\left[\frac{A^2}{\cos^2x+f^2/\Omega^2}+\frac{B^2}{\sin^2x+g^2/\Omega^2}-\frac{2AB(\sin x\cos x+fg/\Omega^2)}{(\sin x\cos x+fg/\Omega^2)^2+\Omega^{-2}(g\cos x-f\sin x)^2}\right]. \tag{19}$$

TABLE I.

$2l/\lambda$	1/4	1/2	3/4	1	5/4	3/2	7/4	2	15/4
$\bar{\sigma}/\lambda^2$	6×10^{-4}	.151	.023	.163	.022	.176	.066	.219	.127

Assuming that the wires are randomly oriented in space, the average cross section, $\bar{\sigma}$, is

$$\bar{\sigma}=\int_0^{\pi/2} d\theta \sin\theta\, \sigma(\theta), \tag{20}$$

where $\sigma(\theta)$ is given by Eq. (19). The evaluation of $\bar{\sigma}/\lambda^2$ requires numerical integration of Eq. (20). For $2l/a=900$, the results are given in Table I.

The parameter Ω increases as the radius of the antenna decreases. The terms of Eq. (19) are of order $1/\Omega^2$, except when $\cos x$ or $\sin x$ become small; i.e., the cross section will be small ($\sim 1/\Omega^2$) except for values of x nearly $\pi/2$, $3\pi/2$, etc. (odd resonances) and π, 2π, etc. (even resonances). Figures 5 to 8 show plots of $\sigma(\theta)/\lambda^2$ as a function of θ as computed from Eq. (19).

The broadside cross section is of interest for comparison with experiment and with method (B). For this case $\theta=90°$, $y=0$. If we let y approach zero, then $A\to 2x\cos x-\sin x$; $B\to 0$; $f\to 2\cos x\,\mathrm{Si}2x+\frac{1}{2}[\gamma(x)-\sin^2 2x](x\cos x-\sin x)^{-1}$; g remains finite, so that the odd term gives no contribution broadside. This is easily seen physically. For an odd distribution of current, contributions to the field broadside will cancel in pairs.

Substituting in Eq. (19) we obtain

$$\frac{\sigma(\theta=90°)}{\lambda^2}=\frac{3}{2\pi}\frac{(x\cos x-\sin x)^2}{\Omega^2\cos^2 x+\{2\cos x\,\mathrm{Si}2x+\frac{1}{2}[\gamma(x)-\sin^2 2x][x\cos x-\sin x]^{-1}\}^2}. \tag{21}$$

For $\theta=90°$, $\sigma(\theta)/\lambda^2$ is plotted in Fig. 4, for $2l/a=900$. Equation (19) reduces, in limiting cases, to the results obtained by Chu. At odd resonances ($x=\pi/2$, $3\pi/2$, etc.) $\sin x=1$, $\cos x=0$. Then the contribution of the odd terms will be of order $1/\Omega^{-2}\times$ (even terms). If we neglect the odd terms then we find

$$\sigma(\theta)/\lambda^2=\tfrac{3}{8}\pi^{-1}[A/f(1-y^2)]^2, \quad \text{with} \quad f^2=\tfrac{1}{4}[\gamma(x)]^2; \quad A^2=4\cos^4 xy.$$

The corresponding averaged cross section is

$$\bar{\sigma}/\lambda^2=\tfrac{3}{2}\pi^{-1}\gamma(x)^{-2}[x(\mathrm{Si}4x-\tfrac{1}{2}\,\mathrm{Si}8x)+\tfrac{1}{2}\,\mathrm{Cin}4x-\tfrac{1}{8}\,\mathrm{Cin}8x]. \tag{22}$$

Using the asymptotic expansions $\mathrm{Si}z\sim\frac{1}{2}\pi-(\cos z/z)$; $\mathrm{Cin}z\sim\log\gamma z+\sin z/z$; we have

$$\frac{\bar{\sigma}^2}{\lambda^2}\simeq\frac{3}{16\pi}\frac{4\pi^2 l/\lambda-\frac{3}{2}+3\log(8\pi l\gamma/\lambda)-\log 2}{[\log(8\pi l\gamma/\lambda)]^2}, \tag{22a}$$

which is the expression obtained by Chu (Eq. (4)). A similar derivation for the even resonances yields the same final formulas (22) and (22a).

For long wires ($x\to\infty$), we have, provided we are not at resonance and so long as $y\neq 0$:

$$f\to\sigma(y)\cos x; \quad g\to\sigma(y)\sin x; \quad A\to x(1-y^2)\cos x; \quad B\to x(1-y^2)\sin x.$$

Substituting in Eq. (19) we find that the return cross section is zero (for $y\neq 0$); i.e., for long nonresonant wires the return signal is a sharp broadside lobe.

For large values of x, one finds from Eq. (21),

$$\frac{\sigma(\theta=90°)}{\lambda^2}\simeq\frac{3}{2\pi}\frac{x^2}{\Omega^2+\pi^2}=\frac{3\pi l^2}{2}\frac{1}{[\log(2/\gamma\beta a)]^2+\pi^2/4}, \tag{23}$$

which is identical with the expression obtained by Chu (cf. Eq. (5), with $\theta=90°$ and $\langle\cos^4\varphi\rangle_{Av}=\frac{3}{8}$).

III. DETAILS OF METHOD B

The fundamental integral equation to be satisfied after removal of the time factor is that already given as our Eq. (1). The constants A_1 and A_2 are to be determined by the requirement that the current vanishes at the end of the wire.

We seek to satisfy Eq. (1) approximately by a solution of the form

$$I(z)=\alpha e^{iqz}+\gamma_1\cos\beta z+i\gamma_2\sin\beta z. \tag{24}$$

The coefficient α is determined so as to cancel the part of the right side of Eq. (1) which is proportional to e^{iqz}. As in the paper of Gray, we write

$$\int_{-l}^{+l} r^{-1}I(\xi)e^{-i\beta r}\,d\xi=I(z)\int r^{-1}\cos\beta r\,d\xi+\int r^{-1}[I(\xi)-I(z)]\cos\beta r\,d\xi-i\int r^{-1}I(\xi)\sin\beta r\,d\xi. \tag{25}$$

The limits of integration are to be understood throughout to be $\pm l$. In $\int r^{-1}\cos\beta r d\xi$ we must take into account the finite radius of the wire (otherwise the integral diverges), and following the usual procedure of antenna theory take the origin of r as at the center of the wire. In the other members, on the other hand, the integrals converge at $r=0$ so that the wire here may be regarded as of negligible thickness. For a more thorough discussion of this point see Miss Gray's paper;[5] it will be assumed that the reader has some familiarity with the procedure used there.

With these approximations we have

$$\int_{-l}^{+l}\frac{\cos\beta r}{r}d\xi=Z(z),\quad\text{with}\quad Z(z)=\log\frac{[(l+z)^2+a^2]^{\frac{1}{2}}+(l+z)}{[(l-z)^2+a^2]^{\frac{1}{2}}-(l-z)}-\mathrm{Cin}\beta(l+z)-\mathrm{Cin}\beta(l-z), \tag{26}$$

$$\begin{aligned}\int r^{-1}e^{iq\xi}e^{-i\beta r}d\xi=\tfrac{1}{2}e^{iqz}\big[&2Z(z)+2\,\mathrm{Cin}\beta(l-z)+2\,\mathrm{Cin}\beta(l+z)-\mathrm{Cin}(\beta+q)(l-z)-\mathrm{Cin}(\beta-q)(l+z)\\&-\mathrm{Cin}(\beta-q)(l-z)-\mathrm{Cin}(\beta+q)(l+z)-i\,\mathrm{Si}(\beta+q)(l-z)-i\,\mathrm{Si}(\beta-q)(l+z)\\&-i\,\mathrm{Si}(\beta-q)(l-z)-i\,\mathrm{Si}(\beta+q)(l+z)\big]+\tfrac{1}{2}e^{iqz}\big[\mathrm{Cin}(\beta+q)(l-z)\\&+\mathrm{Cin}(\beta-q)(l+z)-\mathrm{Cin}(\beta+q)(l+z)-\mathrm{Cin}(\beta-q)(l-z)\\&+i\{\mathrm{Si}(\beta+q)(l-z)+\mathrm{Si}(\beta-q)(l+z)-\mathrm{Si}(\beta+q)(l+z)-\mathrm{Si}(\beta-q)(l-z)\}\big].\end{aligned} \tag{27}$$

The coefficients of e^{iqz} in Eq. (27) are slowly varying functions of z, and we shall replace them by their mean values. Actually the deviations from the mean values are considerable near the very ends of the wire. Consequently, it may appear to the reader that a very sizable error is committed by using mean values in the current formulas when we apply the boundary conditions at the end of the wire. This point will be discussed more fully in the appendix, where it will be shown that the objection is not a serious one. The second of the two factors enclosed in [ ] in Eq. (27) is an odd function of z, so that its mean value is zero. Furthermore

$$\langle Z(z)\rangle_{Av}=\tfrac{1}{2}l\int Z(z)dz=2[\log(2l/a)+\log 2-\mathrm{Cin}2\beta l-(\sin 2\beta l/2\beta l)]\sim 2[\log(\lambda/\pi a)-0.577], \tag{28}$$

$$\langle\mathrm{Cin}k(l+z)\rangle_{Av}=\mathrm{Cin}2kl+(\sin 2kl/2kl)-1\sim\log 2kl+0.577-1,$$

$$\langle\mathrm{Si}k(l+z)\rangle_{Av}=\mathrm{Si}2kl+(1/2kl)[\cos 2kl-1]\sim\tfrac{1}{2}\pi.$$

The approximations following the wavy lines are contingent on kl being somewhat large compared to unity, and may be considered adequate for our purposes except when the wire is less than a half wave long. Even with wires a half wave-length or so long, the error involved in using the asymptotic formulas is by no means negligible; if, for instance $(2l/a)=900$, the cross section at the first resonance is raised six percent when the asymptotic expansions are not made. Since the formulas based on

these asymptotic expansions are much easier to compute with than are those involving the Si and Cin functions, and since we are usually interested in wires at least half a wave long, we shall carry through the calculations on the assumption that the use of asymptotic approximations is legitimate. However, we shall later give some of the more complicated final expressions which are obtained when these approximations are not made. The expression (27) now becomes Ke^{iqz}, where

$$K=2\{\log(\lambda/\pi a)-0.577\}+2\log(1/\sin\theta)-i\pi.$$

The appropriate value of the constant α in Eq. (24) is thus

$$\alpha=i\omega\cos\varphi E_0/K\beta^2\sin\theta. \tag{29}$$

We now proceed to determine the relation between γ_1, γ_2 and the constants A_1, A_2 of Eq. (1). Using the same type of approximation as in Eq. (27) we obtain

$$\int r^{-1}\cos\beta\xi e^{-i\beta r}d\xi=L\cos\beta z;\quad \int r^{-1}\sin\beta\xi e^{-i\beta r}d\xi=L\sin\beta z,$$

where

$$L=2[\log(\lambda/\pi a)-0.577]+\log 2\beta l+0.577-\log 2-i\pi/2-1.$$

Thus

$$\gamma_1=A_1/L;\quad i\gamma_2=A_2/L. \tag{30}$$

We must now determine the constants A_1 and A_2 so as to satisfy the boundary condition $I(\pm l)=0$. Here it is not sufficient merely to set the expression (24) equal to zero at $z=\pm l$, which would give $\gamma_1=-\alpha\cos ql/\cos\beta l$; $\gamma_2=-\alpha\sin ql/\sin\beta l$, in other words infinite current at resonance. Instead we can obtain a finite current at resonance and proper damping and radiation resistance only by demanding that the second, rather than first approximation to the current, vanish at the boundary. This second approximation is obtained by iterating once the first approximation to the current, or in other words using the first approximation to $I(\xi)$ and $I(z)$ in the second and third, but not the first term in the right side of (25). Clearly the first term is much more sensitive than the other two to the value of $I(z)$, as it involves an integral which would be infinite if the wire radius, a, were equal to zero, whereas the other integrals always remain finite even with $a=0$. The boundary conditions for determining A_1 and A_2 can thus be taken to be

$$\int r^{-1}[I(\xi)-I(\pm l)]\cos\beta r d\xi-i\int r^{-1}I(\xi)\sin\beta r d\xi=(i\omega\cos\varphi/\beta^2\sin\theta)E_0e^{\pm iql}$$
$$+A_1\cos(\pm\beta l)+A_2\sin(\pm\beta l); \tag{31}$$

as is seen by substituting (25) in (1) with $z=\pm l$, and with $I(\pm l)=0$ in the first right-hand member of (25). The approximation (24) may be used for $I(\xi)$ and $I(l)$ in evaluating the left side of (31), and r has the value $|l\pm\xi|$.

The satisfaction of the boundary conditions at the two ends of the wire is equivalent to satisfying the condition at one end separately for the problem of an "even" impressed field $E_0\cos qz$ and an "odd" one $iE_0\sin qz$, rather than lumping both in the combination e^{iqz}. Instead of regarding the boundary conditions as determining A_1 and A_2, we can equally well regard them as specifying γ_1, γ_2 inasmuch as γ_1, γ_2 and A_1, A_2 are related by Eq. (30); it is more convenient to solve for γ_1, γ_2 than A_1, A_2, since the former enter directly into the expression (24) for the current distribution. When we utilize (29), (30), and (27) (approximated in the usual way for large l) we thus find that (24) yields the following expressions for determining γ_1, γ_2:

$$(i\omega\cos\varphi E_0/K\beta^2\sin\theta)\{[\log(1/\sin\theta)-\tfrac{1}{2}i\pi]\cos ql-\tfrac{1}{2}i\log[(1+\cos\theta)/(1-\cos\theta)]\sin ql\}$$
$$+\gamma_1\{\cos\beta l(\tfrac{1}{2}\log 2\beta l+0.288-\tfrac{1}{2}\log 2-\tfrac{1}{4}i\pi)-\tfrac{1}{2}i(\log 4\beta l+0.577)\sin\beta l+\tfrac{1}{4}\pi\sin\beta l\}$$
$$=(i\omega\cos\varphi E_0/\beta^2\sin\theta)\cos ql+\gamma_1 L\cos\beta l, \tag{32}$$

$$(i\omega\cos\varphi E_0/K\beta^2\sin\theta)\{[\log(1/\sin\theta)-i\pi/2]\sin ql+\tfrac{1}{2}i\log[(1+\cos\theta)/(1-\cos\theta)]\cos ql\}$$
$$+\gamma_2\{\sin\beta l(\tfrac{1}{2}\log 2\beta l+0.288-\tfrac{1}{2}\log 2-\tfrac{1}{4}i\pi)+\tfrac{1}{2}i(\log 4\beta l+0.577)\cos\beta l-\tfrac{1}{4}\pi\cos\beta l\}$$
$$=(i\omega\cos\varphi E_0/\beta^2\sin\theta)\sin ql+\gamma_2 L\sin\beta l. \quad (33)$$

We may, without too much error, replace $\log(1/\sin\theta)$ and $\log(1+\cos\theta)/(1-\cos\theta)$ by zero in these expressions. The justification for this is that the bulk of the scattering comes from $\theta>30°$, so that the omitted terms are unimportant, and their inclusion would excessively complicate the angular dependence and preclude our obtaining analytical expressions for the cross section averaged over angle. We shall also similarly neglect the term $\log(1/\sin\theta)$ in the quantity K of Eq. (29). Of course, these minor angular terms could be included, but they yield nothing worth while. The expression for the current may now, in virtue of (24), (29), (32), (33) be written as

$$I(z)=(i\omega\cos\varphi E_0/\beta^2\sin\theta)[(F'+iF'')e^{iqz}+2(G'+iG'')\cos\beta z\cos ql+2i(H'+iH'')\sin\beta z\sin ql], \quad (34)$$

$$F'=\Omega'/(\Omega'^2+\pi^2),\quad F''\doteq\pi/(\Omega'^2+\pi^2),\quad \Omega'=2\log(\lambda/\pi a)-1.154, \quad (34a)$$

$$2G'=\Psi(\beta l)[\Psi(\beta l)^2+\Xi(\beta l)^2]^{-1}-\pi\Omega'^{-1}G'',\quad 2G''=\Xi(\beta l)[\Psi(\beta l)^2+\Xi(\beta l)^2]^{-1},$$
$$2H'=\Psi(\beta l-\tfrac{1}{2}\pi)[\Psi(\beta l-\tfrac{1}{2}\pi)^2+\Xi(\beta l-\tfrac{1}{2}\pi)^2]^{-1}-\pi\Omega'^{-1}H'', \quad (35)$$
$$2H''=\Xi(\beta l-\tfrac{1}{2}\pi)[\Psi(\beta l-\tfrac{1}{2}\pi)^2+\Xi(\beta l-\tfrac{1}{2}\pi)^2]^{-1},$$

$$\Psi(x)=-(\Omega'-\Delta)\cos x+\tfrac{1}{4}\pi\sin x,\quad \Xi(x)=\tfrac{1}{2}(\log 4\beta l+0.577)\sin x-\tfrac{1}{4}\pi\cos x,\quad \Delta=-\tfrac{1}{2}\log\beta l+0.712. \quad (35a)$$

The terms $-\pi G''/\Omega'$, $-\pi H''/\Omega'$ occurring at the very ends of our formulas for G' and H' are important only very near resonance, where G'' and H'' are abnormally large. In writing down these terms, we have neglected Δ, etc., in comparison with Ω' so that their denominators are simply Ω'. This approximation is allowable as the terms $-\pi G''/\Omega'$, $-\pi H''/\Omega'$ are never of dominant importance.

Resonance occurs when there is a peak in the cross section plotted against wave-length. If the wire is sufficiently thin, so that $2l/a$ is of the order 10^3, the only important terms which vary acutely with wave-length are the G terms at the resonances 1, 3, 5$\cdots$ and the H ones at 2, 4, 6. The problem of locating the resonance is that of finding the position of the maximum of $G'^2+G''^2$ or $H'^2+H''^2$, and resonance can be regarded as occurring when the denominator of the fractions in Eq. (35) is as small as possible. If the wire is not too long, or in other words if $\log\beta l$ can be regarded as very small compared to $2\log(2l/a)$, the resonance is located nearly at the point where the first of the two squared terms composing the denominator is equal to zero. Then the forced and resonant vibrations are 90° out of phase. With this approximation, resonance occurs when the factor $(\Omega'-\Delta)\cos\beta l-\tfrac{1}{4}\pi\sin\beta l$, or $(\Omega'-\Delta)\sin\beta l+\tfrac{1}{4}\pi\cos\beta l$ vanishes. The positions of the odd and even resonances are thus not given by $\cos\beta l=0$ or $\sin\beta l=0$, as commonly assumed, but rather by

$$\cot\beta l=\pi/4(\Omega'-\Delta)\quad\text{or}\quad -\tan\beta l=\pi/4(\Omega'-\Delta). \quad (36)$$

This relation is the same as Eq. (6) of Part I. If asymptotic expansions are not used, Eq. (36) is replaced by

$$\begin{pmatrix}\cot\beta l\\ -\tan\beta l\end{pmatrix}=\frac{\tfrac{1}{2}\,\mathrm{Si}4\beta l}{2[\log(2l/a)+\log 2-1]-\tfrac{1}{2}\,\mathrm{Cin}4\beta l-\mathrm{Cin}2\beta l-(\sin 4\beta l/4\beta l)+1}. \quad (36')$$

Substitution of (36′) for (36) alters the resonance frequency only negligibly except at the first maximum, and even here the change is slight, (e.g., 0.3 percent in βl if $2l/a=900$). A more important refinement is the allowance for the fact that the minima of the denominators of G or H are not located exactly where their first terms vanish. Correction for this fact leads to the formula

$$\begin{pmatrix}\cot\beta l\\ -\tan\beta l\end{pmatrix}=\frac{\pi(1+\epsilon)}{4(\Omega'-\Delta)}\quad\text{with}\quad \epsilon=\frac{[\log(8\pi l/\lambda)+0.577]^2+2[\log(8\pi l/\lambda)+0.577][\Omega'-\Delta]}{[2(\Omega'-\Delta)]^2}. \quad (36'')$$

The difference between (36) and (36″) is particularly noticeable if the wire is long enough to contain several wave-lengths. For instance if $2l/a=900$, use of (36″) rather than (36) increases the shift of the first peak (measured from the Chu value) by only 10 percent, but the 10th peak by 28 percent. The numerical figures quoted in Sec. I are based on (36″) rather than (36), and in the first peak, avoidance of asymptotic expansions in the leading term is avoided by inserting the correction factor $1+\epsilon$ in (36′) rather than (36). It must be cautioned that if $2l/a$ is of the order 10^2, so that the convergence of our method becomes slow due to the inadequate size of Ω, none of the formulas (36), (36′), (36″) should be used for locating the maximum, as then the influence of the cross terms FG or FH becomes important and the resonance must be located by plotting the final expression (38) for the averaged cross section as a function of wave-length rather than merely maximizing $G'^2+G''^2$ or $H'^2+H''^2$. Thus if $2l/a=80$ it turns out that the shift given by (36″) is about 50 percent larger than what is obtained by locating the peak in the complete expression for the cross section.

The reflected field can be determined from $I(z)$ as given by Eq. (34) by following the same procedure as in Eqs. (11) and (12). We thus obtain

$$\sigma=\frac{\cos^2\varphi(4\pi R^2)|E|^2}{|E_0|^2}$$

$$=4\pi\cos^4\varphi\left|\int_{-l}^{+l}dze^{iqz}[(F'+iF'')e^{iqz}+2(G'+iG'')\cos\beta z\cos ql+2i(H'+iH'')\sin\beta z\sin ql]\right|^2$$

$$=(4\lambda^2/\pi)\cos^4\varphi\{a_1^2(F'^2+F''^2)+(a_2+a_3)^2\cos^2xy(G'^2+G''^2)+(a_2-a_3)^2\sin^2xy(H'^2+H''^2)$$
$$+2(a_2^2-a_3^2)\sin xy\cos xy(G'H'+G''H'')+2a_1(a_2+a_3)\cos xy(F'G'+F''G'')$$
$$+2a_1(a_2-a_3)\sin xy(F'H'+F''H'')\},\quad(37)$$

where

$$x=2\pi l/\lambda,\quad y=\cos\theta,\quad a_1=\tfrac{1}{2}y^{-1}\sin 2xy,\quad a_2=(1+y)^{-1}\sin[x(1+y)],\quad a_3=(1-y)^{-1}\sin[x(1-y)].$$

$\sigma(\theta)$ can be obtained from (37) by replacing $\cos^4\varphi$ by its mean value $\frac{3}{8}$. (For the case of crossed polarization see the remarks in Sec. II following Eq. (18).) To find the value of $\bar{\sigma}$, Eq. (37) should in addition be integrated from $y=0$ to $y=1$. (It must not be integrated from -1 to $+1$ as in evaluating the Si functions we have assumed their arguments positive, which requires $y>0$.)

The integrals are evaluable in terms of $\mathrm{Si}(x)$, $\mathrm{Ci}(x)$ and elementary functions.[10] It is convenient to make asymptotic expansions of $\mathrm{Si}(x)$ and $\mathrm{Ci}(x)$ after the integrals have been calculated. In some of the terms, however, it turns out that the factor multiplying $\mathrm{Si}(x)$ or $\mathrm{Ci}(x)$ contains a first power of x explicitly rather than involving x only through trigonometric functions, and in such terms it is not sufficient to use the approximations $\mathrm{Si}(x)\sim\frac{1}{2}\pi$, $\mathrm{Ci}(x)=0$, but rather we must employ the somewhat more accurate asymptotic developments $\mathrm{Si}(x)\sim\frac{1}{2}\pi-\cos x/x$, $\mathrm{Ci}(x)\sim\sin x/x$ in order to obtain answers correct to terms of the zeroth order in x. By proceding in this fashion it is found that the averaged cross section $\bar{\sigma}$ finally becomes

$$16\pi\bar{\sigma}/3\lambda^2=(F'^2+F''^2)(2x\pi-1)+(G'^2+G''^2)[2x\pi-1+\log 4x+0.577+(4x\log 2+\pi)\sin 2x$$
$$+(\tfrac{1}{2}-2\{\log 4x+0.577\})\cos 2x-(\log 2)\cos 4x]$$
$$+(H'^2+H''^2)[2x\pi-1+\log 4x+0.577-(4x\log 2+\pi)\sin 2x$$
$$+(2\{\log 4x+0.577\}-\tfrac{1}{2})\cos 2x-(\log 2)\cos 4x]$$
$$+2(G'H'+G''H'')[4x(\log 2)\cos 2x-\tfrac{1}{2}\sin 2x]$$
$$+4(F'G'+F''G'')[(7\pi/4)\sin x-\tfrac{1}{2}(\log 4x+0.577)\cos x-\tfrac{1}{2}(\log 2)\cos 3x]$$
$$+4(F'H'+F''H'')[\tfrac{1}{4}\pi\cos x-\tfrac{1}{2}(\log 4x+0.577)\sin x+\tfrac{1}{2}(\log 2)\sin 3x].\quad(38)$$

[10] For detailed evaluation of the integrals see report 411-103 of the Radio Research Laboratory, Harvard University (NDRC Div. 15). This report also contains more graphs of the angular cross sections than given in our Figs. 5–8.

Short wires in case the wire is not long enough compared to the wave-length to permit the use of asymptotic expansions, the preceding formulas must be modified as follows: Eq. (37) is still applicable, but the coefficients F, G, H, must be redefined. Equation (34a) is replaced by

$$F'=\Omega''/(\Omega''^2+\mathrm{X}^2),\quad F''=\mathrm{X}/(\Omega''^2+\mathrm{X}^2),\quad \mathrm{X}=2[\mathrm{Si}2\beta l+(2\beta l)^{-1}(\cos 2\beta l-1)],$$

$$\Omega''=2[\log(2l/a)+\log 2-\mathrm{Cin}2\beta l-(\sin 2\beta l/2\beta l)].$$

The formulas (35) for G and H are still valid if the coefficients $\pi\Omega'^{-1}$ in (35) are replaced by $2\Omega''^{-1}\mathrm{Si}2\beta l$, and if the definitions (35a) are modified to

$$\Psi(x)=-(\Omega''-\Delta'')\cos x+\tfrac{1}{2}\,\mathrm{Si}4\beta l\sin x,\quad \Xi(x)=\tfrac{1}{2}\,\mathrm{Cin}4\beta l\sin x-[\tfrac{1}{2}\mathrm{Si}4\beta l+(4\beta l)^{-1}(\cos 4\beta l-1)]\cos x,$$

$$\Omega''-\Delta''=2[\log(2l/a)+\log 2-1]-\tfrac{1}{2}\,\mathrm{Cin}4\beta l-\mathrm{Cin}2\beta l-(\sin 4\beta l/4\beta l)+1.$$

The explicit expression for the resulting averaged cross section is given in reference 10, and will not be reproduced here, as it is quite cumbersome.

For $2l/a=900$, the averaged cross section at the first resonance turns out to be six percent lower when asymptotic expansions are avoided. The lower values have been used in drawing the first peak in Figs. 2 and 3, but serious error would not have resulted had we used the asymptotic formulas. For the second and higher peaks, the results are not appreciably influenced by employing asymptotic expansions. On the other hand, when the frequency is lowered much below the first resonance, it is very essential to avoid using the asymptotic formulas.

When the frequency is quite small compared to the first resonant frequency, or in other words if the wire is cut much too short for resonance, it is very difficult to compute with the non-asymptotic formula that replaces (38). The cross section is expressed as a difference of terms which nearly cancel and which must hence be very accurately evaluated to obtain a significant answer.

However, for very short wires, simple formulas may be obtained by using for the coefficients the approximate values

$$F'=1/[2\log(2l/a)+2\log 2-1],\quad G'=-F'(1+x^2)/2,\quad H'=-F'/2x,$$

and developing the expression (34) for the current or the integrand of (37) as a Taylor's series in x and retainining only the terms of lowest order. In this way one finds that before averaging the cross section is

$$\sigma=(\lambda^2x^6/9\pi)(\cos^4\varphi)(1-y^2)^2[\log(4l/a)-1]^{-2},\tag{39}$$

while the averaged cross section is

$$\bar{\sigma}=(\lambda^2x^6/45\pi)[\log(4l/a)-1]^{-2},\quad (x=2\pi l/\lambda).\tag{40}$$

Equations (39) and (40) can safely be used if the frequency is twenty percent or less of the first resonant frequency (i.e., $\lambda/l\geqq 20$). Equations (39) or (40) show that for wires very short compared to the wave-length, the cross section is proportional to the sixth power of the wire length, and inversely proportional to the fourth power of the wave-length. This behavior is reasonable, as in the low frequency limit the dimensions of the object and the wave-length also enter in the sixth and inverse fourth powers in the known formulas for other types of scatterers (e.g., spheres), as well as in the general Rayleigh theory of scattering by small particles.

We can, in fact derive (39) in a quite independent fashion by computing the Rayleigh scattering. It suffices to consider the case $\varphi=y=0$ where the wire axis A is parallel to the incident vector E_0, as it is readily seen that for very long waves the cosine of the angle between A and E_0 is involved to the fourth power, thus accounting for the factor $\cos^4\varphi(1-y^2)^2$ in (47). The broadside radiation of a dipole of moment M has a Poynting vector $\frac{1}{4}\pi^{-1}c^{-3}R^{-2}(d^2M/dt^2)^2$. In the long wave-length limit we can safely take $d^2M/dt^2=-(2\pi\nu)^2a_0E_0$, where a_0 is the static polarizability of the wire. The cross

section is then $a_0^2(2\pi/\lambda)^4 4\pi$. We now need only the value of a_0, and this we can take from the soluble problem[11] of a very prolate ellipsoid of revolution of semi-major axis and semi-minor axis a in a static field parallel to the axis of symmetry. Since the wire is a conductor, we take the dielectric constant as ∞. The polarizability is then the volume of the ellipsoid divided by the demagnetizing factor D, and for the infinitely prolate case the value of D is $(4\pi a^2/l^2)[\log(2l/a)-1]$. We thus obtain a formula identical with (39) except that $\log 2l/a$ occurs in place of $\log 4l/a$. The difference is of minor consequence since $2l/a$ is large, and is no doubt due either to the non-equivalence of an ellipsoid and cylinder, or to the fact that our replacement of $Z(z)$ by a constant $\langle Z\rangle_{Av}$ as in (28) is of necessity an approximation.

The cross section falls off very rapidly as the frequency is lowered from the first resonance. Consequently in Fig. 2 or Fig. 3 the ordinate can be regarded as sensibly equal to zero when the abscissa is less than about half the value associated with the first resonance. Part of the drop of the curve as one approaches the origin is caused by the fact that $\bar{\sigma}/\lambda^2$ rather than $\bar{\sigma}$ is being plotted. λ increases when the abscissa (proportional to frequency) is lowered. However, most of the decrease of $\bar{\sigma}/\lambda^2$ is caused by the $\bar{\sigma}$ rather than $1/\lambda^2$ factor. For instance, if $2l/a=900$, the value of $\bar{\sigma}/\lambda^2$ yielded by (40) at $x=0.3$ (frequency one-fifth that of the first resonance $x=1.5\sim\pi/2$) is 0.00000012, and the cross section $\bar{\sigma}$ is only one sixty-thousandth of its value at the first resonance. The values of $\bar{\sigma}/\lambda^2$ at frequencies forty, sixty, eighty, and one hundred percent of the first resonance ($x=0.6$, $x=0.9$, $x=1.2$, $x=1.50$) are 0.000043, 0.0014, 0.0071, 0.184, respectively, if $2l/a=900$.

APPENDIX. SOME NOTES ON THE CONVERGENCE OF METHOD B

If we decompose the fundamental integral Eq. (1) into its forced and resonant parts, then the equation satisfied by either portion is mathematically of the type form

$$\int r^{-1}I_p(\xi)e^{-ikr}d\xi=D_p\cos kz, \qquad (41)$$

where I_p refers to only the forced or resonant part of the current ($p=f$, r, respectively) and where k means $q=\beta\cos\theta$ for the forced and $\beta=2\pi/\lambda$ for the resonant case. For simplicity we consider only the portion of the solution which is even as regards reflection in the origin, as the convergence questions connected with the even and odd members are fundamentally similar. We seek to solve (41) by a trial function of the form $E_p\cos kx$. The left-hand side of (41) then turns out to be of the structure

$$E_p[f_p(z)\cos kz+g_p(z)\sin kz], \qquad (42)$$

(Cf. Eq. (27)) where $f_p(z)$ is a slowly varying function of z, and $g_p(z)$ may be disregarded in the first approximation. We next replace f_p by its mean value, and thus take

$$E_p=D_p/\bar{f}_p. \qquad (43)$$

[11] E. C. Stoner, *Magnetism and Matter*, p. 39.

Against this procedure it may be objected by some readers that actually $f_p(z)$ does vary with z, and so should not be replaced by a constant in such a debonnaire fashion. In fact, at the ends of the wire $f(z)$ has approximately half its value at the center, which is also nearly its mean value, provided of course the wire length l is large compared to its radius, as we assume throughout. Now for computation of the radiation from the wire, it seems fairly clear that the approximation $f_p=\bar{f}_p$ is not responsible for much error, since the ends of the wire contribute only a fraction of the total radiation. However, it may well seem at first sight that the use of (42) is a bad mistake in applying the boundary condition $I(\pm l)=0$, i.e., in satisfying Eq. (31), for it is at the ends of the wire that the difference between f_p and $\bar{f}_p$ is largest. We shall now show that this objection is not as serious as it first seems. We may distinguish between two cases: (a) wires which contain at most a few wave-lengths, so that $\log(l/\lambda)$ is small compared with $\log(\lambda/a)$, and (b) wires which are so extended as to contain an enormous number of wave-lengths, so that $\log(l/\lambda)$ is comparable with, or greater than, $\log(\lambda/a)$.

First we shall dispose of case (a). Here as can be seen from the study of Eq. (27) the distinction between $f_p(z)$ and $\bar{f}_p$ is important only at distances from the ends of the wire which are comparable with the wire radius, and small compared

with the wave-length. However, because of the fact that the current vanishes at the ends of the wire, the substitution of $\bar{f}_p$ for f_p leads to no serious error when we remember to include the sum of the resonant and forced terms rather than to consider them separately. Individually they would show abrupt discontinuities near the end of the wire if we assumed them inversely proportional to $f_p(z)$. Because $\log(l/\lambda)$ is by hypothesis small compared to $\log(\lambda/a)$ in case (a), the value of f_p is roughly the same for the forced and resonant members, as can be seen from Eqs. (27) and (30). Hence for estimating the orders of errors, we can replace f_f, f_r by a common expression f, and the point of our argument is that in the "end zone," i.e., the region a small fraction of a wave-length from the end of the wire, the difference between the expressions

$$\text{and} \qquad \begin{matrix} f^{-1}(D_f \cos qz + D_r \cos\beta z) \\ \bar{f}^{-1}(D_f \cos qz + D_r \cos\beta z) \end{matrix} \qquad (44)$$

is of minor importance. The reason for this statement is that at the ends of the wire the terms $D_f \cos qz$ and $D_r \cos\beta z$ nearly cancel. The cancellation, it was pointed out in Part I, is not complete, but still it is enough to insure that throughout the end zone either form of expression (44), and hence the difference between the two forms, is only of the order $I(0)/\Omega$ (with $\Omega \sim \log(\lambda/a)$). This is sufficient accuracy since our solution only pretends to be accurate to the order $I(0)$. Here $I(0)$ denotes the order of magnitude of the current down most of the wire (not necessarily at the center) and is of the order $\omega E/\beta^2\Omega$ away from resonance and $\omega E/\beta^2$ at resonance. This argument can be stated somewhat more exactly as follows: If we iterate (1) or (25) to obtain a second approximation to the current, the difference as compared with (24) is

$$\begin{aligned} \Delta I = f(z)^{-1}\Big\{ & -\int r^{-1}[I_0(\xi) - I_0(z)] \cos\beta r d\xi \\ & + i\int r^{-1} I_0(\xi) \sin\beta r d\xi \\ & + (i\omega \cos\varphi/\beta^2 \sin\theta) E_0 e^{iqz} \\ & + A_1 \cos\beta z + A_2 \sin\beta z \Big\} - I_0(z), \end{aligned} \qquad (45)$$

where $I_0(z)$ denotes the first approximation to the current, given by (24) and where the significant part of $f(z)$ is given by (26). Because of the boundary condition (31) one finds that $I_0(l)$ is of the order $1/\Omega$ compared with $I_0(0)$. The factor in braces in (45) vanishes at the ends of the wire, and reaches values of the order of $I_0(0)\bar{f}$ only when one moves a wave-length or so away from the ends. Except at the very ends of the wire, the distinction between f and $\bar{f}$ disappears, so that the factor in braces in Eq. (45) is nearly the same as $f(z)I_0(z)$. Thus ΔI is everywhere of the order $I_0(0)/\Omega$. Similarly one can show that each successive approximation gives a contribution of the order $1/\Omega$ times the preceding one. Our procedure is hence convergent.

In case (b), however, the situation is a different one. The value of $f_p(z)$ is essentially different for the forced and resonant parts of the solution, as f_f has the structure $A \log(\lambda/a) + B$, while f_r has the form $C \log(\lambda/a) + D \log(l/\lambda) + E$ and so increases without limit when the wire contains more and more wave-lengths, whereas in (a) we assumed that $\log(l/\lambda)$ was small compared with $\log(\lambda/a)$. In the end zone the correction ΔI furnished by the second approximation still is of the order $I_0(0)/\Omega$, but becomes of the order $I_0(0)$ at distances from the end of the wire comparable with the wave-length, but large compared with the radius of the wire and small compared with its total length. Since the correction is comparable in order with the first approximation for part of the wire, it may seem that all semblance of convergence is lost. However, we believe that the resulting error is not serious. In the first place, the difficulty arises only in connection with the resonant rather than forced part of the solution, as the extra term $D \log(l/\lambda)$ occurs only in connection with the former, and in the latter most of the contribution comes from the "close-in" rather than the "far-away" portion since

$$\int_\epsilon^\infty \cos q\xi \frac{e^{-i\beta r}}{r} d\xi$$

converges. Hence our forced member is reasonably well determined, and for long wires this is the main effect. Furthermore, the fact that the

integral varies only slowly with position on the wire, together with the fact that most of the radiation does not come from too near the end zone, means that the amplitude of even our resonant term is probably not in error by a factor 2 or so until $\log(l/\lambda)$ becomes large rather than merely comparable with $\log(\lambda/a)$. When $\log(l/\lambda)$ is large compared with $\log(\lambda/a)$, the resonant terms are unimportant compared with the forced, and so any quantitative percentage error in the resonant part of the theory in this region is inconsequential as long as it gives resonant terms which are small compared with the forced. In other words, our theory behave correctly in the limit of infinitely long wires, where it agrees with Chu. Before reaching the limit, but by the time $\log(l/\lambda)$ becomes comparable with $\log(\lambda/a)$, the difference between the heights of the peaks and valleys is small compared with the elevations of the valleys, so that accuracy in this difference is unimportant. We might add that practically we are not concerned, anyway, with wires so long that $\log(l/\lambda)$ is comparable with $\log(\lambda/a)$, so that case (b) is of rather academic interest.

In closing, it is perhaps well to make a few remarks comparing our procedure in method (B) to that of Hallén[4] (or King and Harrison[3]), of Gray,[5] and of King and Middleton.[6] In each instance one is concerned with obtaining a first approximation to an integral of the form $\int r^{-1}\cos k\xi e^{-i\beta r}d\xi$ with the singularity at the origin avoided by integrating down the center of the wire, so that $r^2=(\xi-z)^2+a^2$. Hallén approximates the integral by $\cos kz\int r^{-1}d\xi$. When the upper limit of integration is infinity, the integral $\int r^{-1}\cos k\xi e^{-i\beta r}d\xi$ converges when $k\neq\beta$, whereas $\int r^{-1}d\xi$ does not. Thus, it is clear that the Hallén procedure is not appropriate for long wires. This difficulty is avoided by Miss Gray, who approximates the integral by

$$\cos kz\int r^{-1}e^{-i\beta r}d\xi.$$

This is not an unreasonable step when $k\neq\beta$, as then both the original and substituted integrals are convergent. Hence the Gray scheme is a fairly suitable one for the forced part of the solution, as here $k\neq\beta$. In fact, for the broadside case $k=0$ which figures particularly prominently in the forced part of the scattering, the original form of the integral does not differ from that substituted by Miss Gray. In this particular case, there is no essential distinction between the Gray scheme of approximation and our own which resembles that of King and Middleton. (We might mention parenthetically, that the Gray procedure was not intended specifically for the problem of the receiving antenna, to the forced part of which it applies quite well, but rather for the resonant radiating antenna, to which the same difficulties apply as in the resonant portion which we now discuss. On the other hand, it was intended primarily for the half wave antenna, which is so short that the proper behavior, as l approaches infinity, is irrelevant. Even for the half-wave case, the method of King and Middleton is somewhat more accurate than that of Miss Gray.) Certainly, the type of substitution employed by Miss Gray is not a happy choice for the resonant terms if the wire is so long as to contain a great number of wave-lengths. The difficulty is that the resonant part of the problem has $k=\beta$, so that $\int r^{-1}\cos k\xi e^{-i\beta r}d\xi$ diverges (through to half the Hallén value) when the limit is infinite, whereas the integral substituted by Gray converges. Correspondingly, the amplitude of the resonant member, which by (43) is inversely proportional to the substituted integral, remains finite if the Gray approximation is applied to an infinitely long wire, whereas actually it should go to zero. This difficulty is avoided in our type of procedure which is essentially the same as that of King and Middleton and consists in replacing $\int r^{-1}\cos k\xi e^{-i\beta r}d\xi$ by $\cos kz\int r^{-1}\cos k(z-\xi)e^{-i\beta r}d\xi$ in first approximation. (Cf. Eq. (27) or (42).) The factor multiplying $\cos kz$ is then an integral which converges for infinitely long wires for the forced part of the solution and diverges for the resonant part, whereas Hallén has divergence for both portions, and Gray has convergence. Correspondingly in the limit of very long wires, the forced amplitude remains finite, approaching the Chu value asymptotically, and the resonant member approaches zero as should be the case, whereas the first approximation of Hallén would make both amplitudes tend to zero, and that of Gray would make them both stay finite.

X-Ray Scattering at Small Angles by Finely-Divided Solids. I. General Approximate Theory and Applications*

C. G. SHULL** AND L. C. ROESS
Beacon Research Laboratory of The Texas Company, Beacon, New York

(Received August 29, 1946)

The general approximate theory of x-ray scattering at small angles by finely divided solids is reviewed. It is assumed that the x-ray scattering data can be interpreted in terms of a particle size distribution, with particle-to-particle scattering negligible. Scattered intensity curves for Maxwellian, Gaussian, and rectangular size distributions are calculated, and several procedures for obtaining a size distribution from the experimental scattering data are described. Details of the experimental technique are given, and evidence is presented to show that appreciable error can result if crystal-monochromated radiation is not used. General procedures are given for applying corrections to the experimental data for the slit geometry used. Scattering data, mass distribution curves, and average particle sizes are presented for amorphous silica gels and for crystalline oxides of alumina, nickel and iron. These data are shown to correlate well with the results of crystal size measurements by x-ray diffraction line broadening and with specific surface measurements. The average particle size values determined from the experimental data are shown to have considerable significance, at least for the type of materials considered here.

INTRODUCTION

THE usefulness of x-ray scattering at small angles in the study of finely-divided solids has been demonstrated by many investigators.[1] Carbon blacks have been studied by Warren and his collaborators,[1,2] by Guinier,[3] and by Krishnamurti,[1] cellulose in various forms by Kratky and his collaborators,[4] by Hosemann[5] and by Guinier,[3] while Guinier[3,6] has applied the method to ovalbumine, rubber, colloidal silver, ramie, and the hardening of alloys. Catalyst studies have been reported by Guinier,[3] Elkin, Shull, and Roess,[7] and Jellinek and Fankuchen.[8]

The interpretation of the x-ray intensity scattered at small angles is by no means unambiguous.[9] At least two specialized points of view have been emphasized in the literature: (1) the Guinier[1] and Hosemann[1] theory, which emphasizes particle form factor scattering and assumes that particle-to-particle scattering can be neglected, and (2) Kratky's view[4,10] that, at least for fibrous materials, such as cellulose, a statistical distribution of Bragg reflection planes is responsible for the observed scattering.

Basically it is the distribution of electron density which produces the scattering, and therefore nothing more than this distribution, if that much, can be obtained without ambiguity from the x-ray data. An average electron density, the Patterson distribution,[11] can be calculated, at least in principle, from the observed x-ray data. Such an average electron density having been determined, its interpretation in terms of more

* Much of the material in this paper was presented by C. G. Shull at two Gibson Island conferences: the ASXRED meeting in 1944 and the AAAS Catalyst Session in 1945.

** Now at Clinton Laboratories, Oak Ridge, Tennessee.

[1] J. A. Gray and W. H. Zinn, Can. J. Research **2**, 291–293 (1930); P. Krishnamurti, Ind. J. Phys. **5**, 473–488 (1930); H. Mark and J. Hengstenberg, in H. Mark, *Physik und Chemie der Zellulose*, Verlagsbuchhandlung, Julius Springer (Berlin, 1932), p. 139; S. B. Hendricks, Zeits. f. Krist. **83**, 503–504 (1932); B. E. Warren, J. Chem. Phys. **2**, 551–555 (1934); A. Guinier, Comptes rendus **206**, 1641 (1938); O. Kratky, Naturwiss. **26**, 94 (1938); R. Hosemann, Zeits. f. Physik **113**, 751–768 (1939); The ASXRED *Bibliography on X-Ray Small Angle Scattering* (1946) has additional references.

[2] B. E. Warren, Phys. Rev. **49**, 885 (1936); J. Biscoe and B. E. Warren, J. App. Phys. **13**, 364–371 (1942).

[3] A. Guinier, Ann. de physique **12**, 161–237 (1939); H. Brusset, J. Devaux, and A. Guinier, Comptes rendus **216**, 152–154 (1943).

[4] O. Kratky and F. Schoszberger, Zeits. f. physik. Chemie **B39**, 145–154 (1938); O. Kratky, Naturwiss. **30**, 542–543 (1942); O. Kratky, A. Sekora, and R. Treer, Zeits. f. Elektrochemie **48**, 587–601 (1942); O. Kratky and A. Wurster, Zeits. f. Elektrochemie **50**, 249–255 (1944).

[5] R. Hosemann, Zeits. f. Physik **114**, 133–169 (1939); Zeits. f. Elektrochemie **46**, 535–555 (1940).

[6] A. Guinier, Proc. Phys. Soc. **57**, 310–324 (1945).

[7] P. B. Elkin, C. G. Shull, and L. C. Roess, Ind. Eng. Chem. **37**, 327–331 (1945).

[8] M. H. Jellinek and I. Fankuchen, Ind. Eng. Chem. **37**, 158–164 (1945); Ind. Eng. Chem. Anal. Ed. **18**, 172–175 (1946) (with E. Solomon).

[9] An excellent discussion is given in A. Guinier, J. Chim. Phys. **40**, 133–150 (1943). See also R. Hosemann, Zeits. f. Elektrochemie **46**, 535 (1940).

[10] Kratky, Zeits. f. Elektrochemie **46**, 556 (1940), discussion of Hosemann's paper.

[11] A. L. Patterson, Zeits. f. Krist. **A90**, 517–542 (1935). D. Wrinch, *Fourier Transforms and Structure Factors* (American Society for X-Ray and Electron Diffraction, 1946), p. 12.

directly useful physical pictures, such as particle size distributions, offers considerable difficulty, and requires that further assumptions be made.

The most useful method of interpreting the small angle x-ray data may well depend upon the nature of the materials being studied. It has seemed to us that the particle size (or mass) distributions resulting from Hosemann's theory, which assumes particle-to-particle scattering to be negligible, are of great value in forming physical pictures of the solid materials which we have studied (silica gels, silica-alumina catalysts, alumina gels, and alumina-base catalysts). We have, therefore, consistently used this method of interpreting the data, and have endeavored to find evidence supporting it from investigations of these materials by entirely independent means, such as physical adsorption and the broadening of ordinary x-ray diffraction lines.

Once this assumption of negligible particle-to-particle scattering is made, the procedure becomes straightforward. The angular distributions of x-ray intensity scattered at small angles by a series of particle mass distributions obtained by varying two parameters in several types of distribution functions have been calculated. The observed data are compared with the calculated curves, after taking into account any necessary corrections for the geometry of the apparatus, and the mass distribution giving the best fit is determined. Spherical particle shape is assumed in all of the work reported here, although calculations have been made[12] for randomly oriented spheroids also.

The justification for these assumptions can only be found in the usefulness of the particle size distributions obtained and in the agreement between predictions based on them and data obtained independently. We believe that on these grounds the assumptions have been shown to be justified for the materials we have studied.

It is possible to invert the x-ray data to give the mass distribution function directly.[13] This procedure was discovered too late for use in presenting our data. It is unlikely that significantly different results would be obtained for the materials studied here.

[12] L. C. Roess and C. G. Shull, J. App. Phys. **18**, 308 (1946).
[13] L. C. Roess, J. Chem. Phys. **14**, 695–697 (1946).

GENERAL THEORY OF X-RAY SCATTERING BY A DISTRIBUTION OF RANDOMLY ARRANGED PARTICLES

For purposes of mathematical analysis we consider a scattering specimen which contains small particles arranged in a random fashion. The intensity of x-radiation scattered at a small angle ϵ by a single particle is given by

$$I(\xi) = I_e \rho_e^2 V^2 S(R, \xi), \tag{1}$$

where

$$\xi = (2\pi/\lambda)\epsilon, \tag{2}$$

I_e is the Thomson scattering factor for a single electron and is essentially constant for the angles to be considered, ρ_e is the electron density and V the volume of the particle, and $S(R, \xi)$ is the scattering function characteristic of the particle size R and its geometrical shape. The scattering function S is related to the particle structure as the atomic form factor is related to the structure of an atom.

When many particles N are present, as is always the case experimentally, and if their contributions to the scattered intensity are independent of each other, then obviously the scattered intensity is given by

$$I(\xi) = I_e N \rho_e^2 V^2 S(R, \xi). \tag{3}$$

This is the equation used by Guinier[3] in his early studies.

If a distribution of particle sizes is envisaged, as Hosemann[1] has suggested,

$$I(\xi) = I_e \rho_e^2 \int_0^\infty N(R) V^2(R) S(R, \xi) dR \tag{4}$$

where $N(R)dR$ is the total number of particles having sizes in the range R, dR. This integral equation can be put into a somewhat more usable form by introduction of a mass distribution function and by expressing the particle volume in terms of the particle size. Thus

$$I(\xi) = K I_e \rho_e^2 \int_0^\infty M(R) R^3 S(R, \xi) dR, \tag{5}$$

with $M(R)dR$ representing the total mass of particles in the size range R, dR and K being a constant proportional to the total mass.

TABLE I. Relationship between average particle size and parameters in Maxwellian type of distribution.

n	0	1	2	3	4	5
$\bar{r}/r_0$	0.227	0.693	1.183	1.677	2.176	2.674

In proceeding further, it is necessary to assume a particular particle shape in order to permit evaluation of the scattering function S. The scattering function for the general case of spheroidal particles (which includes spherical, rod-shaped, and plate-shaped particles) has been evaluated in an exact form and will be discussed in the second paper[12] of this series. Guinier[3] has introduced an approximate scattering function

$$S_0(R, \xi) = \exp\left[-\frac{r^2}{3}\xi^2\right], \qquad (6)$$

which agrees exactly at very small angles with the exact scattering function for spherical particles. Deviations are obtained, however, at the larger angles and the effect of these on the interpretation of experimental data will also be discussed in the companion paper. In Eq. (6), Guinier has defined r as the radius of gyration (defined as in the usual mechanical case) of the particle. However, the introduction of the radius of gyration is not of sufficient generality to make the Guinier function a good approximation for very asymmetrical particles, as Guinier[3] has shown.[14]

The integral Eq. (5) along with the Guinier scattering function has been used by Hosemann,[5] by Elkin, Shull, and Roess,[7] and by Jellinek, Solomon, and Fankuchen[8] in their studies. Since, in general, not very much is known in advance about the particle shape or whether there is a preferred shape, it would seem that the use of the Guinier scattering function would be as significant as any. A comparison of the results obtained by interpreting a typical set of experimental data with both the Guinier scattering function and the exact scattering function for spherical particles has shown agreement within about 20 percent for the calculated average particle size. In the present paper, the experimental data have all been interpreted by use of the approximate scattering function and the resultant particle size distributions described in terms of a particle diameter.

[14] See also section on Numerical Results in reference 12.

Methods of Data Interpretation

In applying Eq. (5) to the interpretation of experimental data, it is necessary to perform a mathematical inversion of the data in order to obtain the desired particle size distribution. A direct inversion procedure making use of the exact scattering function for spheroidal particles has been introduced by Roess,[13] but as mentioned earlier this was discovered too late for application to the present experimental data. Several indirect methods are available, however, which provide a simple and easily-performed procedure for obtaining the particle size distribution, and these have been used in the present study. Basically these indirect methods involve a matching of the experimental scattering curve with either one or a suitable combination of standard scattering curves which have been calculated in advance for selected distributions of particle size. Three types of distributions have been studied: Maxwellian, Gaussian, and rectangular, and these will be considered individually.

Maxwellian Type of Particle Size Distribution

Hosemann[1] has suggested that the particle size distribution might be represented by an expression of the type $r^n \exp[-(r/r_0)^2]$, where n and r_0 are constants whose values are to be adjusted to the experimental data. Following this idea, we let

$$M(r) = \frac{2}{r_0^{n+1}\Gamma\left(\frac{n+1}{2}\right)} r^n \exp[-r^2/r_0^2], \qquad (7)$$

where the coefficient is that which gives a total mass of unity. The average particle size $\bar{r}$, which is defined as that size which divides the mass distribution in half, has been calculated for this distribution in terms of the parameters r_0 and n, and the resulting values are listed in Table I. It is interesting that $\bar{r}/r_0$ varies almost exactly linearly with n for $n \gtrsim 1$.

If Eq. (7) and the Guinier scattering function,

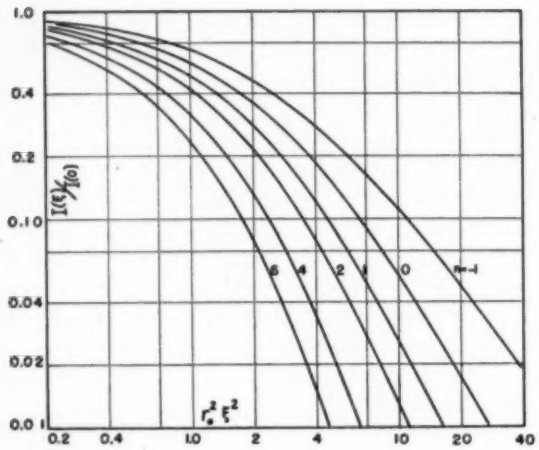

FIG. 1. Calculated scattering curves for Maxwellian type of particle size distribution.

Eq. (6), are inserted into Eq. (5), we obtain

$$I(\xi)=KI_e\rho_e^2\frac{2}{r_0^{n+1}\Gamma\left(\frac{n+1}{2}\right)}\times\int_0^\infty r^{n+3}\exp[-(\tfrac{1}{3}\xi^2+r_0^{-2})r^2]dr, \quad (8)$$

and this integrates directly to

$$I(\xi)=\frac{2KI_e\rho_e^2\Gamma\left(\frac{n+4}{2}\right)r_0^3}{\Gamma\left(\frac{n+1}{2}\right)}\times[\tfrac{1}{3}r_0^2\xi^2+1]^{-[(n+4)/2]}. \quad (9)$$

The requirement of finite total mass in the distributions of Eq. (7) restricts values of n to those greater than -1.

Equation (9) represents the intensity distribution to be expected if the particle size distribution has the form of Eq. (7). Conversely if Eq. (9) can be made to fit the experimental data by adjustment of its parameters, then the particle size distribution is obtainable directly from Eq. (7). The adjustment of the parameters can be conveniently done by either of two graphical methods, (a) a curve matching and resolution process, and (b) a curve shifting procedure.

The former procedure makes use of the *standard scattering curves* shown in Fig. 1. These have been calculated[15] according to Eq. (9). If the experimental scattering curve (plotted as log$I$ *versus* logξ^2) can be matched to one of these standard scattering curves by suitable displacement of the two graphs along horizontal and vertical axes, the particle size distribution is represented by Eq. (7) with the parameter n determined by the selected standard curve and r_0 determined by comparing the location of the ξ^2 axis on the experimental graph in relation to the $r_0^2\xi^2$ axis of the standard curve graph. If, however, the experimental data do not match any of the standard curves it is necessary to resolve the experimental curve into the sum (or difference) of two or more component curves each of which is a good match for one of the standard curves. The parameters of the component curves will be determined in the same fashion as in the earlier one-component match and the relative amplitudes of the distributions will be determined by the relative intensities of the component scattering curves. It has been found generally that one standard curve will represent the experimental data, but even when additional component curves have been found necessary the whole resolution process can be carried out in less than one-half hour.

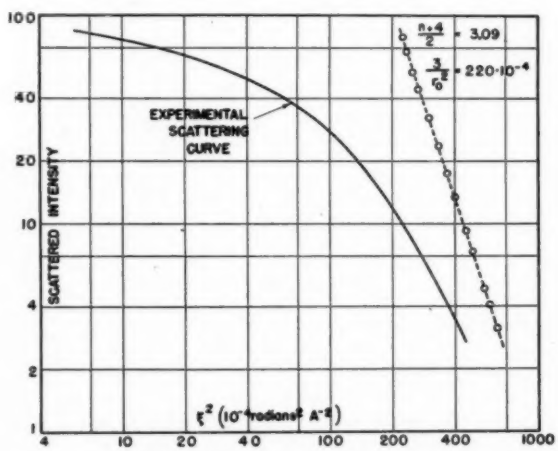

FIG. 2. Typical experimental scattering curve for alumina gel illustrating the shifting procedure for determining the particle size distribution parameters.

[15] The calculated values for the scattered intensity produced by various particle size distributions have been tabulated and are available from the authors upon request.

The second method for determining the particle size distribution does not involve the use of the standard curves but is nevertheless quite similar to the former method. Equation (9) can be put into a logarithmic form

$$\log I(\xi)=\log K_1-\left(\frac{n+4}{2}\right)\log[\xi^2+3/r_0^2], \quad (10)$$

with K_1 a constant. From this equation it can be seen that a graph of the experimental intensity *versus* (ξ^2+3/r_0^2) on a double logarithmic scale should show a linear relationship between these variables. Moreover the slope of the line through the experimental data would be $-[(n+4)/2]$ and hence n would be determined. It is not possible to plot the above variables directly, since r_0 is also an undetermined parameter, but the data can be plotted simply as I *versus* ξ^2 (again on double logarithmic paper) and then various values of $3/r_0^2$ added to ξ^2 until a straight line is obtained. Figure 2 illustrates the use of this shifting procedure. The experimental data are represented by the solid line and upon adding a fixed quantity ($220\cdot10^{-4}$ radians^2 A^{-2}) to the abscissa of the experimental values, the circled points are seen to agree closely with a straight line. The parameters n and r_0 are immediately available and the particle size distribution can be represented by Eq. (7). In cases where the shifting process does not lead to a single straight line, the experimental curve can be broken into component curves each of which can be shifted into a straight line. Additional terms are therefore necessary in describing the true particle size distribution. Again this process can be performed in a short time.

Gaussian Distribution of Particle Size

Let the particle size distribution be represented by

$$M(r)=\frac{2}{\sqrt{\pi}}\frac{\beta}{r_0}\frac{1}{1+H(\beta)}\exp\left[-\frac{\beta^2}{r_0^2}(r-r_0)^2\right], \quad (11)$$

where the coefficient has been selected to make the total mass unity. Substitution of Eqs. (11) and (6) into Eq. (5) gives upon integration

$$I(\xi)=\frac{KI_e\rho_e^2}{\sqrt{\pi}}\frac{r_0^3}{\beta^4[1+H(\beta)]}D(\beta, r_0\xi) \quad (12)$$

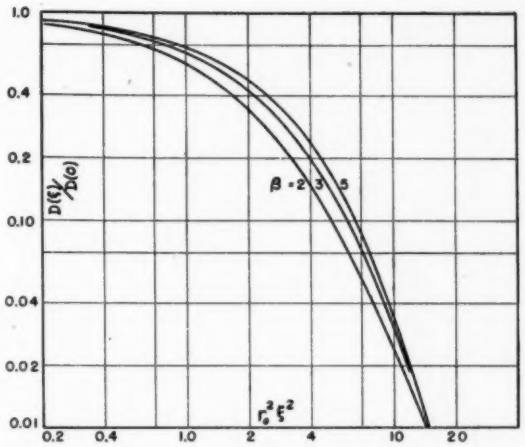

FIG. 3. Calculated scattering curves for Gaussian type of particle size distribution.

with

$$D(\beta, r_0\xi)=\beta^{-13/2}\tau^4\left\{(1+\tau^2)\exp(-\beta^2)\right.$$

$$\left.+\frac{\sqrt{\pi}}{2}\tau\exp(\tau^2-\beta^2)[2\tau^2+3][1+H(\tau)]\right\}, \quad (13)$$

where

$$\tau^2=\frac{3\beta^4}{3\beta^2+r_0^2\xi^2}$$

and

$$H(x)=\frac{2}{\sqrt{\pi}}\int_0^x\exp(-u^2)du.$$

From Eq. (12) it is seen that the angular dependence of the scattered intensity is wholly within the function D. This function has been evaluated for various values of β, and a typical family of curves is shown in Fig. 3. It should be mentioned that the parameter β in the distribution given by Eq. (11) determines the sharpness of the distribution, whereas r_0 is the average particle size.

The curves given in Fig. 3 can be used in the same fashion as those of Fig. 1 in interpreting experimental data. If the data can be matched to one of the curves, one expression of the type given by Eq. (11) suffices to describe the particle size distribution. If a simple matching cannot be performed it is necessary to perform the resolution process as outlined for the Maxwellian type of distribution.

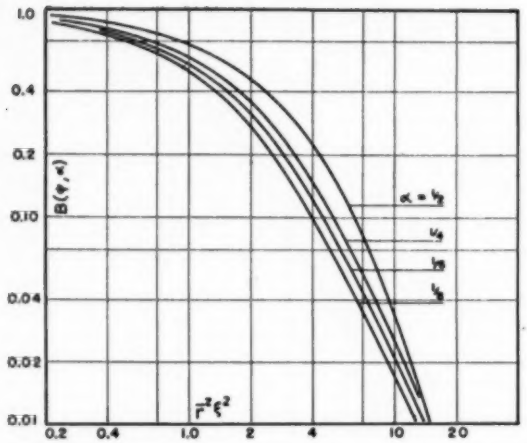

FIG. 4. Calculated scattering curves for rectangular type of particle size distribution.

Rectangular Distribution of Particle Size

Let the particle size distribution be represented by

$$M(r)=\frac{1}{r_2-r_1} \quad \text{for} \quad r_1\leqslant r\leqslant r_2$$

$$=0 \text{ otherwise.} \tag{14}$$

Equation (5) now integrates into

$$I(\xi)=\frac{2KI_e\rho_e^2(1-\alpha^4)}{(1-\alpha)(1+\alpha)^3}\bar{r}^3B(\psi,\alpha), \tag{15}$$

where

$$B(\psi,\alpha)=\frac{2}{(1-\alpha^4)\psi^4}\{(1+\alpha^2\psi^2)\exp(-\alpha^2\psi^2) - (1+\psi^2)\exp(-\psi^2)\} \tag{16}$$

with

$$\alpha=\frac{r_1}{r_2}, \quad \bar{r}=\frac{r_1+r_2}{2} \quad \text{and} \quad \psi^2=\frac{4}{3}\frac{\bar{r}^2}{(1+\alpha)^2}\xi^2. \tag{17}$$

In Eq. (17), $\bar{r}$ is the average particle size of the rectangular distribution. The angular variation of the scattered intensity is given by the function B, and this is graphed in Fig. 4. Curves of this type may be used to evaluate the particle size distribution in a fashion similar to that outlined above.

Comparison of the Scattering Curves Calculated for Different Distributions

The standard scattering curves which have been given in the preceding sections are all seen to possess three distinct features: (a) a flat section at the very small angles, (b) a curved region (the knee of the curve) at intermediate angles and (c) a steep, linear section at the larger angles. Because of the difficulty of making absolute intensity measurements, the interpretation of the experimental data is based on the shape of the experimental scattering curve, rather than on its absolute level. Since a fit between the observed curve and one of a family of calculated curves is made by effectively multiplying the ordinates and abscissae of the former by arbitrary factors (displacement in the vertical and horizontal directions until a match is found), it is seen that no significant match can be found if the experimental curve has been obtained in an angular region which does not include the curve knee.

In comparing the families of curves in Figs. 1, 3, and 4, it is found that some members in one family are very similar in shape to others in another family. Specifically, the curve for $\beta=2$ in Fig. 3 is very similar (over the angular range illustrated) to the curve for $\alpha=1/4$ in Fig. 4. This means that very accurate and extensive experimental data would be required in order to select the correct distribution form. However, the average particle sizes, obtained by matching an experimental curve with both of these calculated curves, agree very closely in value. Hence it appears that the curve matching method may introduce some ambiguity as to the distribution form but does lead to quite definite values of the average particle size for those cases in which the particle geometry is such that the Guinier scattering function can be used.

Figures 5 and 6 illustrate several particle size distribution curves and their appropriate calculated scattering curves. Distributions A, B, and

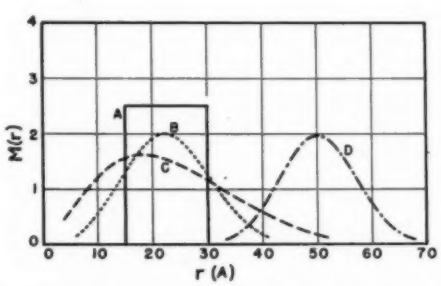

FIG. 5. Various types of particle size distributions.

C all have closely the same average particle size. The scattering curves for A, B, and C differ somewhat in the knee curvature with the sharpest distribution (A) showing the most curvature in the scattering curve. Distribution D corresponds to a considerably different average particle size and the resultant scattering curve differs markedly from the other curves.

Experimental Technique

A schematic diagram of the camera used in determining x-ray scattering at small angles is shown in Fig. 7. Basically the camera consists of two parts: (a) a crystal monochromator for insuring that x-rays of only one wave-length pass into the camera, and (b) the scattering chamber which is an evacuated cylinder about 15 cm in diameter and 60 cm in length. Both calcite and rocksalt crystals are used as monochromating crystals: the former when a high degree of collimation is desired and the latter when higher intensity and less collimation is found necessary in the primary x-ray beam. The x-radiation coming from the monochromator passes into the evacuated scattering chamber through a thin beryllium window and then through slits A and B of respective opening 0.13 by 1.6 and 0.13 by 2.5 mm. These slits serve both to limit the width of the primary beam and to eliminate the weaker component of the $K\alpha$ doublet when a calcite crystal is used. If only one slit is used, the well resolved $K\alpha$ doublet will pass through the camera, and be-

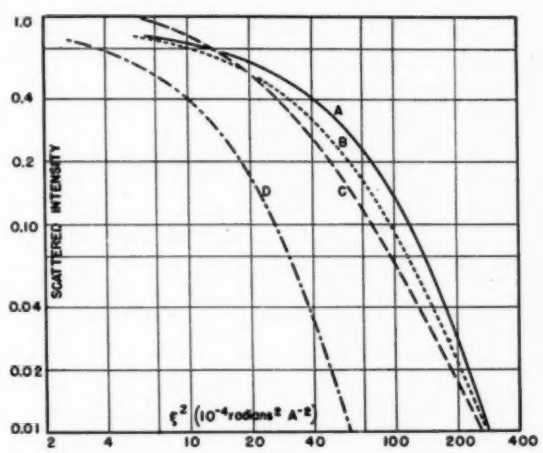

FIG. 6. Calculated scattering curves for the distributions given in Fig. 5.

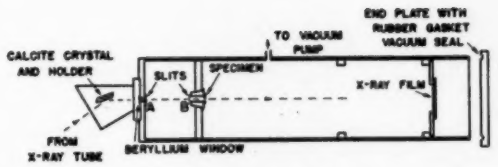

FIG. 7. Schematic diagram of small angle x-ray scattering camera.

cause of the angular separation of its components an unsymmetrical scattering pattern will be obtained. By proper alignment of the calcite crystal and the two slits, a homogeneous primary beam $K\alpha_1$, can be obtained. The half width of this beam after passage through slit B has been determined to be 0.10 mm, and at a distance of 50 cm beyond this slit this value has increased to only 0.14 mm. Thus it is seen that very little divergence is present in the beam reflected from the calcite crystal. This collimation is very desirable when the x-ray scattering is to be studied at the very small angles.

The scattering specimen is placed immediately behind the second slit and the scattered radiation recorded on a piece of photographic film located at one of several positions in the scattering chamber. It has been found convenient to pulverize the sample by grinding to a particle size of the order of one micron (much larger than the particles whose size is to be studied by the scattering) and to pack this powder into a rectangular opening about (4 by 2 mm) in a flat metal plate. The thickness of the plate determines the specimen thickness and this can be selected so as to be of optimum value. No binder has been found necessary in this technique. A beam stop of width 0.5 mm is placed 1 cm in front of the film to absorb the primary beam. Specimen to film distances from 60 to over 400 mm have been used, depending upon the range of scattering angles to be investigated. At the conclusion of the main scattering exposure of duration 10 minutes up to 30 hours depending upon the scattering power of the specimen, the beam stop is removed and a short exposure of the primary beam is made. A typical exposure is reproduced in Fig. 8. The image of the primary beam and the scattered radiation on either side of the beam can be seen.

The intensity distribution across the equator (perpendicular bisector of the primary beam

FIG. 8. Typical small angle x-ray scattering photogram.

image) of the film is determined with a microphotometer of scanning area 0.04 by 0.5 mm. Since the scattered x-ray intensity varies over a considerable range (several hundred or a thousand to one) a series of exposures are made with increasing exposure times in order that a large range of photographic density may be covered without exceeding the range in which the x-ray intensity is proportional to the density on any one film. After the individual films are microphotometered, the component intensity curves are combined by graphical matching into a complete scattering curve.

Some tests have been performed in which the use of crystal monochromated radiation is compared with that of filtered and unfiltered x-radiation. Figure 9 shows a series of scattering curves obtained for a sample of alumina with three types of primary radiation. The geometrical conditions of exposure (beam divergence, etc.) were kept unchanged from one exposure to another. It will be seen that intensity errors as large as 50 percent are obtained with unfiltered radiation. Upon filtering out the $K\beta$ radiation component, intensity errors as large as 20 percent are still present, caused by the white radiation band which is transmitted through the filter. The average particle size values as calculated from the filtered and crystal monochromated radiation curves differ by about 25 percent.

It has been mentioned earlier that slit openings, rather than pinholes, were used to define the primary beam. This has been done in order to utilize the increased intensity of scattering available with a slit system. Such technique, however, requires that a correction be applied to the data since the scattered intensity distribution will be altered. Hosemann[1] has considered the case in which the slit openings are infinitely long, but this situation will not be satisfied under the usual experimental conditions. The general theory of slit correction has been worked out and will be outlined in Appendices A and B of this report. As will be shown there, two methods of applying the correction are available and either one may be used.

Experimental Results

The above procedure of analysis has been applied to several dozen finely divided samples in this laboratory. In general, scattering data were taken over the scattering angle range from about 0.2 to 2.5 degrees. As mentioned above, for the best interpretation of the data it should cover the region of interesting curvature. This region will depend in an approximately inverse fashion on the average particle size: with small particle systems the larger scattering angles are most interesting, while the smaller scattering angles are most profitably studied for systems of large average particle size.

In view of the interpretative assumptions discussed earlier, it is highly desirable to compare the results of x-ray scattering analysis with those obtained by other independent techniques. With crystalline materials the crystal size (as contrasted with the particle size) can be evaluated from studies of the width of x-ray diffraction lines, and for both crystalline and amorphous materials, low temperature gas adsorption can be used for obtaining information on the state of subdivision. Both methods have been used in our studies wherever possible.

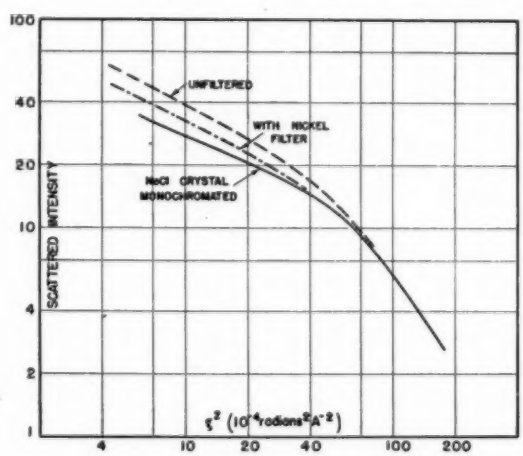

FIG. 9. Comparison of experimental scattering curves obtained with unfiltered, filtered and crystal monochromated primary radiation.

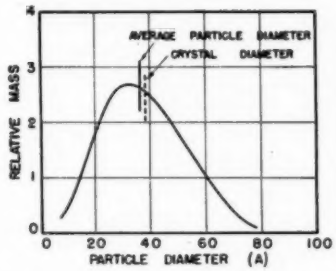

FIG. 10. Particle size distribution obtained for a sample of alumina gel.

In determining the crystal size, the Jones[16] technique of correcting the line broadening for geometrical effects was used. Values of the Scherrer constant used in the crystal size evaluation were those given by Stokes and Wilson[17] and Murdock.[18]

A typical particle size distribution[19] obtained for a sample of alumina gel is shown in Fig. 10. The experimental data and their analysis for this alumina gel have been given in Fig. 2. From the distribution curve, an average particle size can be readily evaluated. For the distribution given in Fig. 10 the average particle size has been determined as 36 angstroms and this has been marked on the distribution curve by the full vertical line. Also shown on the distribution curve by the broken vertical line is the crystal size (38 angstroms) as determined from the diffraction line broadening. The agreement between the crystal and particle sizes is well within the experimental error.

Figure 11 illustrates the correlation which has been obtained between average crystal and average particle sizes. The line drawn represents equivalence of the two values. It is to be emphasized that the particle size may be either equal to or larger than the crystal size, since agglomeration of crystals into larger particles may be present. Crystals larger than particles would not be expected however. The four shaded points to the lower right of the line are believed to signify this agglomeration effect. These four materials were Al_2O_3-MoO_3 catalysts which had been prepared in a special manner. Independent evidence supporting this hypothesis is obtained from the gas adsorption studies in which the particle size correlated better than the crystal size with the specific surface.

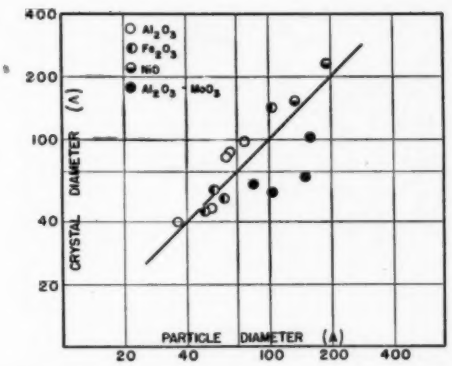

FIG. 11. Correlation between average crystal and particle sizes for a variety of materials. The solid points are believed to represent crystal agglomeration into larger particles.

The unshaded points in Fig. 11 indicate fair agreement between the crystal and particle size. It would appear from the general sequence of the data that the crystal size is a little larger than the particle size, and this may reflect the difference in degree of weighting which the two determinations afford. Jones[16] has shown that the crystal size values will be weighted to the larger sizes and this may account for the observed displacement of values from the line.

Low temperature gas adsorption analysis has been widely used[20] in the study of finely divided solids and this technique provides interesting data for comparison with the x-ray scattering data. One can easily determine the specific surface (surface area per unit mass) and over-all porosity of such solids by this method. It can be shown that the specific surface S of a collection of spherical particles of diameter D is given by

$$S = -\frac{6\int_0^\infty \frac{M(D)}{D}dD}{\rho\int_0^\infty M(D)dD} \tag{18}$$

$$= \frac{6}{\rho\bar{D}} \tag{19}$$

[16] F. W. Jones, Proc. Roy. Soc. **166**, 27 (1938).
[17] A. R. Stokes and A. J. C. Wilson, Proc. Camb. Phil. Soc. **38**, 313 (1942) and **40**, 197 (1944).
[18] C. C. Murdock, Phys. Rev. **63**, 223 (1943).
[19] When using the Guinier exponential scattering function, the particle size distribution is obtained in terms of the radius of gyration of the particle. For spheres, the particle diameter is $2(5/3)^{\frac{1}{2}}$ times the radius of gyration.
[20] P. H. Emmett, Ind. Eng. Chem. **37**, 639 (1945).

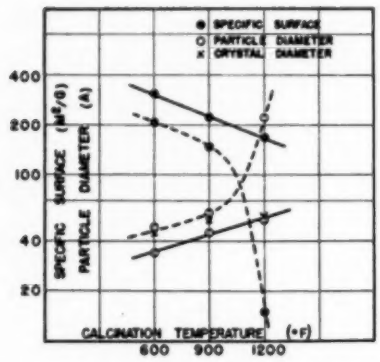

FIG. 12. Average particle size and specific surface variation with calcination temperature for two iron oxide preparations. Solid line—preparation *A*, broken line—preparation *B*.

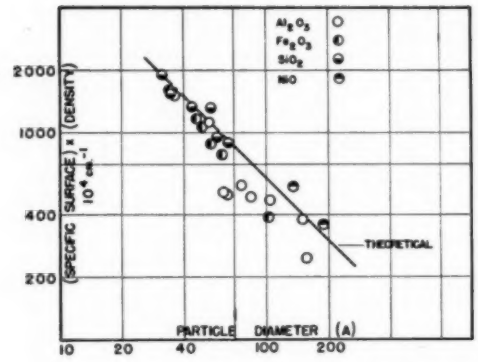

FIG. 13. Correlation between specific surface and particle size for a variety of materials.

where ρ is the particle density (not over-all apparent density) and $\bar{D}$ is an average particle size. Thus a linear relationship should exist between $S\rho$ and $1/\bar{D}$.

The specific surface and average particle sizes for a large number of materials have been determined.[21] Typical of the results of such investigations have been those published[7] for various silica-alumina preparations. It was found there that modifications in preparation technique brought about changes in the specific surface of the gel which were followed in all cases by appropriate qualitative changes in the average particle size as determined by small angle x-ray scattering technique.

Figure 12 illustrates additional comparative data obtained by gas adsorption and x-ray scattering analyses. Two preparations of iron oxide were heat treated at the temperatures shown on this graph and the specific surface and average particle size values were obtained. It is seen that for preparation *B* the specific surface falls rapidly and the particle size increases rapidly upon heat treatment about 1000°F. Preparation *A* on the other hand is seen to be quite stable in regard to either measurement at temperatures through 1200°F. Also shown on the graph are several crystal size values and these are seen to agree closely with the particle size determinations.

Equation (19) predicted a linear relationship between $S\rho$ and $1/\bar{D}$ and Fig. 13 summarizes our data with regard to this. The line shown on this graph is that given by Eq. (19). Considerable deviations are to be noted for individual points but the general trend of the data follows fairly well that to be expected. Data for both amorphous and crystalline materials are represented on this graph.

[21] We are indebted to Dr. P. B. Elkin for supplying us with the gas adsorption results.

ACKNOWLEDGMENT

It is a pleasure to acknowledge the stimulation and encouragement received from Professor B. E. Warren of M.I.T., and several illuminating discussions of interpretational details with Professor A. L. Patterson of Bryn Mawr.

APPENDIX A. METHOD OF CORRECTING THE SCATTERED INTENSITY DISTRIBUTION OBTAINED WITH A SLIT-SHAPED BEAM TO THAT FOR A PINHOLE BEAM

The experimental data given in the body of this paper were all taken with a slit-shaped primary beam, whereas the theory given is applicable only to data taken for a pinhole beam of very small cross section. Fortunately it is possible to change the experimental intensity distribution into a form equivalent to that which would have been obtained if a pinhole primary beam had been used. The theory of data interpretation given in the body of this paper and the companion paper can then be applied to this modified scattering curve.

A ray diagram of the x-ray optics in the scattering camera is shown in Fig. 14. The x-rays coming from the crystal or target focal line (not shown), in front of the first slit (of length $2l_1$), fan

out from this slit in a vertical plane. Those which pass through the second slit (length $2l_2$), and strike the specimen, are scattered through the scattering angle and may be either (1) recorded on a piece of photographic film placed in a plane perpendicular to the camera axis, or (2) detected by a Geiger counter behind a scanning slit opening. In either case the intensity distribution is determined by means of a scanning slit of finite length ($2y_0$) at different positions along the equator axis. It is obvious that the intensity at any point in the scanning area is a result of the superposition of various intensity elements as scattered through different scattering angles by different scattering elements in the sample.

Consider a specimen element ds which is struck by a ray making an angle η with the camera axis. From the camera geometry it is seen that

$$\begin{aligned} d&=\epsilon L,\\ u&=\alpha L,\\ g&=\eta L+s, \end{aligned} \tag{20}$$

since all of the angles under consideration are small (less than 3°). The angle α is characteristic of the position of the scanning slit in the plane of intensity measurement. Since

$$d^2=u^2+(g-y)^2,$$

it follows that

$$\epsilon^2=\alpha^2+\left(\eta+\frac{s-y}{L}\right)^2,$$

$$=\alpha^2+\sigma^2 \tag{21}$$

with

$$\sigma=\eta+\frac{s-y}{L}. \tag{22}$$

$g(\alpha)$ will be considered to represent the intensity striking the scanning area with center at angular position α, and $I(\epsilon)ds$ the intensity of scattering at an angle ϵ by a specimen element ds. Since $g(\alpha)$ is the summation of the intensity produced by all specimen elements and all primary rays, it follows upon averaging over the scanning area, that

$$g(\alpha)=\frac{1}{2y_0}\int_{-y_0}^{y_0}dy\int_{-l_2}^{l_2}ds\int_{(s-l_1)/L_3}^{(s+l_1)/L_3}I(\epsilon)d\eta. \tag{23}$$

The problem remaining is the determination of $I(\epsilon)$ when $g(\alpha)$ is known. Suppose $I(\epsilon)$ to be represented by

$$I(\epsilon)=\sum_i T_i\exp(-t_i^2\epsilon^2), \tag{24}$$

with as many terms included in the summation as are necessary to describe the function. It follows from Eqs. (21) and (23) that

$$g(\alpha)=\frac{1}{2y_0}\sum_i T_i\exp(-t_i^2\alpha^2)\int_{-y_0}^{y_0}dy\int_{-l_2}^{l_2}ds \times\int_{(s-l_1)/L_3}^{(s+l_1)/L_3}\exp(-t_i^2\sigma^2)d\eta, \tag{25}$$

$$=\sum_i T_i f(t_i)\exp(-t_i^2\alpha^2), \tag{26}$$

$$=\sum_i T_i'\exp(-t_i^2\alpha^2), \tag{27}$$

with

$$f(t_i)=\frac{1}{2y_0}\int_{-y_0}^{y_0}dy\int_{-l_2}^{l_2}ds\int_{(s-l_1)/L_3}^{(s+l_1)/L_3}\times\exp(-t_i^2\sigma^2)d\eta, \tag{28}$$

and

$$T_i'=T_i f(t_i). \tag{29}$$

The function $f(t_i)$ is independent of α and depends only upon values of t_i and the camera geometry, and the latter remains fixed during the various exposures of one specimen (assuming the specimen-to-detector distance remains unchanged). Equations (24) and (27) permit the desired transformation of $g(\alpha)$ into $I(\epsilon)$ in the following fashion. If $g(\alpha)$ can be represented by a series of exponential terms, each with known values of t_i and T_i', then $I(\epsilon)$ can be represented by the same exponential series but with different term amplitudes, T_i.

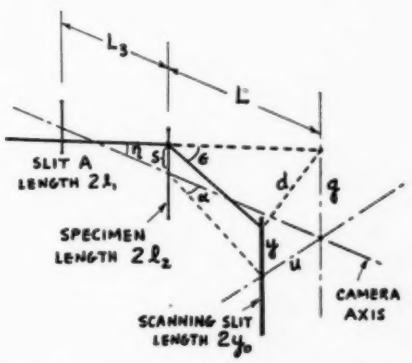

FIG. 14. Ray diagram of the x-ray optics in the scattering camera.

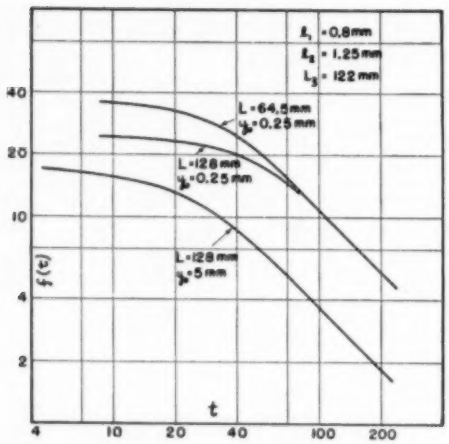

FIG. 15. Slit correction function calculated for various experimental conditions.

The triple integral in Eq. (28) has been integrated with the result that

$$\begin{aligned}\frac{4hct_i^3}{L_3}f(t_i)=\frac{\sqrt{\pi}}{2}\{&[1+2t_i^2(a+c)^2]H[t_i(a+c)]\\&+[1+2t_i^2(c-a)^2]H[t_i(c-a)]\\&-[1+2t_i^2(b+c)^2]H[t_i(b+c)]\\&-[1+2t_i^2(c-b)^2]H[t_i(c-b)]\}\\&+t_i\{(a+c)\exp[-t_i^2(a+c)^2]\\&+(c-a)\exp[-t_i^2(c-a)^2]\\&-(b+c)\exp[-t_i^2(b+c)^2]\\&-(c-b)\exp[-t_i^2(c-b)^2]\},\end{aligned}\tag{30}$$

where

$$\begin{aligned}h&=1+\frac{L_3}{L},\\a&=\frac{hl_2+l_1}{L_3},\\b&=\frac{hl_2-l_1}{L_3},\\c&=y_0/L,\end{aligned}\tag{31}$$

and

$$H(x)=\frac{2}{\sqrt{\pi}}\int_0^x\exp(-v^2)dv.$$

Equation (30) has been evaluated numerically for various t_i and the function $f(t_i)$ is graphed in Fig. 15 for the experimental conditions generally used in our particular scattering camera. In the present study a microphotometer slit opening of length 0.5 mm was used for scanning across the photographic film and typical curves for this scanning area are given in Fig. 15. If a scanning slit of longer length had been used (as would have been done with a Geiger counter) the values of $f(t_i)$ would have been changed and this is also illustrated in Fig. 15. It is to be emphasized that $f(t_i)$ depends only upon the camera geometry and need be evaluated just once.

The representation of $g(\alpha)$ by a series of exponential terms can be conveniently performed graphically. When the experimental intensity distribution is graphed on log intensity *versus* α^2 axes, the curve can be resolved into the sum of a series of straight lines (as is done in analyzing complex radioactive decay curves, for instance). Each straight line corresponds to one of the terms in Eq. (27) and t_i and T_i' can be determined from the slope and intensity axis intercept, respectively, of the straight line. Knowing the values of $f(t_i)$ from Fig. 15, the true scattering curve (for pinhole conditions) can then be reconstructed by use of Eq. (24).

APPENDIX B. SIMPLIFIED METHOD OF APPLYING THE SLIT CORRECTION WHEN THE EXPONENTIAL SCATTERING FUNCTION IS USED

In Appendix A a general method of correcting the scattered intensity for the slit geometry is given. When the Guinier scattering function is used in interpreting the data, a second and more easily performed procedure is available for taking into account the slit effect. In this procedure the correction is applied to the final particle size distribution rather than to the original intensity data.

The basic integral expression for the intensity of x-ray scattering at an angle ϵ by a small scattering specimen ds has been given (Eq. (5)) as

$$I(\xi)ds=KI_e\rho_e^2\int_0^\infty M(r)r^3\exp(-\tfrac{1}{3}r^2\xi^2)drds,\tag{32}$$

with $\xi=(2\pi/\lambda)\epsilon$. When many specimen elements and many primary and scattered rays are contributing to the observed intensity, additional integrations must be performed as has been discussed in Appendix A. Applying Eqs. (21) and (23) to (32), the observed intensity dis-

tribution is given by

$$g(\alpha)=KI_e\rho_e^2\int_0^\infty M(r)r^3 \times\exp\left(-\frac{4\pi^2}{3\lambda^2}r^2\alpha^2\right)dr\frac{1}{2y_0}\int_{-y_0}^{y_0}dy\int_{-l_2}^{l_2}ds \times\int_{(s-l_1)/L_3}^{(s+l_1)/L_3}\exp\left(-\frac{4\pi^2}{3\lambda^2}r^2\sigma^2\right)d\eta, \quad (33)$$

$$=KI_e\rho_e^2\int_0^\infty M(r)r^3 \times\exp\left[-\frac{4\pi^2}{3\lambda^2}r^2\alpha^2\right]drf\left(\frac{2\pi}{\sqrt{3}\lambda}r\right), \quad (34)$$

with $f[(2\pi/\sqrt{3}\lambda)r]$ given by Eq. (28). Let

$$M(r)f\left(\frac{2\pi}{\sqrt{3}\lambda}r\right)=M'(r). \quad (35)$$

It follows that

$$g(\alpha)=KI_e\rho_e^2\int_0^\infty M'(r)r^3\exp\left[-\frac{4\pi^2}{3\lambda^2}r^2\alpha^2\right]dr, \quad (36)$$

and this expression has the same form as the original integral expression for pinhole conditions. Thus the function $M'(r)$ can be obtained by procedures given in the body of this paper. Following this, the true particle size distribution can be derived with the use of Eq. (35).

Back Number Prices

ATTENTION is called to the new price scale for single copies and back volumes of this journal as listed on the second cover page. The new price scale was effective March 1, 1947.

The increase is the result of increased handling costs and the fast-diminishing supply of older issues. The increase will make it possible for exhausted issues to be reprinted with no great burden placed on current subscribers for this reprinting.

X-Ray Scattering at Small Angles by Finely-Divided Solids. II. Exact Theory for Random Distributions of Spheroidal Particles

L. C. Roess and C. G. Shull*
Beacon Research Laboratory of The Texas Company, Beacon, New York
(Received August 29, 1946)

The theory of the scattering of x-rays at small angles is given for a continuous distribution in size of randomly spaced and oriented spheroidal particles having arbitrary, but fixed, shape. Families of scattering curves are presented for spheres, and for spheroids ranging in shape from flat disks to long rods. Both Maxwellian and rectangular types of particle mass distribution are used. A fit between the experimental and a calculated scattering curve enables one, under favorable circumstances, to determine the mass distribution in the test sample. However, an unambiguous interpretation of the experimental scattering curve on the basis of the small angle scattering theory is not possible without additional evidence from independent investigations of such quantities as particle shape and sample specific surface.

INTRODUCTION

IT has been pointed out in the preceding paper[1] that a reasonable, though by no means entirely unambiguous, approach to the interpretation of x-ray scattering at small angles can result from the calculation of the scattering to be expected from assumed mass distributions of particles having a definite shape, followed by an estimation of the actual mass distribution and particle shape by obtaining a fit between the observed scattered intensity curve and one of a series of calculated intensity curves. It is the object of this paper to present the exact theory for the x-ray scattering at small angles by a continuous distribution of randomly spaced spheroidal particles having an arbitrary, but fixed, shape. Scattering by spheres is, of course, a special case of the theory, while the scattering by disks of finite radius but vanishing thickness, and by rods of finite length but vanishing radius form two limiting cases.

ASSUMPTIONS

It is desirable to state clearly and exactly the assumptions on which the calculations are based:

1. The particles have whatever form of random spacing necessary to produce incoherency in the radiation scattered by individual particles, so that the total intensity is the sum of the individual intensities.
2. The particles have random orientation.
3. The incident x-ray beam is composed of monochromatic and parallel rays, and is of negligibly small cross-sectional extent.
4. The interaction of the scattered radiation with the incident radiation inside the sample to produce an index of refraction is ignored. This effect should be noticeable only at extremely small angles.[2] A closely related assumption is that multiple scattering can be neglected.
5. The effects of finite sample size are ignored. They also should be noticeable only at extremely small angles.
6. The effects of variations on an atomic scale of the electron density distribution inside a particle are ignored.
7. The particles all have the same shape.[3]
8. Absorption of x-radiation inside a particle can be neglected.

GENERAL THEORY

The general equation for the scattered intensity $I(\xi)$ is[4]

$$I(\xi)=AI_e\rho_e^2\int_0^\infty V^2(R)N(R)\langle S(R,\xi)\rangle_M dR, \quad (1)$$

$$=AI_e\frac{\rho_e^2}{\rho}\int_0^\infty V(R)M(R)\langle S(R,\xi)\rangle_M dR, \quad (2)$$

with

$$\xi=\frac{4\pi}{\lambda}\sin\theta, \quad (3)$$

λ = wave-length,
$2\theta=\epsilon$ = scattering angle,

* Now at Clinton Laboratories, Oak Ridge, Tennessee.
[1] C. G. Shull and L. C. Roess, J. App. Phys. 18, 295 (1947).
[2] R. von Nardroff, Phys. Rev. 28, 240–246 (1926).
[3] The mathematical methods used in this paper have also been applied to calculate the scattered intensity for particle distributions varying in both shape and size.
[4] R. Hosemann, Zeits. f. Physik 113, 751–768 (1939). See also Eq. (4) of reference 1.

I_e = Thomson scattering factor for a single electron,[5]
A = absorption factor,[6]
ρ_e = average electron density of particle, electrons per cm^3,
ρ = mass density of individual particles, gram cm^{-3}.

$V(R)$ is the volume of a particle characterized by the size parameter R, $\langle S(R, \xi)\rangle_{Av}$ is the scattering function (the shape function[7] or form factor for the particle averaged over-all orientations), and $N(R)dR$ and $M(R)dR$ are, respectively, the number and the mass of the particles having size parameters in the range R, dR.

SHAPE FUNCTIONS FOR SPHEROIDS

Patterson[7] and Guinier[8] have shown that the shape function for a spheroid having principal axes R, R, vR in a system of Cartesian coordinates (x, y, z) is

$$S(R\xi, v) = S(u) = 9\left(\frac{\sin u - u\cos u}{u^3}\right)^2, \quad (4)$$

with

$$u = R\xi(\sin^2\vartheta + v^2\cos^2\vartheta)^{\frac{1}{2}}. \quad (5)$$

In Eq. (5), ϑ is the angle between the z axis and the difference $\mathbf{s}-\mathbf{s}_0$ between the unit vectors $\mathbf{s}_0$ and $\mathbf{s}$ which specify the direction of the incident and scattered beams, respectively.

The effect of random orientation of the spheroids can be obtained most simply by considering the spheroid fixed, and averaging over-all directions of the vector $\mathbf{s}-\mathbf{s}_0$. This is equivalent to integrating S over the surface of a sphere, and gives

$$\langle S(R\xi, v)\rangle_{Av} = \frac{1}{4\pi}\int_0^{\pi}\int_0^{2\pi} S[R\xi(\sin^2\vartheta + v^2\cos^2\vartheta)^{\frac{1}{2}}]\sin\vartheta d\vartheta d\varphi,$$

or, putting $x = \cos\vartheta$,

$$\langle S(R\xi, v)\rangle_{Av} = \int_0^1 S[R\xi(1+(v^2-1)x^2)^{\frac{1}{2}}]dx. \quad (6)$$

It follows directly from formulas given by Watson[9] that Eq. (4) may be written

$$S(u) = \frac{9\pi}{2}\frac{J_{3/2}{}^2(u)}{u^3}, \quad (7)$$

$$= {}_1F_2(2; 4, (5/2); -u^2). \quad (8)$$

The generalized hypergeometric function is defined[10] by

$${}_pF_q(\alpha_1, \alpha_2, \cdots\alpha_p; \beta_1, \beta_2, \cdots\beta_q; z) = \sum_{m=0}^{\infty}\frac{(\alpha_1)_m(\alpha_2)_m\cdots(\alpha_p)_m z^m}{m!(\beta_1)_m(\beta_2)_m\cdots(\beta_q)_m}, \quad (9)$$

with

$$(\alpha)_0 = 1; \quad (\alpha)_m = \alpha(\alpha+1)\cdots(\alpha+m-1). \quad (10)$$

Obviously ${}_pF_q$ is an integral function when $q \geqslant p$.

Substituting Eq. (8) in Eq. (6), and integrating term by term, using[11]

$$\int_0^1 [1+(v^2-1)x^2]^m dx = {}_2F_1(-m, \tfrac{1}{2}; \tfrac{3}{2}; 1-v^2), \quad (11)$$

one obtains

$$\langle S(R\xi, v)\rangle_{Av} = \sum_{m=0}^{\infty}\frac{(2)_m(-R^2\xi^2)^m}{m!(4)_m(5/2)_m} \times {}_2F_1(-m, \tfrac{1}{2}; \tfrac{3}{2}; 1-v^2), \quad (12)$$

$$= {}_1G_2(2; 4, (5/2); -R^2\xi^2, v), \quad (13)$$

where we define

$${}_pG_q(\alpha_1, \alpha_2, \cdots\alpha_p; \beta_1, \beta_2, \cdots\beta_q; z, v) = \sum_{m=0}^{\infty}\frac{(\alpha_1)_m(\alpha_2)_m\cdots(\alpha_p)_m z^m}{m!(\beta_1)_m(\beta_2)_m\cdots(\beta_q)_m} \times {}_2F_1(-m, \tfrac{1}{2}; \tfrac{3}{2}; 1-v^2). \quad (14)$$

For spherical particles, $v=1$, ${}_2F_1(-m, \frac{1}{2}; \frac{3}{2}; 0) = 1$, and $\langle S(R\xi, 1)\rangle_{Av} = S(R\xi)$.

In the limit $v \to 0$

$${}_2F_1(-m, \tfrac{1}{2}; \tfrac{3}{2}; 1-v^2) \to {}_2F_1(-m, \tfrac{1}{2}; \tfrac{3}{2}; 1) = \frac{(1)_m}{(\frac{3}{2})_m}, \quad (15)$$

so that

$$\langle S(R\xi, 0)\rangle_{Av} = {}_2F_3(1, 2; 4, (5/2), \tfrac{3}{2}; -R^2\xi^2). \quad (16)$$

[5] Because of the small angular range involved, the state of polarization of the incident beam has negligible effect on the angular variation of intensity.
[6] The absorption may be assumed independent of angle for the small angles under discussion.
[7] A. L. Patterson, Phys. Rev. **56**, 972–977 (1939).
[8] A. Guinier, Thèses (Masson et Cie, Paris, 1939), or Ann. de Physique **12**, 161–237 (1939).
[9] G. N. Watson, *Theory of Bessel Functions* (Cambridge University Press, Cambridge, 1922), pp. 54 and 147.
[10] For example, reference 9, p. 100.
[11] Note that Eq. (11) is valid for any value of m if $v \neq 0$.

This is the scattering function for a disk of radius R and vanishingly small thickness.

If we let $v\to\infty$, but simultaneously $R\to 0$ in such a way that $Rv\to L$, the spheroid approaches a rod of length $2L$ and vanishingly small radius. The scattering function for such a rod may be obtained most simply from Eq. (6).

$$\lim_{\substack{R\to 0\\ v\to\infty\\ Rv\to L}}\langle S(R\xi,v)\rangle_{Av}=\langle S_\infty(L\xi)\rangle_{Av}=\int_0^1 S(L\xi x)dx \quad (17)$$

$$={}_2F_3(\tfrac{1}{2},2;4,(5/2);\tfrac{3}{2};-L^2\xi^2), \quad (18)$$

since

$$\frac{1}{2m+1}=\frac{(\frac{1}{2})_m}{(\frac{3}{2})_m}. \quad (19)$$

By direct integration, using Eq. (4), it can readily be shown that

$$\langle S_\infty(x)\rangle_{Av}=\frac{6}{5}\frac{Si(2x)}{x}-\frac{3}{2x^4}-\frac{9}{10x^6}$$
$$+\frac{3\cos 2x}{5x^2}\left(1-\frac{1}{2x^2}+\frac{3}{2x^6}\right)+\frac{3}{10}\frac{\sin 2x}{x^3}\left(1+\frac{6}{x^2}\right), \quad (20)$$

in which

$$Si(x)=\int_0^x\frac{\sin t}{t}dt. \quad (21)$$

A similar closed expression for $\langle S(R\xi,0)\rangle_{Av}$ has not been found.

MASS DISTRIBUTION FUNCTIONS

Hosemann[4] introduced the Maxwellian type of mass distribution function[12]

$$M(R)=B\left(\frac{R}{R_0}\right)^n e^{-(R/R_0)^2};$$
$$B=\frac{2}{R_0\Gamma\left(\frac{n+1}{2}\right)}, \quad (22)$$

which has a maximum at

$$R_{\max}=(n/2)^{\frac{1}{2}}R_0, \quad (23)$$

and showed that a wide variety of distribution forms could be obtained by varying the parameters n and R_0. Consideration of the more general function

$$M(R)=B\left(\frac{R}{R_0}\right)^n e^{-(R/R_0)^m} \quad (24)$$

has shown that no advantage with respect to variety of the mass distribution form is gained by choosing $m\neq 2$, while considerable simplicity is lost in evaluating the integral in Eq. (2).

It must be pointed out here that, since the incident beam has a finite cross section, the effective scattering specimen has a finite volume, so that

$$M(R)=0, \quad R>R',$$

where R' is of the order of the beam radius. A mass distribution function expressed by

$$\left.\begin{aligned} M(R)&=BR^n(R'-R)^\mu, && 0\le R\le R'\\ &=0, && R>R'\end{aligned}\right\} \quad (25)$$

in which μ is very large, has been tried and found to give results essentially the same as the Maxwellian type. The increased simplicity of the analysis using the latter type is thus sufficient to justify its use, despite the infinite range of R.

INTENSITY SCATTERED BY MAXWELLIAN MASS DISTRIBUTIONS

Since for a spheroid

$$V(R)=\frac{4\pi}{3}vR^3, \quad (26)$$

substitution of Eqs. (26), (22), and (13) in Eq. (2), and term by term integration gives, using Eq. (14),

$$I(\xi,v)=K\sum_{m=0}^{\infty}\frac{(2)_m\left(\frac{n+4}{2}\right)_m(-R_0^2\xi^2)^m}{m!(4)_m(5/2)_m}$$
$$\times{}_2F_1(-m,\tfrac{1}{2};\tfrac{3}{2};1-v^2), \quad (27)$$

$$=K\,{}_2G_2\left(2,\frac{n+4}{2};4,(5/2);-R_0^2\xi^2,v\right), \quad (28)$$

with

$$K=AI_e\frac{4\pi vR_0^3\rho_e^2}{3\rho}\frac{\Gamma\left(\frac{n+4}{2}\right)}{\Gamma\left(\frac{n+1}{2}\right)}. \quad (29)$$

[12] With the value of B given in Eq. (22), the total mass is unity.

Equation (27) is the formal solution of the scattering problem. It is worth noting that the parameter R_0 enters directly as a scale factor, while the parameter n affects the shape of the intensity function.

The series in Eq. (27) converges for all values of ξ, R_0, n, and v. However, numerical calculation by direct summation of the series becomes impractical for large values of $R_0\xi$ or $R_0\xi v$. In these ranges asymptotic series must be used for the calculation; the form of these series depends upon the value of v. Three ranges of v are important:

$$v \ll 1; \quad v \cong 1; \quad \text{and} \quad v \gg 1.$$

In each range, a suitable form of ${}_2F_1(-m, \frac{1}{2}; \frac{3}{2}; 1-v^2)$ must be used.[13]

It can be shown that Eq. (27) can be written

$$I(\xi,v)=\frac{K}{(1-v^2)^{\frac{1}{2}}} \times\left\{ {}_3F_3\left(1, 2, \frac{n+4}{2}; 4, \frac{5}{2}, \frac{3}{2}; -R_0^2\xi^2\right) -\frac{v^2}{2}\sum_{m=0}^{\infty}\frac{\left(\frac{n+4}{2}\right)_m(-R_0^2\xi^2v^2)^m}{(4)_m(5/2)_m} \times {}_2F_1(\tfrac{1}{2}, m+1; m+2; v^2)\right\}. \quad (30)$$

Equation (30), while valid for all values of v, is useful for numerical calculation when $v \ll 1$. For large $R_0\xi$ an asymptotic expansion[13] of the first term is required.

Equation (27) can also be written

$$I(\xi,v)=K\sum_{m=0}^{\infty}\frac{(2)_m\left(\frac{n+4}{2}\right)_m(-R_0^2\xi^2)^m}{m!(4)_m(5/2)_m} \times {}_3F_3\left(2+m, \frac{n+4}{2}+m, \frac{1}{2}; 4+m, \frac{5}{2}+m, \frac{3}{2}; -R_0^2\xi^2(v^2-1)\right). \quad (31)$$

Equation (31) is also valid for all values of v and, when used with the asymptotic expansion[13] for the ${}_3F_3$ terms, is suitable for numerical calculation when $v \gg 1$.

When $v \cong 1$, the series in Eq. (27) suffices for numerical calculation when used with its asymptotic expansion[13] for large $R_0\xi$.

INTENSITY SCATTERED BY RECTANGULAR MASS DISTRIBUTIONS

If the mass distribution is defined as follows

$$\left.\begin{aligned} M(R)&=\frac{1}{R_2-R_1}, \quad R_1 \leqslant R \leqslant R_2 \\ &=0, \quad \text{otherwise}\end{aligned}\right\} \quad (32)$$

so that it is normalized to unit mass, the scattered intensity given by Eq. (2) becomes, using Eq. (26),

$$I(\xi,v)=\frac{K'}{R_2-R_1} \times\{R_2^4{}_2G_3(2, 2; 4, 3, (5/2); -R_2^2\xi^2, v) -R_1^4{}_2G_3(2, 2; 4, 3, (5/2); -R_1^2\xi^2, v)\}, \quad (33)$$

with

$$K'=AI_e\frac{4\pi v\rho_e^2}{3\rho}. \quad (34)$$

If we put $\alpha=R_1/R_2$, Eq. (33) can be written

$$I(\xi,v)=\frac{K'R_2^3}{1-\alpha} (2)_m(2)_m\,{}_2F_1(-m, \tfrac{1}{2}; \tfrac{3}{2}; 1-v^2) \times\sum_{m=0}^{\infty}\frac{\times(-R_2^2\xi^2)^m(1-\alpha^{4+2m})}{m!(4)_m(3)_m(5/2)_m}. \quad (35)$$

The series (divided by $1-\alpha^4$) has been calculated for $v=1$ and $\alpha=0$, 0.5, 0.9, and 1.0. (When $\alpha=1$, the intensity is that produced by a group of spheres all having the same radius R_2, and is given by Eq. (8) with $u=R_2\xi$.)

NUMERICAL RESULTS

Calculated scattered intensity curves[14] are plotted on a double logarithmic scale on Figs. 1 to

[13] A summary of the formulas giving the relevant asymptotic series, as well as a discussion of the procedure used in obtaining them, has been prepared and is available from the authors on request.

[14] Numerical values have been tabulated, and are available from the authors upon request.

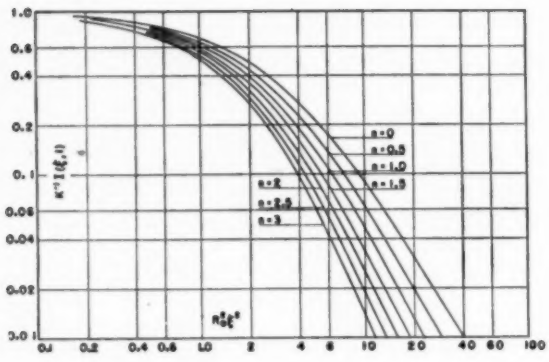

FIG. 1. Calculated intensity scattered by Maxwellian distributions of spheres, $v=1$ (Eq. (27)).

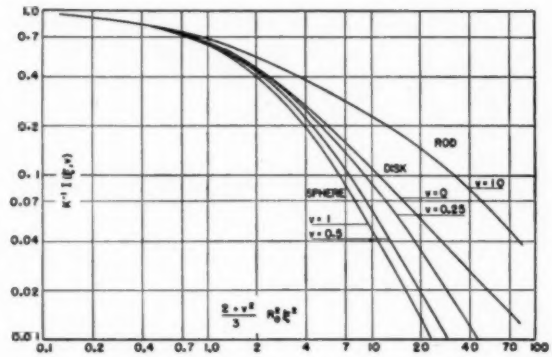

FIG. 2. Calculated intensity scattered by the same Maxwellian distribution of spheroids having various shapes.

5. Figure 1 shows the effect of varying the parameter n (which controls the form of the mass distribution) on the shape of the angular distribution of the intensity scattered by a Maxwellian distribution of spheres. The increased curvature observed as n increases is associated with an increased sharpness in the mass distribution. As is shown by the asymptotic expansions, all curves for $n>0$[15] approach the same slope (-2) as $R_0^2\xi^2$ becomes large.

Figure 2 shows the effect of particle shape ($v=0$, $\frac{1}{4}$, $\frac{1}{2}$, 1, 10) on the angular distribution of the intensity scattered by a mass distribution having a fixed form ($n=1$). The abscissa are chosen proportional to the radius of gyration[16] of the particle in order to make the curves merge at small values of $R_0\xi$. Distinct differences are apparent between the disk-shaped ($v=0$) and rod-shaped ($v=10$) particles. The smaller slopes at large $R_0\xi$ values are predicted by the asymptotic expansions: for $v=0$ the limiting slope is -1 and for v very large the limiting slope is $-\frac{1}{2}$.

Figures 3 and 4 show the effect of varying n on the shape of the angular distribution of the intensity scattered by oblate spheroids having the fixed shape parameters $v=0$ and $v=\frac{1}{4}$, respectively.

Figure 5 shows the calculated angular distribution of scattered intensity produced by rectangular mass distributions (cf. Eq. (32)) having various values of $\alpha=R_1/R_2$. The curvature is considerably greater than that associated with the Maxwellian distributions. Also, although it is not shown on the plot, the scattered intensity shows a series of maxima and minima, for $\alpha=1$, 0.9, and 0.5 at $R_2\xi$ values greater than those for which the curves are drawn.

It may be shown by superposition that the curve for $v=\frac{1}{2}$, $n=1$ on Fig. 2 has very nearly the same shape as that for $v=1$, $n=\frac{1}{2}$ on Fig. 1, while the curves $v=1$, $n=0$ and $v=\frac{1}{4}$, $n=5$ form a similar isomorphic pair. These examples show that when both particle shape and mass distribution form are varied, near coincidences can occur, rendering the interpretation in the scattered intensity curves very uncertain. Obviously, if a distribution in particle shape were also considered, the possible ambiguity would become even greater. Other independent evidence must be taken into account in deciding between the various possibilities. In general, a mass distribution

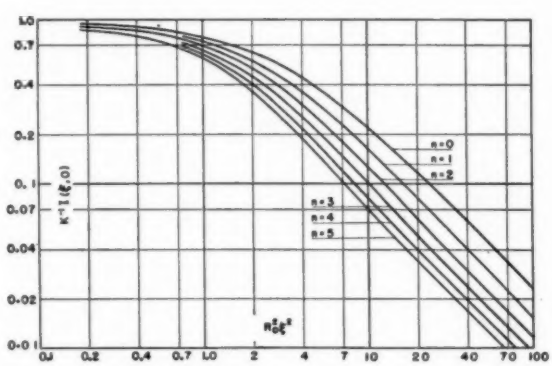

FIG. 3. Calculated intensity scattered by Maxwellian distributions of thin disks, $v=0$.

[15] When $n=0$ the leading term in the asymptotic expansion is proportional to $\dfrac{\ln R_0\xi}{(R_0\xi)^4}$.

[16] $R_v=\left(\dfrac{2+v^2}{5}\right)^{\frac{1}{2}}R$, cf. A. Guinier, Ann. de Physique **12**, 161–237 (1939).

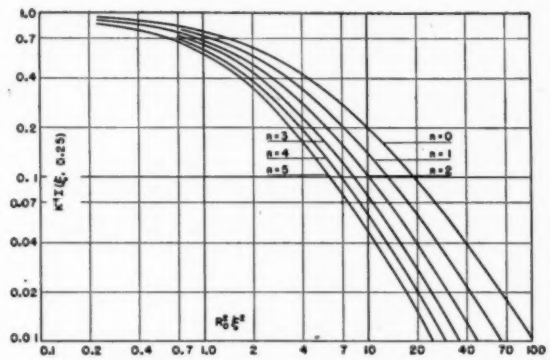

FIG. 4. Calculated intensity scattered by Maxwellian distributions of oblate spheroids, $v=0.25$.

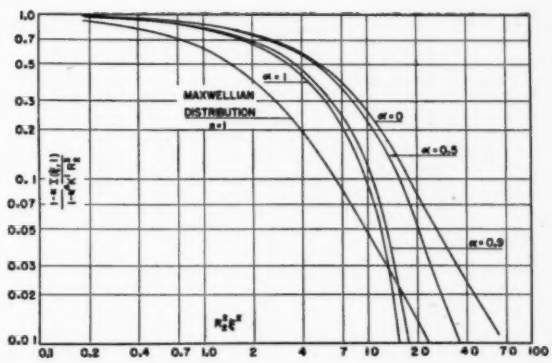

FIG. 5. Calculated intensity scattered by rectangular distributions of spheres (Eq. (35)). $\alpha=R_1/R_2$. The intensity fluctuations at large values of $R_2^2\xi^2$ are not shown. The intensity scattered by a Maxwellian distribution of spheres is also plotted for comparison.

having a small value of n is improbable, so that the ambiguity of the above examples could be at least partially resolved by this argument. If a crystalline material is under investigation, independent information on particle shape can be obtained from x-ray line width measurements.[17]

In each of the examples cited above only one scattering curve is involved. When the radius of gyration of the average particle in each of the two mass distributions calculable from each scattering curve is computed, it is found that those of the spheroidal particles are appreciably greater than those of the spherical particles. This shows that when a given intensity curve is interpretable in terms of two or more distributions of differently shaped particles, the resulting average radii of gyration are by no means identical, as would be required, for example, by the approximate theory using the Guinier scattering function.[1]

The matching of the scattered intensity curves with the experimental data has been discussed in the previous paper.[1]

[17] For the crystalline materials discussed in reference 1, no evidence for shape asymmetry has been found from line width measurements.

ERRORS DUE TO USE OF THE GUINIER SCATTERING FUNCTION

The exact scattering function for randomly oriented particles of fixed size and shape has a primary peak centered at zero scattering angle and a series of secondary peaks at larger angles whose amplitudes decrease as some negative power of the angle. In contrast, the Guinier function used in the approximate theory given in the preceding paper[1] has a primary peak only, and decreases exponentially at larger angles. This neglect of the secondary peaks leads to appreciable errors in the calculated scattered intensity at relatively large angles.[18] However, these errors are small for $R_0\xi$ values up to 1.5 or 2, and since the region enclosing the knee of curve[1] rarely extends to $R_0\xi$ values greater than 2.5 to 3, no really serious errors of interpretation result from the use of the Guinier function in place of the corresponding exact scattering function, when the particles are reasonably symmetrical in shape.

[18] This may be illustrated by the asymptotic proportionality of the Guinier function scattered intensity to $(r_0\xi)^{-(n+4)}$, while the exact function for spheres gives $(R_0\xi)^{-4}$ for all $n>0$.

Excess Noise in Cavity Magnetrons

ROBERT L. SPROULL*
RCA Laboratories, Princeton, N. J.†
(Received October 17, 1946)

The magnetron oscillator of some frequency-modulation radars also furnishes the "local oscillator" excitation for the crystal mixer of the receiver. Excess noise generation by the magnetron was observed to reduce greatly the receiver sensitivity. This noise exhibited a strong dependence upon anode voltage and current, and changed with time in a perplexing manner. After many experiments, a hypothesis of the cause of excess noise was developed, and further experiments confirmed this hypothesis. The noise is thought to be caused by ionization of atoms of the cathode oxide coating, which atoms are removed from the cathode by electron bombardment. In order to reduce the generation of excess noise, and still preserve the advantages of an oxide-coated cathode, a special shape of cathode has been developed. The coated regions of this cathode are sheltered from electron bombardment, and the noise is much reduced. Use of cathodes of this general type should also produce magnetrons with longer operating lives than present tubes.

THE magnetron oscillator in some[1] frequency-modulation, continuous-wave radars also furnishes the "local oscillator" excitation of the crystal mixer of the receiver. It was observed that the magnetron oscillations were frequently modulated with large amounts of noise, thereby impairing the sensitivity of the receiver. The cause of this excessive noise modulation (many times ordinary shot noise) was made the subject of a special investigation, the results of which are reported here. Excess noise is not noticed in the usual use of a magnetron as a transmitter tube, since the signal-to-noise ratio is at least 60 db. However, the noise phenomena may

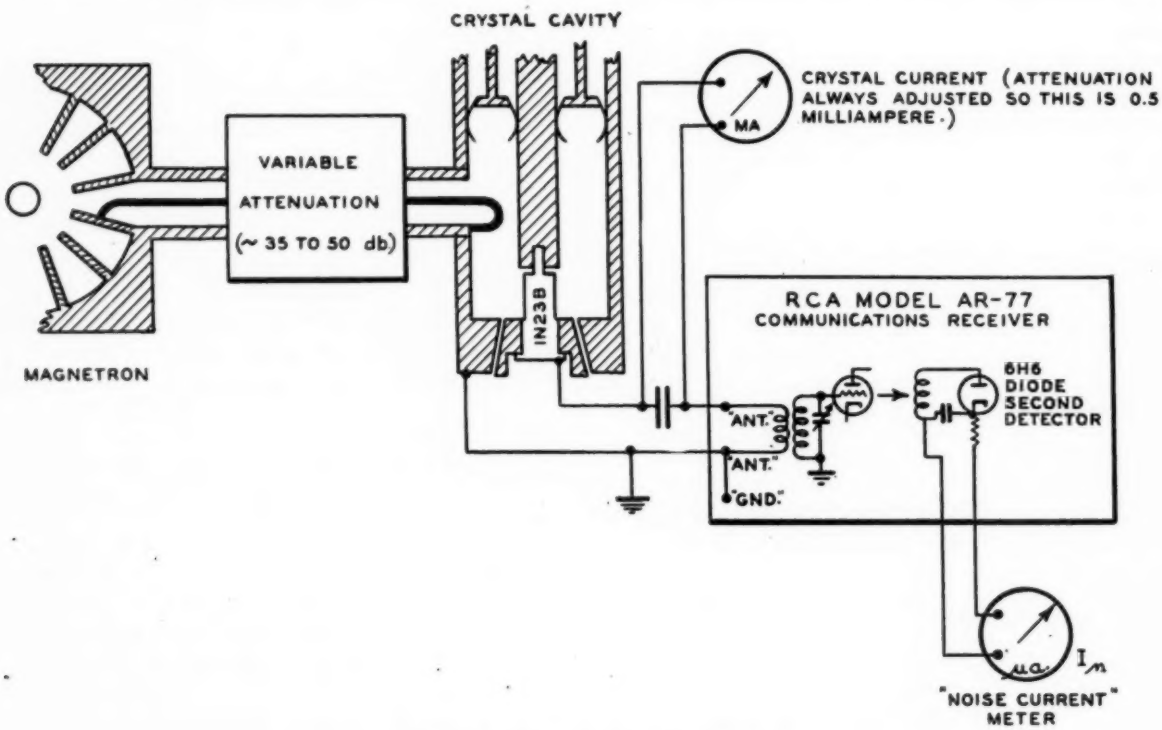

FIG. 1. Noise comparison apparatus.

* Now at Cornell University, Ithaca, N. Y.
† This paper is based on work done for the U. S. Navy under Contract NXsa 35042.
[1] Such as the AN/APQ-19, developed in this laboratory.

increase our understanding of magnetron operation, are important in special applications of magnetrons, and are of interest in any development of receiving tubes utilizing magnetic fields.

I. DESCRIPTION OF THE NOISE PHENOMENA

Figure 1 shows the experimental arrangement used to detect noise modulation and to estimate its magnitude. Since the magnitude of the oscillating field in the crystal cavity was kept constant by varying the attenuation between the magnetron and this cavity, the receiver detector current "I_n" was roughly inversely proportional to the signal-to-noise ratio of the magnetron oscillations.

Figure 2 shows the "noise current" I_n as a function of magnetron d.c. anode voltage (V_a) for several anode currents (I_a) in a 4000 megacycle, continuous-wave magnetron[2] developed in this laboratory. To obtain such a plot, the magnetic field was varied to produce different values of V_a at constant I_a. It is apparent that at low voltages the total noise current is substantially constant, and in this region the contribution of the magnetron noise to the total receiver noise is small. At some voltage, which we shall call V_{ao}, a relatively sharp break in the curve appears, and above this voltage the magnetron noise dominates noise from other sources and becomes hundreds or thousands of times as large as at low voltages. This region ($V_a > V_{ao}$) of excess noise contained the ordinary operating point of the oscillator. Phenomena very similar to those portrayed in Fig. 2 were also observed in a magnetron[3] of quite different design.

Curves such as those of Fig. 2 are not reproducible in detail. The "peaks" and "valleys" of the curves cannot be repeated even a few minutes after they are observed. The most useful feature for comparing noise phenomena in different tubes is the voltage V_{ao}. Even this parameter changes with time, however, and may have quite different values in two tubes constructed (as nearly as possible) identically. Several tubes must, therefore, be constructed in order to be certain of the dependence or lack of dependence of noise upon some one feature of the design. Figure 2 is representative of the early 4000 megacycle tubes and exhibits the increase in noise with decrease in anode current which was observed with all tubes.

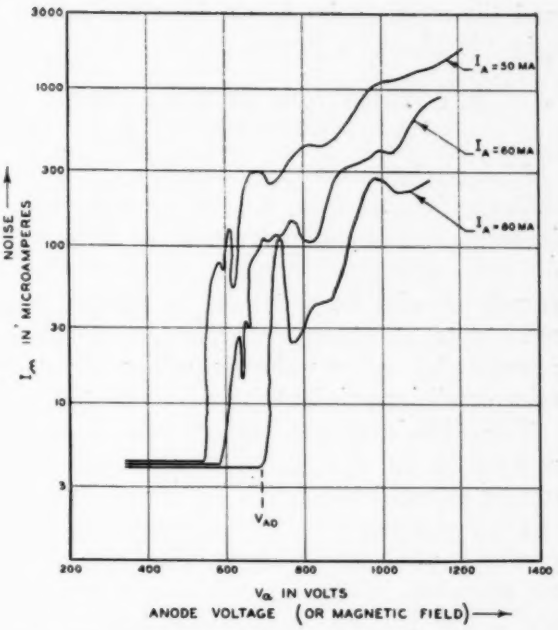

FIG. 2. Noise in early 4000 megacycle magnetrons. At constant anode current, anode voltage and magnetic field are approximately proportional. Therefore the abscissa may be considered (except for units) as either voltage or magnetic field strength.

After vigorous oscillation in these magnetrons has begun at a sufficiently high anode voltage, the cathode heater power may be removed. Back-bombardment of the cathode by electrons which have received energy from the oscillating field produces secondary electrons and warms the cathode sufficiently to produce some thermionic electrons. The excess noise was invariably less when the ordinary heater power was removed. All of the measurements and correlations reported here refer to operation with no applied heater power.

The receiver (Fig. 1) was ordinarily tuned to pass modulation components in the frequency range 1496 to 1504 kilocycles, but other frequency regions were also explored. In general the noise was less the higher the receiver frequency,

[2] G. R. Kilgore, C. Shulman, and J. Kurshan, "A Frequency-Modulated Magnetron for Super-High-Frequencies," Proc. I.R.E. (to be published).

[3] J. S. Donal, Jr., R. R. Bush, C. L. Cuccia, and H. R. Hegbar, "A One-Kilowatt Frequency-Modulated Magnetron for 900 Megacycles," Proc. I.R.E. (to be published).

and the excess noise was quite small at a receiver frequency of 30 megacycles.

II. CORRELATIONS OF NOISE WITH MAGNETRON PROPERTIES

Many tubes were constructed with slightly different features from the ordinary magnetron in order to test the dependence of noise upon different aspects of the design. In each case correlation of noise properties with the changes made was attempted. Correlations were also attempted between noise properties and operating conditions of the tube.

The high-frequency load presented to the magnetron by the antenna and transmission system changed the details of the excess noise, but any standing wave ratios and phases which produced reasonably stable operation with moderate efficiency produced about the same values of V_{ao}. The presence or absence of discontinuities in the straps of the magnetron resonator, the presence or absence of "hats" on the ends of the cathode produced no consistent changes in noise. The geometry and potentials of electrodes near the ends of the cathode affected the noise only very slightly. Small changes in anode diameter produced no effect. A variation of almost a factor of two in cathode size produced marked changes in efficiency and stability; but the noise was little changed except with very small or very large diameters, and in these cases the noise was greater than with intermediate diameters.

These and other experiments were used to show that several more or less obvious hypotheses of the causes of excess noise were not tenable. For example, any axial oscillations (such as observed in magnetron structures many years ago by Megaw[4]) should be strongly affected by end plate potentials, and if the noise were related to such oscillations it should be a function of these potentials. Other hypotheses were concerned with the resonant modes of the resonator and with the space-charge and electric field distributions in the cathode-anode space. The results of the studies with various cathode and anode diameters, the fact that the excess noise was observed in a magnetron of quite different construction, and the occurrence of noise over a wide range of anode voltages and currents, made such hypotheses of the cause of noise very unlikely.

Three successful correlations emerged from this work, but none gave immediately a clear indication of the cause of the noise. These correlations will be briefly described here. The first was a correlation of noise with low efficiency accompanied by high back-bombardment of the magnetron cathode. Tubes which exhibited considerably lower efficiency than others of similar construction were usually very noisy. Experimental tubes were constructed with windows which allowed observation of the cathode during operation, and this correlation was verified in such tubes. This correlation is probably related to the reduction in noise as the normal cathode heater power is removed; in both cases high noise accompanies high cathode temperature.

The second correlation was between excess noise and the length of the cathode sleeve which was coated with oxides. It was found that if the emitting length were confined to less than two-thirds of the length of the anode, the voltage (V_{ao}) at which noise began could be materially increased. It was not certain that the ends of the cathode did not emit electrons, but the carbonate spray was carefully cleaned from all except the central region of the cathode sleeve in the hope that no emission would occur in the end regions. The suggestion was that the r-f and d.c. fields were distorted there, and it might be desirable to prevent the interaction of electrons with such fields.

The third correlation was between noise and the thermionic emission properties of the cathodes. The critical voltage (V_{ao}) was used as a measure of the former, and the heater current required to permit a thermionic current of 50 milliamperes at 100 volts (no magnetic field) was used as a measure of the latter. The correlation coefficient[5] of V_{ao} with this current was 0.79 for thirteen experiments with ten tubes. This shows a definite relation, with low noise accompanying low thermionic activity. This correlation was strengthened by observations on a single tube during the early part of its life, when both the

[4] E. C. S. Megaw, "Fundamental Characteristics of Electronic Oscillations," Nature **137**, 189 (1936).

[5] H. L. Rietz, *Mathematical Statistics*, Open Court (Chicago, 1927), p. 82.

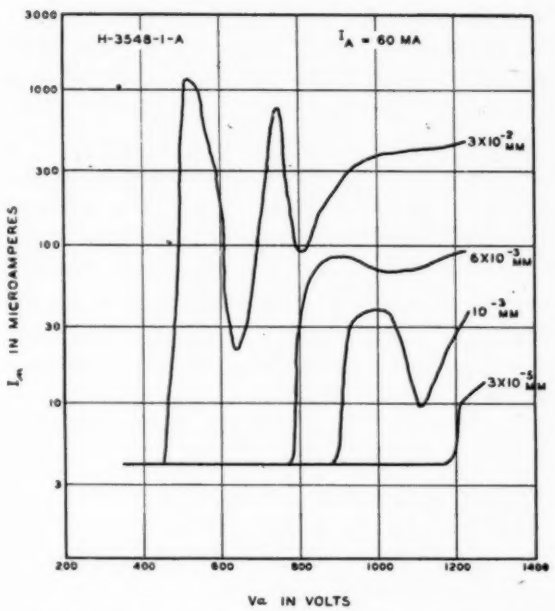

FIG. 3. Noise as a function of pressure. This tube had a helical tungsten filament in place of the usual oxide-coated cathode.

cathode activity and the noise were changing. Magnetrons were constructed with strontium oxide coatings on the cathodes, since the emission from SrO is known[6] to be considerably less than that from the SrO-BaO mixtures ordinarily used. These tubes showed high values of heater current for 50 milliamperes thermionic current, but the noise properties did not differ appreciably from other tubes. This experiment indicated that noise was not directly related to the cathode's thermionic activity, but that for cathodes of the same composition, high noise accompanied high activity.

III. IONIZATION NOISE

One of the first hypotheses of the cause of the excess noise was that it originated in the ionization of gas atoms in the interaction space of the magnetron. To test this, several tubes were continuously pumped while noise data was taken, and neon gas was admitted to vary the pressure. No variation of noise with pressure was observed for pressures less than about 5×10^{-3} mm of mercury. At pressures greater than this, the noise increased and the efficiency decreased rapidly; this behavior was not surprising since at 10^{-2} mm a glow discharge was beginning. The pressures could not be measured inside the magnetron itself, but they were measured in an ionization gauge connected to the magnetron.

Several magnetrons were constructed with tungsten helices in place of the usual oxide-coated cathodes. Two of these were continuously pumped, and noise was observed as a function of pressure. Figure 3 represents the behavior of these tubes. Unlike the results with oxide-cathodes, the data here show a continuous increase in V_{ao} (that is, decrease in noise) as the pressure decreases. For pressures less than 10^{-6} mm, V_{ao} was greater than 1200 volts for tungsten filament tubes. But lowering the pressure below 10^{-3} mm did not change the noise in oxide-coated cathode tubes, and even at 10^{-6} mm V_{ao} was no larger than 800 or 900 volts. If the cause of the noise is the same in the tubes with these two types of cathodes, it must be that there is a condensable gas in the oxide-coated cathode magnetrons which is present in the anode-cathode space but which is not measured by external pressure gauges.

Evidence to support this interpretation came from quite different experiments. Observations upon tubes with windows revealed a luminescence in the anode-cathode space or upon the cathode surface. Spectrographic investigation showed that the line spectra of barium and strontium (the metallic constituents of the cathode coating) were represented by their most persistent lines. Since the lines were quite sharp, it was apparent that the luminescence was not fluorescence of the solid (such fluorescence is also observed on activated cathodes, but its spectrum is broad and diffuse). It appeared therefore that there were substantial quantities of Ba and Sr atoms in the interaction space. At least some of these were ionized, since some of the spectral lines observed were those of the positive, singly-charged ion.

In order to obtain further information about the atoms and ions in the anode-cathode space, "double-triode" tubes were built. In these tubes electrons from the central cathode bombarded both a nickel anode and an oxide-coated anode, which had been activated as if it were a cathode and which could be heated by a tungsten heater. A negative grid was placed in each half of the

[6] M. Benjamin and H. P. Rooksby, "Emission from Oxide-coated Cathodes," Phil. Mag. 15, 810 (1933).

tube, and the positive ion currents to these grids were measured. Both anodes were maintained at approximately the same potential, and the electron currents in the two parts of the tube were the same. The grid current in the nickel anode space was about 0.01 microampere when 10 milliamperes electron current was flowing; this corresponds to roughly 10^{-6} mm pressure of residual gas in the tube. The grid current in the other side of the tube was always many times this value, and when the oxide-coated anode was heated to 700–800°C, grid currents of 10–40 microamperes were observed. It was apparent, therefore, that atoms or ions were released from the bombarded surface, and that these formed a condensable gas phase which could not be observed outside the immediate neighborhood of the bombarded surface. Noise measurements were also made on these tubes; excess noise was observed, and it was substantially proportional to the ion current collected by the grid.

From these experiments it was possible to derive the following interpretation of the phenomena of magnetron noise: (1) Some of the electrons (of the order of 20 percent) emitted from the cathode return to it after gaining considerable energy from the r-f field. If the cathode is oxide-coated, these back-bombarding electrons remove atoms or ions of the cathode material. Any ions emitted quickly return to the cathode, but they alter the space charge in the region of the potential minimum and permit a momentary excess of electrons to be emitted. Atoms emitted have between a 1 percent and a 10 percent chance of being ionized before they strike the anode or other parts of the tube. Ions thus produced alter the space charge and may release other atoms or ions when they bombard the cathode. (2) Noise in excess of ordinary shot noise is produced by these processes. The noise occurring in space-charge limited electron currents when appreciable numbers of positive ions are present has been investigated by Thompson and North.[7] Most of the noise effects observed in the present tests of special triodes are consistent with their work. In general, however, the excess noise in magnetrons is greater than that obtained in any other vacuum tubes, and it would be necessary to assume pressures of the order of 0.1 to 0.01 mm of mercury in a magnetron in order to explain the observed excess noise by simple extrapolation of the work of Thompson and North. (3) The very great noise in magnetrons and the irregular dependence of noise upon time, current, and voltage, may be the result of cumulative or chain effects. The equivalent pressure of barium and strontium atoms near a hot magnetron cathode is of the order of 10^{-2} mm; this figure is derived from measurements on the "double-triode" tubes and is checked by the fact that at neon pressures less than 5×10^{-3} mm the noise in an oxide-coated cathode magnetron was independent of pressure. At such a large pressure the contribution of positive ions to the space-charge distribution is considerable, and increasing the pressure by a factor of ten would cause oscillation to cease and a gas discharge at low voltage to occur. Under operating conditions the magnetron may therefore be on the verge of a Townsend breakdown. The ionization of a single atom may result in a burst of charge reaching the anode that is many times the electronic charge, and a correspondingly large increase in noise may occur. Among the processes which could participate in such a breakdown are ionization by electron impact, removal of atoms from the cathode by electrons, removal of atoms from the anode surface (which is soon contaminated with cathode material) by electrons, secondary electron emission at the cathode, and removal of atoms and electrons from the cathode surface by positive ion bombardment. It is not clear why such a breakdown does not occur, however, instead of merely threatening to occur.

Our interpretation is therefore that the dominating cause of the excess noise is associated with the presence of gas atoms in the interaction space. In a tungsten filament tube, these atoms are of residual gases and by sufficiently extensive pumping and gettering the excess noise may be substantially removed. In an oxide-coated cathode tube which is well out-gassed and gettered, the atoms are at least predominantly atoms removed from the cathode by electron back-bombardment.

The correlations reported in the preceding section give some support to these conclusions. The first correlation (noise *vs.* degree of back-bombardment) is evidently related to the de-

[7] B. J. Thompson and D. O. North, "Fluctuations Caused by Collision Ionization," RCA Review **5**, 88 (1941).

pendence of the rate of removal of cathode material upon the number of bombarding electrons and the cathode temperature, both of which are higher in magnetrons with excessive back-bombardment. Experiments showed that the equivalent pressure of cathode material was an exponentially increasing function of the cathode temperature. Therefore, under conditions of severe back-bombardment, it would be expected that noise would be greater than with moderate bombardment. This is just what was observed.

The reduction in excess noise by reducing the sprayed length of the cathode is presumed to be related to the first correlation. In several tubes with short-spray-length cathodes, the cathodes operated at temperatures less than 700°C. Most full-length-sprayed cathodes operated at considerably higher temperatures. This is evidence of smaller back-bombardment when the electrons do not interact with electric fields near the ends of the anode.

The third correlation is still obscure. It may be that a very active thermionic cathode, which may have a surface layer of barium or strontium atoms, yields more atoms or ions when bombarded with electrons than a less active cathode.

A number of apparently unconnected relations are consistent with the gas-ionization hypothesis of the cause of excess noise: The decrease of noise with increasing I.F. frequency, the decrease of noise when the cathode heater power is removed, the negative results of various experiments with end-plate potentials and geometries, observations of the appearance of anode and cathode surfaces after many hours of operation, the occurrence of excess noise in magnetrons of quite different construction, the lack of dependence of noise phenomena upon cathode and anode diameters, and the irregular changes of noise with time, are all susceptible to explanation by this hypothesis.

There are three outstanding difficulties: (1) The physical process whereby atoms or ions are released from the cathode coating by bombarding electrons is not known, though several processes seem to be capable of producing this result. (2) The exact way in which ions and ionization of emitted atoms combine with the electron flow and the electric and magnetic fields to produce such large amounts of noise is not known. (3) The decrease of noise with increasing anode current does not seem to be explained.

Despite these difficulties, the hypothesis of the cause of the noise is felt to be reasonably well established. More detailed information is required about the mechanism of release of cathode material in order to advance our understanding of noise. Experiments with a mass spectrometer are planned to determine what molecules, atoms, or ions are released. The results of these experiments may make possible a quantitative theory of noise generation. Preliminary results with "double-triode" tubes indicate that at least some of the cathode material is removed as atoms and that the exponential increase of removed atoms (per unit electron current) has an exponent which corresponds to an "activation energy" of 40–50 kilocalories per mole. The heats of sublimation of barium and strontium are 44 and 38 kilocalories. This may be a coincidence, or it may be that electron bombardment produces small patches of barium and strontium, from which atoms readily volatilize at the cathode operating temperature.

IV. PROGRESS IN THE REDUCTION OF EXCESS NOISE

The increase in V_{ao} by reducing the sprayed length of the cathode has already been reported. This change and the improvement of the efficiency and reduction of back-bombardment resulting from further development of the frequency-modulated magnetrons[2] resulted in a large percentage of magnetrons which were not "noisy" in the ordinary operating region, near $V_a = 850$ volts.

The hypothesis of the cause of noise which was advanced in the preceding section suggested that the cathode be modified in order to reduce the excess noise and to raise V_{ao} still further. No hope was entertained of eliminating the back-bombarding electrons, so a means was sought for preventing the removal of cathode material by such electrons. There is considerable evidence that electrons returning to the cathode do not strike at normal incidence, but at angles varying between 45° and tangential incidence. Furthermore, for a fixed magnetic field, the sense of rotation of all electrons about the cathode is the same. These facts permit the construction of a cathode such that returning electrons strike a nickel surface instead of striking the cathode

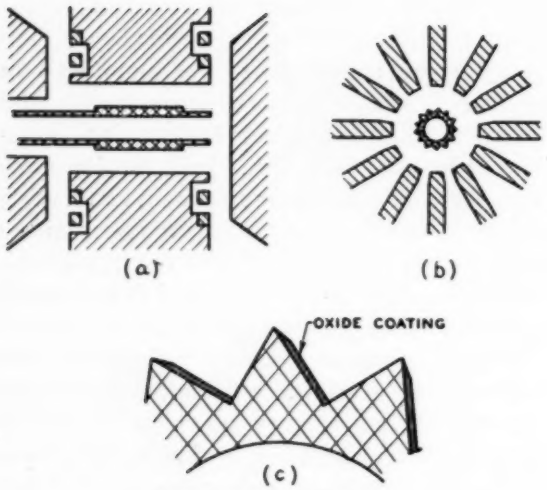

FIG. 4. Grooved cathode.

coating. One such cathode is shown in Fig. 4. The active length of the cathode is in the form of a 13-pointed star; only one side of each star point is coated with oxides. To accomplish this, the entire cathode was coated, and the spray was carefully scraped from areas where it was not wanted. This process was tedious, since the diameter of the cathode was only 0.070 inches, but was quite practical for experimental tubes.

Figure 5 shows the noise behavior of one of the four tubes constructed with the cathode of Fig. 4. By "correct" direction of the magnetic field we mean that direction which allows back-bombarding electrons to strike only the nickel surface (this is the clockwise sense of rotation in Fig. 4). It is evident that the noise is much less if the oxide-coating is sheltered from bombardment. This provides increased confidence in the hypothesis of the cause of noise which was advanced in the preceding section.

Three other tubes with cathodes as shown in Fig. 4 were built. One of these showed somewhat less noise for the "incorrect" direction of magnetic field than for the "correct" direction. This tube exhibited very high back-bombardment, more noise than other tubes of this type, and low efficiency. When it was dissected this tube was found to have a cathode which was not parallel to the axis of the anode. These facts make the information from this test of questionable value, but it is still not understood why this tube exhibited more noise when the electrons were rotating in the proper sense.

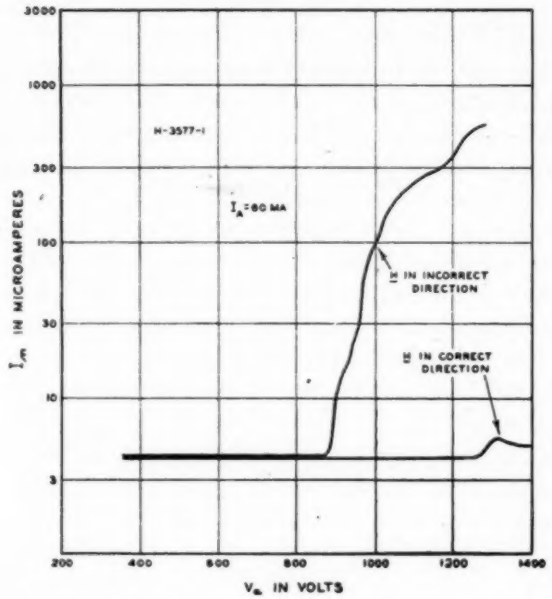

FIG. 5. Noise in magnetron with grooved cathode. When the magnetic field is in the "correct" direction, the oxide-coated surfaces are sheltered from back-bombarding electrons.

The remaining two tubes showed substantially the same behavior as the first (Fig. 5) and therefore confirmed the conclusions from that tube. The net result of all such experiments was that V_{co} is 200–300 volts larger when the magnetic field is applied in the "correct" sense.

An interesting possibility of cathodes of the general type of Fig. 4 is that they may permit substantially longer life than has previously been experienced with magnetrons. There is much evidence (some of it contained in the present work) that cathode life in a magnetron is limited more by the destruction of the cathode by back-bombardment than by the processes of cathode decay observed in ordinary diodes and negative grid tubes. If long life, not low excess noise, were the chief requirement, the oxide-coating could initially cover the entire cathode. Removal of part of the surface by back-bombardment would not cause failure, because at least part of the surface would be sheltered from back-bombarding electrons.

It is a privilege to acknowledge the cooperation of Messrs. G. R. Kilgore, C. I. Shulman, and Dr. J. Kurshan in this study, and the suggestions and encouragement of Dr. L. P. Smith and Dr. I. Wolff.

A Semi-Polar Form of Fourier Series and Its Use in Crystal Structure Analysis

JOSEPH S. LUKESH
Crystallographic Laboratory, Department of Geology, Massachusetts Institute of Technology, Cambridge, Massachusetts

(Received September 27, 1946)

A new form of Fourier series for crystal structure analysis is developed and a graphical method of summation described. The procedure is designed to permit simple and fairly rapid computation and recording of the density contributions of all planes at all points in the unit cell. Its particular advantage is in the case of centrosymmetrical projections where phases must be assigned experimentally. Adjustment of phases involves only re-addition of numbers rather than a complete new summation. The method also requires a minimum of equipment which is easily constructed at negligible expense.

THE distribution of electron density throughout the unit cell of a crystal can be determined by the summation of a Fourier series of the following general type

$$\rho(xyz)=\frac{1}{V}\sum_h\sum_k\sum_l F_{(hkl)}e^{-(2\pi i/N)(hx+ky+lz)} \quad (1)$$

at each point, xyz, for all values of $F_{(hkl)}$. The coordinates, xyz, are given in integral numbers of N, the number of subdivisions of the axes. On expansion, Eq. (1) becomes

$$\rho(xyz)=\frac{1}{V}\left[\sum_h\sum_k\sum_l A_{(hkl)}\frac{\cos 2\pi}{N}(hx+ky+lz)+\sum_h\sum_k\sum_l B_{(hkl)}\frac{\sin 2\pi}{N}(hx+ky+lz)\right]. \quad (2)$$

In most crystal pattern syntheses, the series is restricted to a two-dimensional one whose summation gives a projection of the electron density. Considering only the reflections, $(hk0)$, for instance, the series is

$$\rho(xy)=\frac{1}{A}\left[\sum_h\sum_k A_{(hk0)}\frac{\cos 2\pi}{N}(hx+ky)+\sum_h\sum_k B_{(hk0)}\frac{\sin 2\pi}{N}(hx+ky)\right]. \quad (3)$$

Summation of Eq. (3) at all points, xy, gives a representation of the electron density projected on 001. Projections on 100 and 010 are obtained by considering only the $0kl$ and $h0l$ reflections, respectively.

Because of the tedious nature of the computations involved in even the two-dimensional series, a number of computational aids have been devised. All of these aids are characterized by the trigonometric separation of Eq. (3) into a group of one-dimensional series which can be summed easily by means of strips on which are printed the products of all possible magnitudes of A and B times all possible values of the cosine and sine. Summation is reduced to the addition of previously computed numbers.

Use of the computational aids reduces the labor of any one summation, but it may actually increase the total labor of a crystal structure determination. If one is dealing with a centrosymmetrical projection, the phases are all either 0 or π and the equation to be summed is

$$\rho(xy)=\frac{1}{A}\sum_h\sum_k F_{(hk0)}\cos 2\pi(hx+ky). \quad (4)$$

If the phase of a given reflection is 0, the sign of F is positive; if it is π, the sign is negative. In most structure determinations, the phases are unknown and must be determined by trial and error. Given a trial structure, one may compute phases and these may then be used in the summation. In general, many of the signs will be found to have been incorrectly determined and the electron density will not be a faithful representation of the structure. It will then be necessary to change phases either experimentally or by making adjustments in the trial structure and re-computing. Each time phases are changed, a complete new summation must be made. When accurate parameters are being sought, a number

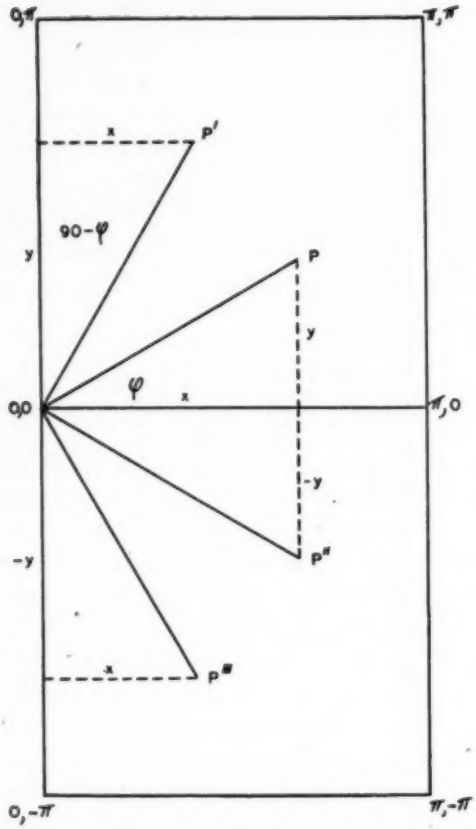

FIG. 1. The relation between rectilinear and semi-polar coordinates for points in a half-unit cell.

of approximations must usually be made before the final electron density map is obtained.

If, instead of summing Eq. (4) by use of strips, one employs a method in which the contributions of each plane at each point are determined individually and recorded, adjustment of phases will not require additional summations. To change signs, one need merely re-add columns of numbers. In the form of Eq. (4), the series requires a great deal of computation. However, if it is put into a new form, to be described in the following section, a graphical method of summation can be used which is both simple and reasonably rapid. In addition, the graphical method has an advantage in that the equipment required is a minimum, consisting of a chart, a scale, and a table of numbers.

THEORY OF THE SEMI-POLAR SERIES

The point, P, in Fig. 1 is conventionally specified by the rectilinear coordinates x and y. As an alternative, one may choose to locate P by the coordinate x and the angle, φ, between the x axis and a line from the origin to P. Since

$$y = x \tan\varphi, \tag{5}$$

the rectilinear coordinate, y, may be replaced by $x \tan\varphi$. Equation (4) becomes

$$\rho(x, x\tan\varphi) = \frac{1}{A}\sum_h \sum_k F_{(hk0)} \times \cos\frac{2\pi}{N}(hx + kx\tan\varphi). \tag{6}$$

In a similar manner, the point, P', in Fig. 1 may be specified by the coordinates $y\tan(90-\varphi)$ and y. In this case, the series is given by

$$\rho[y\tan(90-\varphi), y] = \frac{1}{A}\sum_h \sum_k F_{(hk0)} \times \cos\frac{2\pi}{N}[hy\tan(90-\varphi) + ky]. \tag{6'}$$

For all of the points along a line of constant φ or $90-\varphi$, the tangent is a constant. Equations (6) and (6′) may, therefore, be written

$$\rho(x, c) = \frac{1}{A}\sum_h \sum_k F_{(hk0)} \cos\frac{2\pi}{N}x(h + ck), \tag{7}$$

$$\rho(c', y) = \frac{1}{A}\sum_h \sum_k F_{(hk0)} \cos\frac{2\pi}{N}y(c'h + k), \tag{7'}$$

where c and c' are the tangents of φ and $90-\varphi$. For the points, P'' and P''', the corresponding expressions are

$$\rho(x, -c) = \frac{1}{A}\sum_h \sum_k F_{(hk0)} \cos\frac{2\pi}{N}x(h - ck), \tag{7''}$$

$$\rho(-c', -y) = \frac{1}{A}\sum_h \sum_k F_{(hk0)} \times \cos\frac{2\pi}{N}(-y)(-c'h + k). \tag{7'''}$$

The expressions are the same, except that c, c', and y are negative. Since the cell is centrosymmetrical, only half need be considered.

The important feature of Eq. (7) and its related expressions is that for any given reflection, $hk0$, and any given slope, c, the entire expression in parentheses is a constant. Equation (7) may, then, be written

$$\rho(xc)=\frac{1}{A}\sum_h\sum_k F_{(hk0)}\cos\frac{2\pi}{N}xC. \qquad (8)$$

The density contribution of any plane at each point, x, along the line whose slope is c is found by multiplying F by the cosine of $(2\pi C/N)\cdot 0$ (for $x=0$), $(2\pi C/N)\cdot 1$ (for $x=1$), $(2\pi C/N)\cdot 2$ (for $x=2$), etc. If one is interested in the density at any one point, x, c, Eq. (8) reduces to

$$\rho(xc)=\frac{1}{A}\Big[F_{(hk0)}\cos\frac{2\pi}{N}xC_{(hk0)}+F_{(h'k'0)}\cos\frac{2\pi}{N}xC_{(h'k'0)}+F_{(h''k''0)}\cos\frac{2\pi}{N}xC_{(h''k''0)}+\cdots\Big]. \qquad (9)$$

A POLAR GRID

If the points on the rectilinear grid that is usually used in structure analysis are specified in the semi-polar form just described, there will be

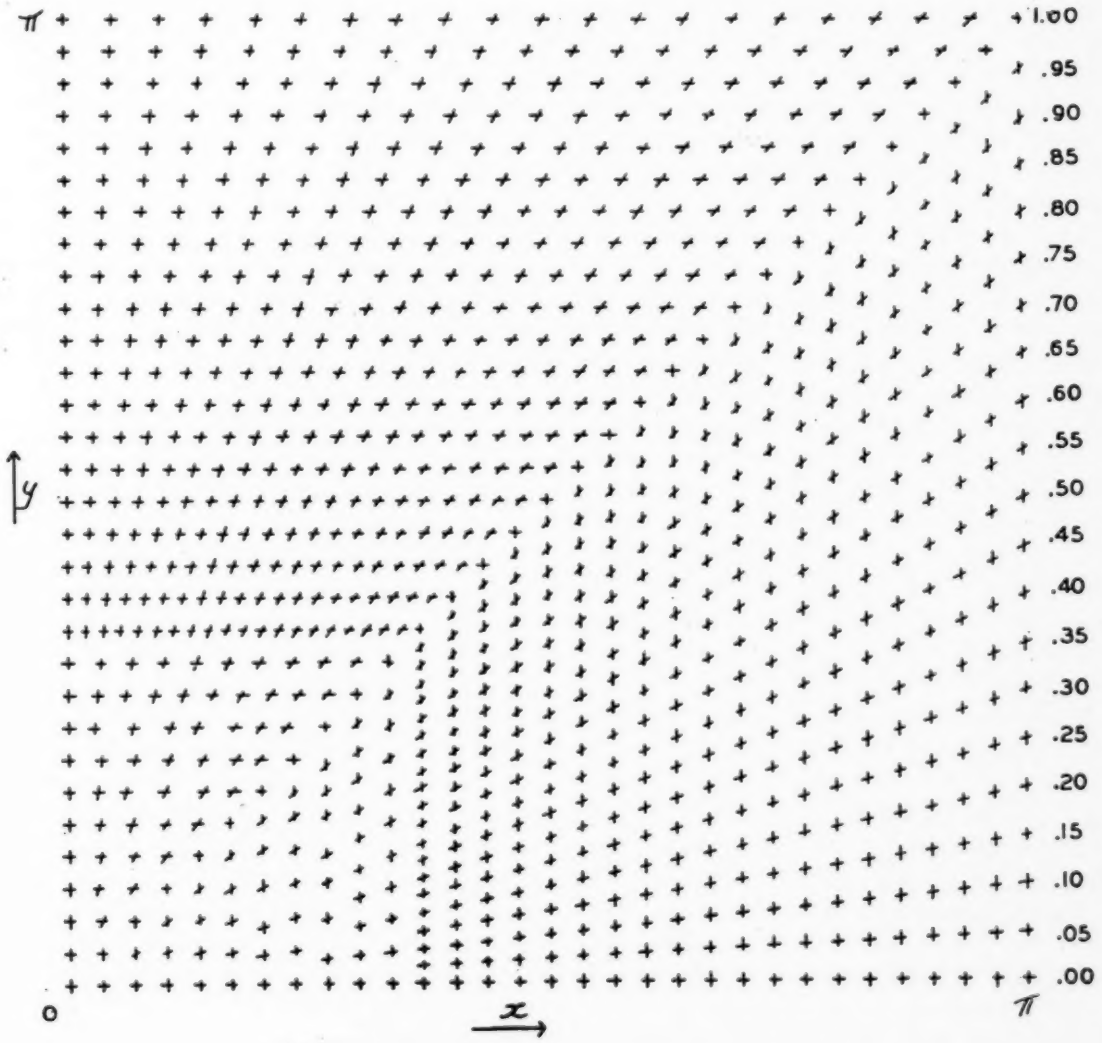

FIG. 2. The polar grid for one-quarter of the unit cell.

TABLE I. Values of $(2\pi/N)\cdot Cx$ for $C=4.80$.

x	$(2\pi/N)\cdot Cx$
0	$(2\pi/N)\cdot$ 0.00
1	$(2\pi/N)\cdot$ 4.80
2	$(2\pi/N)\cdot$ 9.60
3	$(2\pi/N)\cdot$14.40
4	$(2\pi/N)\cdot$19.20
5	$(2\pi/N)\cdot$24.00
6	$(2\pi/N)\cdot$28.80
7	$(2\pi/N)\cdot 33.60=(2\pi/N)\cdot 26.40$
8	$(2\pi/N)\cdot 38.40=(2\pi/N)\cdot 21.60$

TABLE II. Product of F times $\cos(2\pi/N)\cdot Cx$.

x	Cx	$F\cos(2\pi/N)\cdot Cx$
0	0.00	100
1	4.80	89
2	9.60	53
3	14.40	6
4	19.20	−43
5	24.00	−80
6	28.80	−99
7	26.40	−95
8	21.60	−64

a large number of constants, c, corresponding to the tangents of the various angles, and, in general, their numerical values will not be simple numbers. Because of this, computation of the constant, C, will not be easy. Furthermore, there will be only a few points along each line, except in special cases. The value of having a "constant" will be reduced. Both of these difficulties can be eliminated if one abandons the conventional grid in favor of one defined by the intersections of the x and y coordinates with radial lines of simple slopes. For each radial line, there will be $N/2$ points, assuming the summation is made from the origin to π.

A grid suitable for most purposes is formed by allowing N to equal 60. There are, then, thirty divisions along each axis from 0 to π. To approximate the distribution of points formed by such a rectilinear grid, a series of radial lines whose slopes are .05, .10, .15, .20, etc. has been chosen. Intersections of these with the x coordinates locate the points of the grid for the first segment, in Fig. 1, of the cell. For the second segment, a symmetrical array is obtained by using the intersections of the y coordinates and radial lines whose slopes, c', have the same values. The grid thus defined for the first two segments of the cell is shown in Fig. 2. The principal disadvantage, outside of the unconventional array, lies in the fact that there are only twenty points along each of the axes, $x=\pi$ and $y=\pi$. To offset this, points half-way between those shown may be handled by interpolation. The point density near the origin has been reduced by eliminating some of the points, those from the origin to x and y equal four being, actually, coincident with points of the conventional grid.

It might be well at this time to discuss, briefly, the mathematics of the semi-polar coordinate system just developed. Heretofore, the tacit assumption has been made that the unit cell is square so that a point at $x=10$ and $y=5$, for instance, actually lies along a radius which makes an angle with the x axis whose tangent is .50. It may not be immediately obvious that the same relation holds for a rectangular or oblique cell. Actually, the expression, $\tan\varphi=y/x$, is merely a convenient mathematical shorthand for referring to the ratio of units of distance along the y axis to that along the x axis. No matter what the absolute lengths of the two units may be or the angle between the axes, the statement, $\tan\varphi=.50$, simply means that the point is twice as many x units from the origin as y units. This holds, of course, only when the axes are divided into the same number of parts.

GRAPHICAL SUMMATION OF THE SEMI-POLAR SERIES

As was mentioned in an earlier section, for a given plane, $hk0$, and a radial line of slope, c, the term, $(h+ck)$, in Eq. (7) is a constant for all points along the line, and the series may be expressed in the form of Eq. (8). The density contribution of $hk0$ at each point of the grid along the radial line is computed by multiplying the amplitude, F, by the cosines of a series of angles which are multiples of $2\pi C/N$. The discrete values of the cosine so obtained may be computed, once for all, and tabulated. Since they depend only on the geometry of the plane and are independent of the structure, such a table could be used for any structure determination. However, use of a table of cosines would require that multiplication be performed for each plane at each point, which is an extremely tedious task. Inasmuch as Eq. (8) is a periodic cosine function, the product can be determined readily

by graphical means. Given a cosine curve and a vertical scale appropriate to the magnitude of F, it is only necessary to know what points along the axis of the curve correspond to multiples of $2\pi C/N$. These, of course, can be determined in advance and tabulated.

As an example, the density contributions of the plane, 420, along the radial line whose slope is .40 will be determined. The amplitude will be assumed to be +100. The constant, C, in Eq. (8) is given by

$$C = h + ck,$$
$$= 4 + .40 \cdot 2,$$
$$= 4.80.$$

The values of the product, $2\pi C/N$ times x for the first eight points along the radial line are listed in Table I. Because the cosine function is sym-

TABLE III.* Part of the tabulation of C times x as a function of C and x.

C \ x	x=0	1	2	3	4	5	6	7	8	9	10	11	12	13	14
4.00	0.00	4.00	8.00	12.00	16.00	20.00	24.00	28.00	28.00	24.00	20.00	16.00	12.00	8.00	4.00
4.05	0.00	4.05	8.10	12.15	16.20	20.25	24.30	28.35	27.60	23.55	19.50	15.45	11.40	7.35	3.30
4.10	0.00	4.10	8.20	12.30	16.40	20.50	24.60	28.70	27.20	23.10	19.00	14.90	10.80	6.70	2.60
4.15	0.00	4.15	8.30	12.45	16.60	20.75	24.90	29.05	26.80	22.65	18.50	14.35	10.20	6.05	1.90
4.20	0.00	4.20	8.40	12.60	16.80	21.00	25.20	29.40	26.40	22.20	18.00	13.80	9.60	5.40	1.20
4.25	0.00	4.25	8.50	12.75	17.00	21.25	25.50	29.75	26.00	21.75	17.50	13.25	9.00	4.75	0.50
4.30	0.00	4.30	8.60	12.90	17.20	21.50	25.80	29.90	25.60	21.30	17.00	12.70	8.40	4.10	0.20
4.35	0.00	4.35	8.70	13.05	17.40	21.75	26.10	29.55	25.20	20.85	16.50	12.15	7.80	3.45	0.90
4.40	0.00	4.40	8.80	13.20	17.60	22.00	26.40	29.20	24.80	20.40	16.00	11.60	7.20	2.80	1.60
4.45	0.00	4.45	8.90	13.35	17.80	22.25	26.70	28.85	24.40	19.95	15.50	11.05	6.60	2.15	2.30
4.50	0.00	4.50	9.00	13.50	18.00	22.50	27.00	28.50	24.00	19.50	15.00	10.50	6.00	1.50	3.00
4.55	0.00	4.55	9.10	13.65	18.20	22.75	27.30	28.15	23.60	19.05	14.50	9.95	5.40	0.85	3.70
4.60	0.00	4.60	9.20	13.80	18.40	23.00	27.60	27.80	23.20	18.60	14.00	9.40	4.80	0.20	4.40
4.85	0.00	4.65	9.30	13.95	18.60	23.25	27.90	27.45	22.80	18.15	13.50	8.85	4.20	0.45	5.10
4.70	0.00	4.70	9.40	14.10	18.80	23.50	28.20	27.10	22.40	17.70	13.00	8.30	3.60	1.10	5.80
4.75	0.00	4.75	9.50	14.25	19.00	23.75	28.50	26.75	22.00	17.25	12.50	7.75	3.00	1.75	6.50
4.80	0.00	4.80	9.60	14.40	19.20	24.00	28.80	26.40	21.60	16.80	12.00	7.20	2.40	2.40	7.20
4.85	0.00	4.85	9.70	14.55	19.40	24.25	29.10	26.05	21.20	16.35	11.50	6.65	1.80	3.05	7.90
4.90	0.00	4.90	9.80	14.70	19.60	24.50	29.40	25.70	20.80	15.90	11.00	6.10	1.20	3.70	8.60
4.95	0.00	4.95	9.90	14.85	19.80	24.75	29.70	25.35	20.40	15.45	10.50	5.55	0.60	4.35	9.30
5.00	0.00	5.00	10.00	15.00	20.00	25.00	30.00	25.00	20.00	15.00	10.00	5.00	0.00	5.00	10.00

TABLE III. (*Continued*)

15	16	17	18	19	20	21	22	23	24	25	26	27	28	29	30
0.00	4.00	8.00	12.00	16.00	20.00	24.00	28.00	28.00	24.00	20.00	16.00	12.00	8.00	4.00	0.00
0.75	4.80	8.85	12.90	16.95	21.00	25.05	29.10	26.85	22.80	18.75	14.70	10.65	6.60	2.55	1.50
1.50	5.60	9.70	13.80	17.90	22.00	26.10	29.80	25.70	21.60	17.50	13.40	9.30	5.20	1.10	3.00
2.25	6.40	10.55	14.70	18.85	23.00	27.15	28.70	24.55	20.40	16.25	12.10	7.95	3.80	0.35	4.50
3.00	7.20	11.40	15.60	19.80	24.00	28.20	27.60	23.40	19.20	15.00	10.80	6.60	2.40	1.80	6.00
3.75	8.00	12.25	16.50	20.75	25.00	29.25	26.50	22.25	18.00	13.75	9.50	5.25	1.00	3.25	7.50
4.50	8.80	13.10	17.40	21.70	26.00	29.70	25.40	21.10	16.80	12.50	8.20	3.90	0.40	4.70	9.00
5.25	9.60	13.95	18.30	22.65	27.00	28.65	24.30	19.95	15.60	11.25	6.90	2.55	1.80	6.15	10.50
6.00	10.40	14.80	19.20	23.60	28.00	27.60	23.20	18.80	14.40	10.00	5.60	1.20	3.20	7.60	12.00
6.75	11.20	15.65	20.10	24.55	29.00	26.55	22.10	17.65	13.20	8.75	4.30	0.15	4.60	9.05	13.50
7.50	12.00	16.50	21.00	25.50	30.00	25.50	21.00	16.50	12.00	7.50	3.00	1.50	6.00	10.50	15.00
8.25	12.80	17.35	21.90	26.45	29.00	24.45	19.90	15.35	10.80	6.25	1.70	2.85	7.40	11.95	16.50
9.00	13.60	18.20	22.80	27.40	28.00	23.40	18.80	14.20	9.60	5.00	0.40	4.20	8.80	13.40	18.00
9.75	14.40	19.05	23.70	28.35	27.00	22.35	17.70	13.05	8.40	3.75	0.90	5.55	10.20	14.85	19.50
10.50	15.20	19.90	24.60	29.30	26.00	21.30	16.60	11.90	7.20	2.50	2.20	6.90	11.60	16.30	21.00
11.25	16.00	20.75	25.50	29.75	25.00	20.25	15.50	10.75	6.00	1.25	3.50	8.25	13.00	17.75	22.50
12.00	16.80	21.60	26.40	28.80	24.00	19.20	14.40	9.60	4.80	0.00	4.80	9.60	14.40	19.20	24.00
12.75	17.60	22.45	27.30	27.85	23.00	18.15	13.30	8.45	3.60	1.25	6.10	10.95	15.80	20.65	25.50
13.50	18.40	23.30	28.20	26.90	22.00	17.10	12.20	7.30	2.40	2.50	7.40	12.30	17.20	22.10	27.00
14.25	19.20	24.15	29.10	25.95	21.00	16.05	11.10	6.15	1.20	3.75	8.70	13.65	18.60	23.55	28.50
15.00	20.00	25.00	30.00	25.00	20.00	15.00	10.00	5.00	0.00	5.00	10.00	15.00	20.00	25.00	30.00

* *Explanation of Table III.* This table contains that portion of the tabulation of the product of the constant, C, times the coordinate, x, for C between 4.00 and 5.00, inclusive. The values listed are obtained by multiplying C by x, any product larger than 30 being reduced to an equivalent value less than 30. The remainder of the tabulation, covering the rest of the constants, C, from 0 to 30, can be constructed in a similar manner. The values listed in the table are the coordinates along the axis of a cosine curve, graduated in terms of $2\pi/60$, at which a scale should be set in order to determine graphically the product of the amplitude times the appropriate cosine.

metrical about 0 and π; one-half a cycle of the curve is sufficient if all values of the product greater than π are recomputed to a symmetrical value less than π. In the present case, the product is equal to π when C times x is equal to 30.

The products listed in Table I are the angles by whose cosines the amplitude must be multiplied to determine the density contribution of the plane, 420, at each of the first eight points of the grid along the radial line whose slope is .40. If the cosine curve is calibrated in terms of $2\pi/N$, it is only necessary to set the scale at the points 4.80, 9.60, 14.40, etc. and to read off the product. The values so obtained are listed in Table II.

In order to perform the computations for all planes at all points in the cell, it is necessary to tabulate all possible solutions of x times $(h+ck)$ and the related functions. This might at first seem to require an extensive table since the values of h and k may become quite large in large cells. However, the symmetry of the cosine function reduces the number of independent solutions to a finite number. The highest independent value of the product of C times x, and hence of C itself, is that which makes the product $(2\pi C/N)\cdot x$ equal to π. In the present case, the value is 30. Any value of C greater than thirty is symmetrical with one less than thirty. This is evident from $x=7$ and $x=8$ in Table I. Furthermore, since the cosine function is symmetrical about 0, negative value of C are the same as positive, and the sign of C may be disregarded. With N equal to 60, there are only 600 possible values of C, and the products of C times x can be tabulated conveniently. Such a table can be used for all structure determinations. A portion of the table is shown in Table III.

In many cases, it is sufficient to base a grid on N equal to 30. Radial lines of slopes .1, .2, .3, etc. may be used. The tabulation of C times x requires only 150 values of C against 15 values of x.

SUMMATION PROCEDURE

In determining the electron density by the method just developed, it is convenient to compute the density contributions of each plane at each point along a given radial line at the same time, as was done in the example. Worksheets can be prepared for each radial line on which are columns for the indices, the constants for each reflection, the F values, and for the density contributions at each x coordinate. The contributions of each plane, in turn, can then be easily determined by setting the proper scale at the points along the cosine curve indicated in the tabulation of C times x. When all planes have been handled, the columns of density contributions are totaled, and the totals plotted on the polar grid. If the resulting electron density map indicates that adjustments must be made in phases, it is only necessary to re-add the columns.

SUMMARY

A semi-polar form of Fourier series has been developed and a graphical method of summation described. Although the procedure is somewhat more tedious than the conventional strip methods of Fourier series summation, it may be found useful, particularly when phases must be assigned experimentally in centrosymmetrical projections. An added advantage is the simplicity of the equipment, which can be constructed at a negligible cost.

The Insulation of High Voltages in Vacuum

JOHN G. TRUMP
Department of Electrical Engineering

AND

R. J. VAN DE GRAAFF
Department of Physics, Massachusetts Institute of Technology, Cambridge, Massachusetts

(Received December 23, 1946)

Breakdown studies have been made between electrodes in high vacuum at constant voltages from 50 to 700 kv. These further demonstrate the inadequacy of the field emission theory to account generally for high voltage breakdown in vacuum. Experiments are described which investigate some of the "total voltage" breakdown mechanisms, including positive-ion emission by electron impact, electron emission by positive-ion impact and by photons. In the d.c. case these processes contribute to a steady interchange of charged particles between cathode and anode which increases with voltage until breakdown ensues. At higher breakdown voltages the cathode gradient has diminished far below the value for field emission. Measurements of electron emission by electrons with energies up to 300 kv for tungsten, steel, aluminum, and graphite are reported. The possibilities of predicting and of improving the insulating strength of electrode gaps in high vacuum by the study of the coefficients of the electrode materials are discussed.

INTRODUCTION

THE use of vacuum for the insulation of high voltages has become of increasing importance in modern science. In physics, vacuum insulation is essential for the acceleration of charged particles to high energies for nuclear studies, and generally for the production of high energy radiations. In engineering, the primary application of vacuum insulation has been in electronic tubes, including high vacuum rectifiers and high voltage x-ray tubes. The present applications of vacuum to low power switches and low loss high frequency condensers merely suggest the possible future importance which vacuum insulation may have in electrical power engineering.

During the last decade, the technique of producing and maintaining vacuum in large volumes has developed to the extent that vacuum may now be regarded as an available voltage-insulating medium. Nevertheless, although solid, liquid, and gaseous dielectrics have been intensively studied for many years, relatively little effort has been directed toward understanding and developing the unique electrical insulating properties of vacuum. After interruption by the war, the study of vacuum insulation, particularly at high voltages, is being resumed in the Department of Electrical Engineering at M.I.T. Some of the information obtained in these prior studies, as well as comments on our present picture of the mechanism of voltage breakdown in vacuum, is reported herein.

Vacuum insulation may be said to exist when the breakdown strength between metallic electrodes is independent of the pressure of the intervening gas. In an insulating vacuum the mean free path of electrons and positive ions moving in the residual gas must, therefore, be large compared with the inter-electrode gap in order that the contribution of gaseous ionization to the breakdown mechanism be negligible. While this condition may be achieved at atmospheric pressure for gaps of a small fraction of the wave-length of light, for the more ordinary gaps of physics and engineering a residual gas pressure of 10^{-4} mm of Hg or less is generally adequate. Further reduction in pressure does not increase the insulating strength of the gap except insofar as residual gas pressure may affect the absorbed gas and molecular layers of contaminating material which are in equilibrium on the electrode surfaces.

Vacuum insulation is more susceptible to quantitative analysis than any other insulating medium. Being free from the obscurities and limitations of intervening materials, the situation between metallic electrodes immersed in high

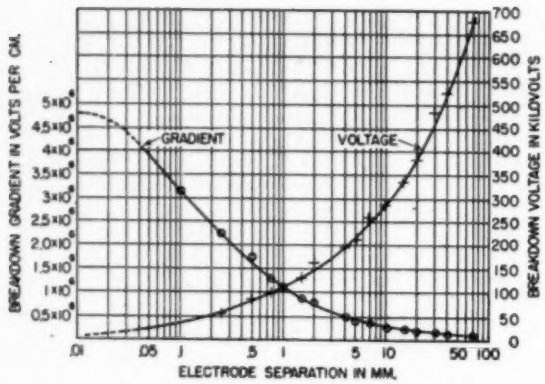

FIG. 1. Breakdown voltages and gradients between 1" stainless steel ball and 2" steel disk in vacuum.

vacuum may be more precisely described in terms of the electric field configuration, the number and energy of the charged particles, and other factors which influence the current flow and breakdown strength. Compared to a gas gap at high pressure, the phenomena in a vacuum gap are fewer and more direct. All of the ionization and recombination processes which occur in the gas are eliminated along with the field-distorting influence of space charge; only the electrodes remain effective in contributing or removing charged particles from the inter-electrode gap.

FIELD EMISSION BREAKDOWN AT LOW VOLTAGES

Much work has been done on vacuum insulation at low d.c. voltages and high field strengths with the object of studying the phenomena of high field emission. These experiments in general were made using well-outgassed electrodes in a highly evacuated chamber, the electrode arrangement consisting variously of concentric cylinders with the inner cylinder a filament easily outgassed by heating, of a point directed at a plane, of two fine crossed wires, or of sphere gaps. These experiments indicated that gradients at the cathode surface of several times 10^6 volts per centimeter could be insulated before breakdown ensued, and that gradients at least ten times higher than this value could be insulated on the anode surface. Hayden[1] reports a maximum cathode gradient of 1.3×10^6 volts per centimeter between outgassed molybdenum spheres. Piersol[2] observed a cathode gradient of 5.4×10^6 volts per centimeter between molybdenum plates outgassed at 1400°C. In the work described in the present paper it was found that at voltages less than 50 kilovolts it is quite easy to support gradients above 10^6 volts per centimeter on steel cathode surfaces after conditioning the surface by permitting low energy flashover.

In the voltage range below 20 kilovolts detectable high field emission from cathode surfaces in vacuum begins at a fairly definite gradient which depends on the electrode material and its surface condition and increases exponentially with increasing gradient until flashover. This effect was first quantitatively analyzed by Schottky,[3] who modified the Richardson thermionic emission equation by reducing the true work function of the metal to account for the attractive influence of the electric field on the escaping electrons. The later experiments of Millikan[4] and others indicated that, unlike the prediction of the Schottky equation, high field emission is substantially independent of the cathode temperature, at least up to about 1200°C, beyond which it is overshadowed by the thermionic emission. This non-dependence has been more adequately explained by the newer Fowler-Nørdheim relation.[5]

Both the Schottky and Fowler-Nordheim relations assume the existence of a smooth cathode surface. Actually, high field emission, like thermionic emission,[6] takes place preferentially from the microscopic projections, crystal edges, and spots of impurities which usually exist on surfaces. This consideration of surface roughness and contamination explains to a considerable extent the discrepancy between the experimentally observed cathode gradients and the higher values predicted by theory. Since field emission varies exponentially with gradient, it is evident that an intensification as small as 10

[1] Hayden, J. A. I. E. E. **41**, 854 (1922).

[2] Piersol, Rep. Brit. Assoc. Advancement Sci. 359 (1924).

[3] Schottky, *Jahrbuch der Radioactivitat und Elektrotechnik* (1915), Vol. 12, pp. 200–205.

[4] Millikan, Eyring, and McKeown, Phys. Rev. **31**, 900 (1928).

[5] Fowler and Nordheim, Roy. Soc. Proc. **A119**, 173–181 and **A121**, 626–639 (1928).

[6] R. P. Johnson and W. Shockley, Phys. Rev. **49**, 433 (1936).

percent because of surface projections would cause most of the field-emission current to flow from such points. The adverse influence on the breakdown gradient of such factors as contaminating surface films, rough electrode surfaces, and low work-function electrodes has become generally appreciated.

It is now well established that voltage breakdown between metal electrodes in high vacuum at high gradients, but relatively low voltages is initiated by high field emission. This emission increases exponentially with gradient and results in local temperature increases and enhanced secondary effects which lead to instability. For many years it has been generally believed that this same high field mechanism accounted for breakdown at high voltages. That this cannot be the case is demonstrated by the data of Fig. 1, in which breakdown voltage and gradient are shown as a function of electrode separation for constant voltages from 20 to 650 kilovolts. It is seen that, while fairly constant gradients of several million volts per centimeter are required to produce breakdown at voltages less than 50 kilovolts, the cathode gradient required at voltages higher than this decreases rapidly. Thus, whereas a gradient of 3000 kilovolts per centimeter is required when the total voltage between the electrodes is 20 kilovolts, a gradient of less than 100 kilovolts per centimeter is the maximum that can be supported at 650 kilovolts. This gradient is evidently inadequate of itself to insure breakdown through the mechanism of high field emission.

HIGH VOLTAGE BREAKDOWN

The explanation of high voltage breakdown suggested some years ago by one of us[7] pictures an interchange of charged particles and photons between cathode and anode. Thus, an electron starting from the cathode and accelerated by the voltage between the electrodes, impinges on the anode with the resultant possible emission of both a positive ion and photons. Such positive ions and some of the photons would return to the cathode and cause further electron emission. When the conditions are such that this interchange becomes cumulative, breakdown results. To represent this mechanism quantitatively, let coefficient A represent the average number of positive ions produced by one electron, and coefficient B the average number of secondary electrons produced by one of these positive ions; similarly, let C represent the photons produced by one electron, and D the secondary electrons produced by an average photon. Then, when the condition

$$AB+CD>1$$

is realized, the interchange becomes cumulative and breakdown ensues. It is evident that these coefficients will be functions of the accelerating voltage between the electrodes and the gradient at the electrode surfaces, as well as of the electrode material and the surface condition. Some preliminary experiments to measure these coefficients were undertaken before the war with the collaboration of J. R. Maull, and work in this direction is now being resumed.

The experimental arrangement for determining coefficient A is shown in Fig. 2. Electrons starting from the filament are accelerated by the voltage between electrodes, and impinge on the upper target, where they are measured. Because of the uniform field, any positive ions produced by these primary electrons return along the same path and are measured by collection in the

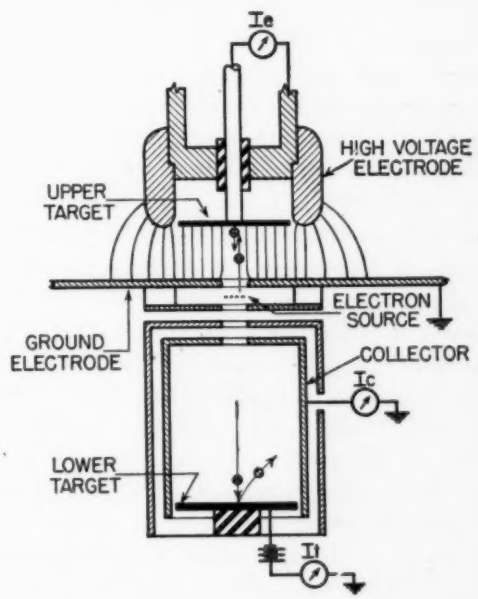

FIG. 2. Electrode arrangement for measuring "breakdown coefficients."

[7] Van Atta, Van de Graaff, and Barton, Phys. Rev. **43**, 158 (1933).

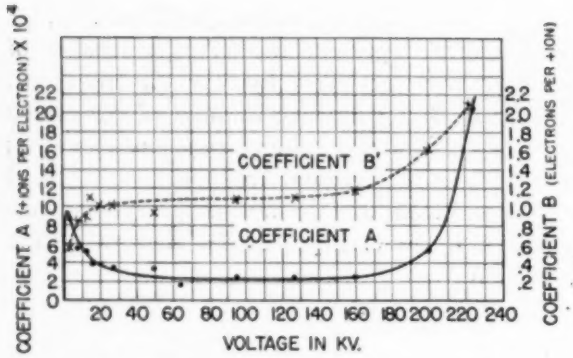
COEFFICIENT A (+IONS PER ELECTRON) X 10⁴
COEFFICIENT B (ELECTRONS PER +ION)
COEFFICIENT B'
COEFFICIENT A
VOLTAGE IN KV.
0 2 4 6 8 10 12 14 16 18 20 22
.2 .4 .6 .8 1.0 1.2 1.4 1.6 1.8 2.0 2.2
20 40 60 80 100 120 140 160 180 200 220 240

FIG. 3. Breakdown coefficients for steel electrodes with 2-cm gap.

Faraday cage. The ratio of the positive-ion current to the electron current is the coefficient A, and can thus be determined over a range of voltages and gradients and different electrode materials. It is noteworthy that the emission of positive ions due to electron impact is assisted in this experiment by the electric field at the anode surface. This is exactly the condition which exists in an actual gap in high vacuum.

Figure 3 shows the coefficient A, the ratio of secondary positive ions to electrons, for a parallel-plane steel gap as a function of the gap voltage. This curve was quite reproducible after the steel target had been outgassed by electron bombardment. The low voltage peak was found to be caused by the ionization of the residual gas and varied closely with its pressure. As would be expected, this residual gas ionization reduces with increasing gap voltage so that at the higher voltages the returning positive ions are owing primarily to secondary ion emission from the anode. The small proportion of residual gas ions to ions from the anode itself accounts for the small dependence on pressure of breakdown voltages in high vacuum.

That a definite positive-ion current could be measured from the electron bombarded target is evidence that this mechanism contributes to breakdown in vacuum. The small value of coefficient A, in this case 2 to 20×10^{-4} in the energy range below breakdown, indicates the cathode coefficient B must be large if this particle mechanism is to be important. The sharp increase in coefficient A near the breakdown voltage is to be noted. The existence of secondary positive-ion emission is also supported by two observations of Anderson in the course of a doctorate research in this program.[8] With constant applied potential and a substantially uniform field, Anderson found deposition of anode (copper) material on the cathode after some minutes of operation near the breakdown value. He also showed a definite, though small, cathode temperature rise under such conditions—this temperature rise being a fraction of one percent of the rise of this same electrode when the polarities were reversed.

It should be expected that the coefficient A will in general differ from one metal to another and show considerable dependence on surface condition.

The same arrangement shown in Fig. 2 may be used to give an idea of the coefficient B, the average number of electrons produced at the cathode by the impact of one high energy positive ion. The returning positive ions, having been accelerated by the full gap voltage, are permitted to impinge on a second target within the collector cage. The resultant secondary electrons are collected as current I_e in this experiment. Figure 3 shows that under these conditions the secondary electrons increase slowly with the energy of the impacting positive ions, the ratio being a small number at energies below 220 kv. This result checks generally with the measurements of Allen,[9] Linford,[10] Hill *et al*,[11] in which secondary electron emission under high energy positive-ion bombardment and low cathode field were found to be small (2 to 20) and usually increased with voltage.

Since, in an actual gap, the cathode is subjected to a high electric gradient which would have the effect of assisting in the escape of electrons, the cathode coefficient shown in Fig. 3 is labeled B' and must be regarded as low, perhaps low by the large factor required to make the particle mechanism of importance in vacuum breakdown. It is evident that a heavy positive ion having an energy of the order of a hundred kilovolts will produce brief, but extremely intense, local heating at its point of impact on the cathode. The effect of a high cathode gradient

[8] Anderson, Elec. Eng. **54**, 1315 (1935).
[9] J. S. Allen, Phys. Rev. **55**, 236 (1939).
[10] L. H. Linford, Phys. Rev. **47**, 279 (1935).
[11] Hill, Buechner, Clark, and Fisk, Phys. Rev. **55**, 463 (1939).

would be to reduce the space charge limitation to electron emission during this short period of intense local heat. Thus under the conditions of high cathode gradient a relatively large number of electrons might escape because of the impact of a single positive ion. Experiments are now planned to determine coefficient B under the complete conditions of voltage and gradient.

Unless retarded by the external circuit, the collapse of the insulating strength of a vacuum gap is characterized by unusually rapid development greatly exceeding that of gaseous or solid insulator gaps. Evidently the conditions for instability are sharply defined and the subsequent discharge is relatively unimpeded. This is to be expected because of the short transit times involved in the energy interchange between electrodes and the absence of space-charge phenomena in the early phases. At an intermediate stage, after the condition for instability has been reached, self-focusing processes probably concentrate the discharge into a thin-cored channel and further enhance the emission of charged particles from the surfaces through thermionic emission. It has been observed that higher voltages can be insulated in the case of somewhat ununiform fields than when the interchange of particles can proceed undeviating along a straight line path between electrodes. The problem of vacuum insulation must be met primarily by reducing the emission characteristics of the electrode surfaces so as to prevent the onset of instability until well beyond the required conditions of voltage and gradient.

EMISSION OF ELECTRONS BY HIGH ENERGY ELECTRON IMPACT

Primarily by replacing the upper target of Fig. 2 with a tungsten filament, the experimental set-up was adapted for measuring the number of secondary electrons emitted due to impact of high energy primary electrons, as a function of voltage and electrode material. Figure 4 shows the ratio of secondary electrons to primary electrons from 30 kv to 340 kv for tungsten, steel, aluminum, and graphite. It is seen that this ratio diminishes with increasing primary energy and that the ratio is a function of the atomic number of the electrode. A study of the energy of these secondary electrons showed a

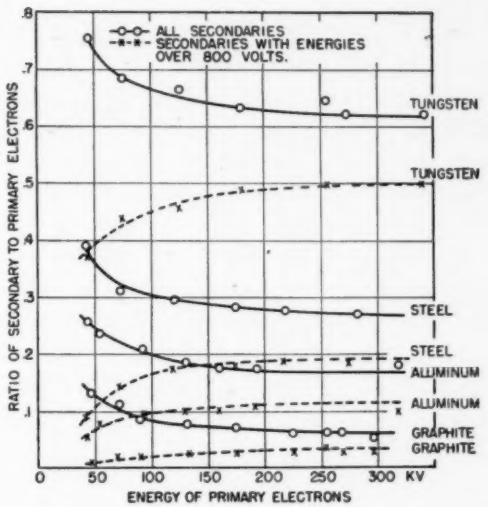

FIG. 4. Secondary emission of electrons by electrons with energies up to 340 kv.

low energy group with energies less than 20 volts. Most of the remainder of the secondaries had energies in excess of 800 volts, some extending in the limit up to the energy of the primaries. As can be seen from the ascending curves of Fig. 4, the proportion of these high energy secondaries increased with voltage, becoming fairly constant above 200 kv. These more energetic electrons result from elastic nuclear scattering and from electron-electron collisions.

To the picture of vacuum breakdown this information adds the concept that electrons from the cathode striking the anode cause repeated opportunities—though each time with diminished energy—to bring about the emission of positive ions and photons. The reduction of this secondary emission coefficient at the higher voltages illustrates how some breakdown factors may actually become diminished at extreme voltage values.

Experiments have been devised, but not yet carried out, for measuring the contribution of the photoelectric mechanism to high voltage breakdown in vacuum. It is well known that the efficiency of x-ray production increases markedly with voltage, though with an increasing tendency for the radiation to continue in the forward direction. Only backward-scattered radiation would be effective in releasing more electrons from the cathode. Although a high electric field at the cathode would assist the photoelectric

emission, the probability of this mechanism being important appears to be small.

The several processes which contribute to the interchange of charged particles are seen to depend in an important way on the total available voltage between the vacuum-immersed electrodes. The breakdown voltage curve of Fig. 1 clearly shows that, at the higher voltage values across a given gap, it is the voltage and not primarily the gradient that affects the insulation performance. For these reasons the term "total voltage mechanism" has been applied to vacuum breakdown in the high constant voltage range.

PULSED MICROWAVE VOLTAGES

Some studies have recently been made by the linear accelerator group at M.I.T. of the insulation of microwave voltages in high vacuum.[12] In a copper cylindrical cavity, 3000 mc voltages in pulses 2 μsec. in duration and calculated at 2×10^6 volts peak were insulated across the 5-cm gap. The pulse nature and high frequency of these insulation tests is in favor of both high voltages and gradients since the time and energy available to accomplish breakdown is limited. It would seem that positive ions can have relatively less influence with this type of voltage and that the breakdown mechanism would depend on high field and photoelectric emission of electrons from both electrode surfaces viewed as alternate cathodes.

POSSIBILITIES FOR REDUCING SURFACE BREAKDOWN COEFFICIENTS

The striking dependence of secondary electron emission on the electrode material illustrates the way in which the breakdown coefficients A and B may also depend on materials, and hence the need of quantitative information on these factors. When these breakdown coefficients are sufficiently known, it should be possible to begin to design and predict the insulation strength of electrodes in vacuum. Moreover, it may prove possible to improve substantially the insulating strength between electrodes in vacuum by various measures which reduce the electrode coefficients. Various possible procedures are suggested, including the use of composite electrode surfaces in which the surface layer is of low atomic number and, therefore, inefficient as a source of heavy secondary particles and x-rays, the use of highly porous surfaces and of grids or insulating films to repress secondaries, the local distortion of the surface field so as to delay the focusing effects of a particle interchange, the magnetic deflection of the interelectrode electrons, and the more complete conditioning of the electrode surfaces. The experimental determination of surface, coefficients under these various conditions can in principle be performed in a more quantitative way than is generally possible in experiments on material insulating media. Such studies should not only widen our understanding of the essential factors in vacuum breakdown, but they may extend insulation strength of high vacuum into the region of usefulness for electrical power engineering and various scientific purposes.[13]

ACKNOWLEDGMENT

It is a pleasure to acknowledge the effective assistance of J. R. Maull in making some of the measurements reported herein.

[12] Halpern, Eberhardt, Rapuano, and Slater, Phys. Rev. 69, 688 (1946).

[13] J. G. Trump, Doctorate Thesis, M.I.T., E. E. Dept. (1933).

Calendar of Meetings

March

22–27 American Society for Metals, Oakland, California
28 Institute of Aeronautical Sciences, Cleveland, Ohio

April

4–5 American Physical Society, Southeastern Section, Salisbury, North Carolina
9–11 Society of Automotive Engineers, New York, New York (Aeronautic Meeting)
14–18 American Chemical Society, Atlantic City, New Jersey
16–18 Society of Automotive Engineers, Chicago, Illinois (Transportation Meeting)
19 Institute of Radio Engineers, Chicago, Illinois
21–25 American Ceramic Society, Inc., Atlantic City, New Jersey
21–25 Society of Motion Picture Engineers, Chicago, Illinois
22–23 American Geophysical Union, Portland, Oregon (Section of Hydrology)
23–26 American Society of Civil Engineers, Phoenix, Arizona
24–26 American Philosophical Society, Philadelphia, Pennsylvania
25–26 American Mathematical Society, Chicago, Illinois
25–26 American Mathematical Society, New York, New York
26 American Mathematical Society, Stanford University, California
28–30 American Geophysical Union, Washington, D. C.
28–30 National Academy of Sciences, Washington, D. C.

May

1–3 American Physical Society, Washington, D. C.
8–10 Acoustical Society of America, New York, New York
17 New England Radio Engineering Meeting, Cambridge, Massachusetts
26–27 Institute of Aeronautical Sciences, Detroit, Michigan